



TECHNISCHE UNIVERSITÄT MÜNCHEN

Institut für Diabetes und Krebs
(Helmholtz Diabetes Center, Helmholtz Zentrum München)
Chair for Metabolic Programming
(TUM School of Life Sciences)

Role of the orphan nuclear receptors TR2 and TR4 in the pathophysiology of obesity and non-alcoholic fatty liver disease

Michaël Jean Hubert

Vollständiger Abdruck der von der Fakultät TUM School of Life Sciences der Technischen Universität München zur Erlangung des akademischen Grades eines

Doktors der Naturwissenschaften

genehmigten Dissertation.

Vorsitzende/-r: Prof. Dr. Martin Hrabè de Angelis

Prüfende/-r der Dissertation:

1. Prof. Dr. Nina Henriette Uhlenhaut
2. Prof. Dr. Stephan Herzig

Die Dissertation wurde am 08.01.2020 bei der Technischen Universität München eingereicht und durch die Fakultät TUM School of Life Sciences am 07.07.2020 angenommen.

Acknowledgements

First and foremost, I want to thank my first and direct PhD supervisor Prof. Dr. Nina Henriette Uhlenhaut for giving me the trust and opportunity to join her research group and work on this project. I am particularly grateful to you for finding this great balance between guiding me and showing the path when I needed help and giving me the freedom to challenge myself and follow my own ideas the rest of the time. In addition to scientific input, I have learned a great deal in terms of self confidence and moving across obstacles thanks to you.

I would like to warmly thank my second supervisor, Prof. Dr. Martin Hrabè de Angelis, for his support, his valuable feedback and his attention to details that were truly inspiring.

My special thanks go also to Prof. Dr. Matthias Tschöp and Prof. Dr. Stephan Herzig for creating a strong scientific environment at the Helmholtz Diabetes Center as well as their support and useful feedback about my project over the years.

Among the Mol Endo group, I first want to thank Ken Dyar and Franzi Greulich for their involvement in my project and their daily scientific and personal support which made my PhD a great teamwork experience. I also wish to thank Céline Jouffe and Laura Escoter Torres, my two biology sisters with whom I shared so many good memories, for better and worse. Céline, I will always remember Super Mouse, “la souris avec une cape”. I also want to thank all past and present members of the team : Kostas, Katerina, Afzal, Kinga, Teresa, Fabiana, Suhail, Sybille, Ivonne, Cinzia, Omar, Kirsten, Ashfaq, Charlotte, Daud, Kristina and Sonja. This experience would not have been as spicy and exciting without you.

I wish to thank Ali Shilleh and Pedro Weickert, two very motivated and talented Master students who helped me a lot in moments of doubt. I wish them the best for the future.

I also want to thank all my friends and colleagues from the Helmholtz Diabetes Center for their help and moral support.

To Diliaana, my almost fluent French speaking friend, merci d’avoir partagé les rires, la sagesse, la musique et la danse de la vie quotidienne avec moi. À mes parents et mon frère, merci pour votre soutien indéfectible et d’avoir placé la poursuite de mon bonheur devant tout le reste. Vous êtes la locomotive qui me donne l’inspiration de croire en mes rêves. Enfin, je remercie Alexandre, le premier et le dernier, dont l’iris est la mosaïque que je contemple pour l’éternité.

Index of Contents

Abstract	iv
Zusammenfassung.....	v
Abbreviations	vi
Index of Figures	ix
Index of Tables.....	xi
1. Introduction	1
1.1 The consequences of obesity, a risk factor for NAFLD.....	1
1.1.1 Obesity impairs adipose tissue function and triggers systemic insulin resistance.....	1
1.1.2 From healthy liver to hepatocellular carcinoma: the multi-hit progression of NAFLD	2
1.2 Nuclear Receptors as regulators of metabolism and drug targets for obesity and NAFLD	4
1.2.1 The Nuclear receptor family and its role in metabolism	4
1.2.2 Structure of the orphan receptors TR2 and TR4	9
1.2.3 TR2/4 as potential regulators of glucose and lipid metabolism.....	11
2. Scope of the thesis.....	14
3. Materials and Methods	15
3.1 Chemicals, commercial kits, antibodies and primers	15
3.2 Animal experiments	17
3.2.1 Transgenic mouse lines.....	17
3.2.2 Housing and diets	19
3.2.4 Genotyping.....	20
3.2.5 Glucose tolerance test	22
3.2.6 Insulin tolerance test	22
3.2.7 Pyruvate tolerance test	22
3.2.8 Body fat composition using Echo-MRI.....	23
3.2.9 Indirect calorimetry, food intake and locomotor activity.....	23
3.3 Molecular biology techniques	23
3.3.1 RNA isolation from tissue	23
3.3.2 cDNA synthesis	23
3.3.3 Real-time quantitative polymerase chain reaction	24
3.3.4 Nuclear protein extraction from liver	24
3.3.5 Western Blot analysis	24

3.4 Tissue assays.....	25
3.4.1 Triglyceride measurement in serum and liver	25
3.4.2 Paraffin embedding of liver and adipose tissues	25
3.4.3 Hematoxylin and Eosin staining	26
3.4.4 Sirius Red staining	26
3.5 Next generation sequencing techniques.....	26
3.5.1 ChIP-Sequencing.....	26
3.5.2 ChIP qPCR.....	27
3.5.3 RNA-Sequencing.....	28
3.6 NGS data analysis	29
3.6.1 ChIP-Sequencing.....	29
3.6.2 RNA-Sequencing.....	29
3.6.3 Metabolite profiling, data processing and analysis.....	29
3.6.4 Statistical analysis.....	30
3.7 Contributions from collaborators	30
4. Results.....	31
4.1 Characterization of adipose tissue-specific TR2/4 dKO mice	31
4.1.1 Generation of adipose-tissue specific TR2/4 dKO mice.....	31
4.1.2 TR2/4 deletion in adipose tissue does not affect glucose metabolism after HFD	32
4.1.3 TR2/4 deletion in adipose tissue does not affect adipose tissue morphology after HFD	33
4.1.4 TR2/4 deletion in adipose tissue does not affect food intake, activity and calorimetric parameters	34
4.2 Characterization of liver-specific TR2/4 dKO mice and TR4 OE mice	35
4.2.1 Generation of liver-specific TR2/4 dKO mice	35
4.2.2 Generation of liver-specific TR4 OE mice.....	36
4.2.3 TR2/4 deletion in liver does not affect glucose metabolism before and after HFD.....	37
4.2.4 TR4 overexpression in liver does not affect glucose metabolism before and after HFD	38
4.2.5 L-dKO mice show microvesicular storage of lipids in the liver.....	40
4.2.6 L-TR4OE mice show early fibrosis on HFD	41
4.2.7 L-TR4OE mice progress faster into NAFLD on a pro-fibrotic diet.....	42
4.3 Genomic binding of TR2 and TR4 in the liver	44
4.3.1 TR2 and TR4 cistromes partially overlap in liver and control mRNA maturation, protein synthesis and degradation and lipid metabolism.	44
4.3.2 TR4 overexpression in the liver increases the number and the amplitude of TR4 binding sites with similar functionality.....	46

4.4 Transcriptional reprogramming of the livers from L-dKO and L-TR4OE mice	50
4.4.1 L-dKO and L-TR4OE mice have minor changes in transcriptional regulation on chow diet.	50
4.4.2 L-dKO mice show reduced inflammation and immune response and increased xenobiotic and lipid metabolism upon HFD.	52
4.4.3 L-TR4OE mice show increased collagen synthesis and fibroblast maturation and reduced drug and lipid metabolism upon HFD.	54
4.5 Metabolite profiling identify a role in PUFA and bile acid synthesis for TR2 and TR4.	55
4.5.1 TR2/4 deletion and TR4 overexpression affect PUFA and bile acid metabolism.	55
4.5.2 L-dKO mice have increased amidated bile acids and n-6 PUFA species in the liver.	57
4.5.3 L-TR4OE mice have accumulation of alternative bile acids and reduced PUFA species in the liver.	60
5. Discussion.....	64
5.1 Hepatic TR2 and TR4 regulate inflammation and fibrogenesis and control the transition between NAFL and NASH.	64
5.2 TR2/4 and FXR as regulators of bile acid metabolism	68
5.3 TR4 and PPARα as regulators of fatty acid metabolism and inflammation.	72
5.4 TR4 antagonism as a therapeutic strategy against NAFLD.	74
References.....	77
Supplemental data.....	88
List of publications.....	100
Curriculum Vitae.....	101

Abstract

The obesity pandemic is responsible for various metabolic complications referenced as the metabolic syndrome. Those conditions include non-alcoholic fatty liver disease, type 2 diabetes mellitus and various forms of cancer. Nonalcoholic fatty liver disease is a progressive disease ranging from hepatic steatosis to advanced steato-hepatitis that increases the risk of hepatocellular carcinoma. Understanding the pathophysiology of the metabolic syndrome and the molecular pathways involved in the progression of the disease is of prime importance to develop efficient treatment strategies.

Nuclear Receptors are ligand-gated transcription factors that bind directly to consensus DNA sequences as homo- or heterodimers to regulate gene expression in a tissue specific manner. They orchestrate and synchronize major biological processes such as cell division, reproduction, immune response and metabolism. In particular, their ability to respond to nutrients as diet-derived ligands and small molecule drugs makes them pharmacological targets of choice for treating metabolic syndrome.

TR2 and TR4 are related orphan nuclear receptors that are co-expressed in many organs, including liver and adipose tissue. Various studies point at a role for TR2/4 in metabolic control but their tissue-specific function and their gene programs are not yet described. Adipose tissue- and liver-specific TR2/4 double knockout (L-dKO) mice were generated and challenged with a high fat diet. While adipose tissue mutant mice showed no differences in adipose tissue physiology, L-dKO mice showed protection against liver fibrosis. On the other hand, liver-specific TR4 overexpressing mice progress faster towards liver fibrosis after a calory-rich nutritional challenge.

RNA-Sequencing in combination with ChIP-Sequencing and metabolomics analysis revealed that TR2/4 activity controls bile acid synthesis and secretion and poly-unsaturated fatty acid metabolism. The action of these receptors is detrimental for the high fat diet response to inflammation and lipotoxicity and promotes fibrogenesis.

Taken together, the results of this study show that TR2/4 and their target genes are involved in the progression of NAFLD and constitute a missing link in the transition between steatotic and fibrotic liver. By controlling PUFA and bile acid metabolism, TR2/4 link metabolism, inflammation and fibrosis. These findings put these two orphan receptors on the front line for ligand identification and potential drug development against non-alcoholic fatty liver disease.

Zusammenfassung

Die Adipositas-Pandemie ist für verschiedene metabolische Komplikationen verantwortlich, die als metabolisches Syndrom bezeichnet werden. Zu diesen Erkrankungen gehören unter anderem die nicht alkoholische Fettleberkrankheit, Typ-2-Diabetes mellitus und verschiedene Krebsarten. Die nicht alkoholische Fettleberkrankheit ist eine fortschreitende Krankheit, die von der Lebersteatose bis zur Steatohepatitis reicht und das Risiko für ein Leberzellkarzinom erhöht. Das Verständnis der Pathophysiologie des metabolischen Syndroms und der molekularen Wege, die am Fortschreiten der Erkrankung beteiligt sind, ist von größter Bedeutung für die Entwicklung effizienter Behandlungsstrategien.

Kernrezeptoren sind ligandengesteuerte Transkriptionsfaktoren, die direkt an Konsensus-DNA-Sequenzen als Homo- oder Heterodimere binden, um die Genexpression auf gewebespezifische Weise zu regulieren. Sie orchestrieren und synchronisieren wichtige biologische Prozesse wie Zellteilung, Reproduktion, Immunantwort und Stoffwechsel. Insbesondere ihre Fähigkeit, auf Nährstoffe als von der Nahrung abgeleitete Liganden und niedermolekulare Arzneimittel zu reagieren, macht sie zu pharmakologischen Zielen für das metabolische Syndrom.

TR2 und TR4 sind verwandte orphan-nukleare Rezeptoren, die in vielen Organen, einschließlich Leber und Fettgewebe, koexprimiert werden. Verschiedene Studien weisen auf eine Rolle von TR2 / 4 bei der Stoffwechselkontrolle hin, ihre gewebespezifische Funktion und ihre Genprogramme sind jedoch noch nicht beschrieben. Fett- und leberspezifische TR2/4 doppel-Knockout (L-dKO) Mäuse wurden gezüchtet und einer fettreichen Ernährung unterzogen. Während fettspezifische TR2/TR4 KO Mäuse keine Unterschiede in der Physiologie des Fettgewebes zeigten, waren leberspezifische-dKO-Mäuse vor diätinduzierter Leberfibrose geschützt. Andererseits entwickeln leberspezifische TR4 überexprimierende Mäuse nach Fütterung mit Hochfettdiät schneller eine Leberfibrose.

Mit Hilfe der RNA-Sequenzierung in Kombination mit ChIP-Sequenzierung und Metabolomanalyse, konnte gezeigt werden, dass die TR2/4-Aktivität die Gallensäuresynthese und -sekretion, sowie den Stoffwechsel mehrfach ungesättigter Fettsäuren kontrolliert. Folglich führt bei fettreicher Ernährung die Aktivität dieser Rezeptoren zu Entzündungen, Lipotoxizität und Fibrogenese.

Zusammenfassend zeigen die Ergebnisse dieser Studie, dass TR2/4 und ihre Zielgene an der Progression der NAFLD beteiligt sind und ein fehlendes Glied im Übergang zwischen steatotischer und fibrotischer Leber darstellen. Aufgrund dieser Erkenntnisse stehen diese beiden Orphan-Rezeptoren an erster Stelle bei der Identifizierung von Liganden und der potenziellen Arzneimittelentwicklung gegen nichtalkoholische Fettlebererkrankungen.

Abbreviations

A-dKO	adipose tissue double knockout
AF	activation function domain
Alb	albumin
ANOVA	analysis of variance
ATM	adipose tissue macrophages
ATP	adenosine tri-phosphate
BA	bile acid
BAT	brown adipose tissue
bp	base pair
BSA	bovine serum albumin
CDCA	chenodeoxycholic acid
cDNA	complementary DNA
ChIP	chromatin immuno-precipitation
Ct	threshold cycle
DBD	DNA binding domain
DIAMOND	diet induced animal model of NAFLD
dKO	double KO
DNA	deoxyribonucleic acid
DNL	<i>de novo</i> lipogenesis
DR	direct repeat
DTT	dithiothreitol
ECL	enzymatic chemoluminescence
EDTA	ethylenediaminetetraacetic acid
EE	energy expenditure
e.g.	exempli gratia
EtOH	ethanol
ETS	E26 transformation-specific
FFA	free fatty acid
fl	floxed
Fw	forward
GEO	gene expression omnibus
GO	gene ontology
GTT	glucose tolerance test
H&E	hematoxylin and eosin

HCC	hepatocellular carcinoma
HEPES	4-(2-hydroxyethyl)-1-piperazineethanesulfonic acid
HFD	high fat diet
HRE	hormone response element
HRP	horse radish peroxidase
IgG	immunoglobulin G
IP	immunoprecipitation
IR	insulin receptor
IR1	inverted repeat 1
ITT	insulin tolerance test
KCl	potassium chloride
KO	knockout
KOH	potassium hydroxide
L-dKO	liver specific double knockout
L-TR4OE	liver specific TR4 overexpressor
LBD	ligand binding domain
LDF	lineage determining factor
MCD	methionine choline deficient diet
MgCl ₂	magnesium chloride
mRNA	messenger RNA
NaCl	sodium chloride
NAFL	non-alcoholic fatty liver
NAFLD	non-alcoholic fatty liver disease
NaOH	sodium hydroxide
NASH	non-alcoholic steato-hepatitis
NP-40	nonyl phenoxyethoxyethanol
NR	nuclear receptor
OE	overexpression
ORF	open reading frame
PBS	phosphate buffered saline
PCR	polymerase chain reaction
pH	potential of hydrogen
PTT	pyruvate tolerance test
PUFA	polyunsaturated fatty acid
qPCR	quantitative PCR
RER	respiratory exchange ratio
RNA	ribonucleic acid

ROS	reactive oxygen species
rpm	rotation per minute
RT-qPCR	real-time qPCR
Rv	reverse
SCAT	subcutaneous adipose tissue
SCD	sickle cell disease
SD	standard deviation
SDS	sodium dodecyl sulfate
SEM	standard error of the mean
Seq	sequencing
SPF	specific-pathogen-free
T2DM	type 2 diabetes mellitus
TBS-T	TRIS buffered saline with Tween 20
TF	transcription factor
TRIS	tris(hydroxymethyl)aminomethane
TSS	transcription start site
UDCA	ursodeoxycholate
UV	ultraviolet
VAT	visceral adipose tissue
WB	western blot
WT	wildtype
ZT	zeitgeber

All gene names are indicated in *italics*. All proteins are written in regular font with capital letters. Compounds and chemical elements are abbreviated according to common chemical nomenclature.

Index of Figures

Figure 1: Obesity induced systemic inflammation impacts insulin signaling in the liver.....	2
Figure 2: Progression of the NAFLD spectrum.....	3
Figure 3: Structural organization of Nuclear Receptors.....	5
Figure 4: The superfamily of orphan nuclear receptors.	6
Figure 5: Models of NR mechanism of action.	7
Figure 6: Mechanism of nuclear receptor cell-type specific gene regulation.	8
Figure 7: Sequence homology of the LBD and DBD of the human TR2, TR4 and the known steroid receptors.	10
Figure 8: Sequence homology of the peptide composition of the mouse TR2 and TR4 proteins.	11
Figure 9: Recombination strategy on <i>Nr2c1</i> and <i>Nr2c2</i> genes using Cre-LoxP system.	18
Figure 10: Insertion and recombination strategy of the TR4 sequence under a CAG promoter.	19
Figure 11: Generation and validation of adipose-tissue specific TR2/4 dKO mice (A-dKO mice).	31
Figure 12: A-dKO mice show no differences in glucose and insulin tolerance after 12 and 20 weeks of HFD.....	32
Figure 13: A-dKO mice show no differences in body weight and composition and adipose tissue morphology after 20 weeks of HFD.	33
Figure 14: A-dKO mice show mild differences in food intake, activity and calorimetric parameters after 12 weeks of HFD.	34
Figure 15: Generation and validation of liver-specific TR2/4 dKO mice (L-dKO mice).	36
Figure 16: Generation and validation of liver-specific TR4 OE mice (L-TR4OE mice).	37
Figure 17: L-dKO mice show no differences in glucose, insulin and pyruvate tolerance on chow diet or after 12 weeks of HFD.	38
Figure 18: L-TR4OE mice show no differences in glucose, insulin and pyruvate tolerance on chow diet or after 12 weeks of HFD.	39
Figure 19: L-dKO and L-TR4OE mice become obese and have hepatic steatosis on HFD.	40
Figure 20: L-TR4OE mice show early liver fibrosis after HFD.	42
Figure 21: L-TR4OE mice are prone to liver fibrosis and L-dKO mice are protected against liver fibrosis on DIAMOND diet.	43
Figure 22: TR2 and TR4 share a strong overlap in the liver and specific binding for TR4.	45
Figure 23: KEGG pathway annotation of TR2 and TR4 cistromes in WT livers.....	46
Figure 24: TR4 binds extra DNA regions in the liver of L-TR4OE mice compared to WT mice.....	47
Figure 25: KEGG pathway annotation of TR4 cistromes in WT and L-TR4OE livers.....	48
Figure 26: TR2 and TR4 bind in the promoter region of common genes while TR4 binds enhancers in lipid and bile acid metabolic genes.....	49
Figure 27: Livers from L-dKO mice show minimal transcriptional reprogramming on chow diet.....	51
Figure 28: Livers from L-TR4OE mice show activation of sterol and lipid metabolic genes on chow diet.	52
Figure 29: L-dKO mice show up-regulation of lipid and xenobiotic metabolism and down regulation of immune response and inflammation upon HFD.....	53
Figure 30: L-TR4OE mice show up-regulation of collagen and fibroblast production and down regulation of xenobiotic and lipid metabolism upon HFD.....	54
Figure 31: Livers of L-dKO mice have changes in their composition of bile acid species and PUFAs upon HFD.	56

Figure 32: Livers of L-TR4OE mice have changes in their composition of fatty acid and bile acid species upon HFD.	57
Figure 33: L-dKO mice have increased amidated primary bile acids from the alternative pathway in the liver after HFD.	58
Figure 34: L-dKO mice have an increase in some long-chain n-6 PUFA species in the liver after HFD..	59
Figure 35: L-TR4OE mice have accumulation of primary bile acids from the alternative pathway in the liver after HFD.	61
Figure 36: L-TR4OE mice have a decrease in dietary and long chain PUFAs in the liver after HFD.	62
Figure 37: Regulation of NASH progression by TR2 and TR4.	71

Index of Tables

Table 1: List of chemicals and reagents.	15
Table 2: List of commercial kits.	16
Table 3: List of primary and secondary antibodies.	16
Table 4: Primer sequences for qRT-PCR.	16
Table 5: Primer sequences for CHIP-qPCR.	17
Table 6: Genotyping PCR reaction.	21
Supplemental Table 1: TR2 CHIP-Sequencing peaks in wildtype liver.	88
Supplemental Table 2: TR4 CHIP-Sequencing peaks in wildtype liver.	88
Supplemental Table 3: TR4 CHIP-Sequencing peaks in L-TR4OE liver.	89
Supplemental Table 4: Genes differentially expressed in livers of L-dKO livers on chow diet.	90
Supplemental Table 5: Genes differentially expressed in livers of L-TR4OE livers on chow diet.	91
Supplemental Table 6: Genes differentially expressed in livers of L-dKO livers after 12 weeks of HFD.	92
Supplemental Table 7: Genes differentially expressed in livers of L-TR4OE livers after 12 weeks of HFD.	94
Supplemental Table 8: PUFA and bile acid profiling in WT and L-dKO livers.	97
Supplemental Table 9: PUFA and bile acid profiling in WT and L-TR4OE livers.	98

1. Introduction

1.1 The consequences of obesity, a risk factor for NAFLD

Obesity prevalence has tripled worldwide since 1975 (WHO, 2018). Developed countries account for most of this massive increase in obesity but developing countries are following similar trends. The new epidemic in chronic liver disease is related to the burden of non-alcoholic fatty liver disease (NAFLD) paralleling the worldwide increase in obesity. NAFLD is estimated to affect 24% of humanity and is predicted to become the leading cause of liver cirrhosis and hepatocellular carcinoma (HCC), two severe conditions lacking treatment options (Younossi et al., 2017).

Obesity is the pathological expansion of the body fat mass that ultimately leads to metabolic dysfunctions and multi-organ complications such as NAFLD, type 2 diabetes mellitus (T2DM) and cardio-vascular diseases (Brunt et al., 2015). A tight relationship between obesity, insulin resistance and NAFLD has been established (Younossi et al., 2017). The first chapter will review the main events happening in the adipose tissue during obesity and the impact it has on systemic insulin resistance and the onset of NAFLD.

1.1.1 Obesity impairs adipose tissue function and triggers systemic insulin resistance

In obesity, excessive lipid accumulation in adipose tissue leads to inflammatory and metabolic events promoting insulin resistance and metabolic syndrome. Weight gain induces hypertrophy and hyperplasia of the subcutaneous adipose tissue that eventually exceeds its maximal storage capacity leading to adipocyte dysfunction and liberation of pro-inflammatory molecules (Brunt et al., 2015; Font-Burgada, Sun, & Karin, 2016). Adipose tissue macrophages (ATM) in healthy fat depots are skewed toward M2 anti-inflammatory phenotype but during obesity, pro-inflammatory M1 macrophages proliferate and become more abundant (Figure 1) (McNelis & Olefsky, 2014). Recruitment of M1 pro-inflammatory macrophages and unbalance with the resident M2 anti-inflammatory macrophages increases the release of pro-inflammatory cytokines such as TNF α , IL-6 and IL-1 β (Weisberg et al., 2003). Those factors will promote lipolysis and free fatty acid (FFA) release from adipocytes in the circulation that will induce ectopic lipid storage in metabolic organs such as the liver and muscle. Also, inflammation and circulating lipids will affect the insulin receptor (IR) pathway and induce insulin resistance. Systemic insulin resistance is the major event that will trigger the complications of obesity such as cardio-vascular diseases, T2DM and NAFLD (Khan, Bril, Cusi, & Newsome, 2019).

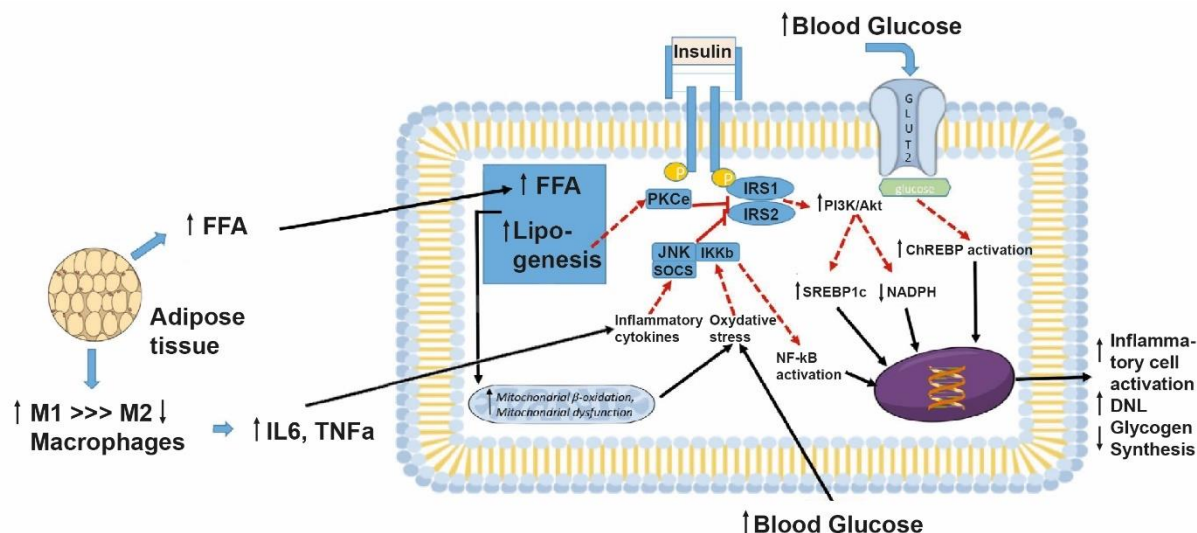


Figure 1: Obesity induced systemic inflammation impacts insulin signaling in the liver. Picture adapted from (Khan et al., 2019).

1.1.2 From healthy liver to hepatocellular carcinoma: the multi-hit progression of NAFLD

The liver is an essential organ for digestion, glucose and lipid metabolism, detoxification, immune response, protein synthesis and secretion and protection of the organism (Adams, 2003). By receiving the blood coming from the digestive track through the portal vein, the liver plays a fundamental role as the first barrier of the organism. It filters, absorbs and metabolizes the nutrients produced by the digestion and enteric absorption of the food. As an accessory digestive organ, it is responsible of bile acid (BA) synthesis from cholesterol to assist lipid breakdown and absorption. During the active and feeding phase, liver orchestrates storage and distribution of nutrients between organs throughout the body. During the resting phase, liver is responsible for providing glucose to the brain and induces FFA liberation by the white adipose tissue (Jensen, Kiersgaard, Sørensen, & Mikkelsen, 2013). As the main gluconeogenic organ, liver has the capacity to produce glucose from non-carbohydrate substrates such as amino acids, glycerol, pyruvate and lactate (Rui, 2014). Switches in metabolic and gene programs are highly dependent on hormone response. Insulin is the main anabolic hormone that promotes glucose absorption by the skeletal muscle and adipose tissue.

In the liver, insulin binds its receptor and activates its substrates IRS1 and IRS2 (Figure 1) (Khan et al., 2019). Insulin is an anabolic hormone that will promote the absorption of glucose in hepatocytes and its storage in the form of glycogen and triglycerides *via de novo* lipogenesis (DNL) (Sanders & Griffin, 2016). During obesity, inflammatory cytokines produced by adipocytes and ATM will impair the action of insulin by promoting inflammation and the downstream regulation of IR (Figure 1) (Chen CC et al., 2003). Insulin resistance in the liver

selectively inhibits the hypoglycemic effects of insulin while maintaining the DNL pathways (Brown & Goldstein, 2008). Hyperglycemia will create oxidative stress and impair mitochondrial function. Glucose will also promote DNL and be a substrate for newly synthesized lipids (Erion et al., 2013). Circulating FFA coming from the diet and the adipose tissue are taken up by hepatocytes and stored as triglycerides. Excess of lipids impact IR targets activity which creates a feed-forward loop towards increased gluconeogenesis that feeds DNL and triglyceride storage in hepatocytes (Samuel & Shulman, 2018).

Chronic hepatic lipid accumulation is defined as hepatic steatosis and is the first stage of NAFLD (Figure 2) (Hardy, Oakley, Anstee, & Day, 2016). Multiple metabolic and inflammatory events will impact the hepatocyte function and determine the progression to the next stages of the disease. Paracrine cytokine production by the activation of the resident Kupffer cells and recruited macrophages will cause local inflammation that will potentiate insulin resistance, mitochondrial dysfunction and hepatocyte damage (Schuppan, Surabattula, & Wang, 2018). Fatty acid overload and metabolism causes a major strain on hepatocyte mitochondria that eventually leads to mitochondrial uncoupling and reactive oxygen species (ROS) production. Also, excess of fatty acids can damage hepatocyte by provoking endoplasmic reticulum stress and activation of death receptors such as FAS (Brunt et al., 2015; Schuster, Cabrera, Arrese, & Feldstein, 2018).

Ultimately, these events will lead to hepatocyte damage and death by senescence or apoptosis that define non-alcoholic steato-hepatitis (NASH) as a more advanced stage of the NAFLD. During NASH, senescent hepatocytes will secrete cytokines such as IL-6, IL-8 and TGF β that will stimulate wound-healing through activation of resident stellate cells into myofibroblast differentiation (Brunt et al., 2015; Torer, Ozenirler, Yucel, Bukan, & Erdem, 2007). These myofibroblasts will compensate for the loss of hepatocyte by producing scar tissue through extra-cellular matrix proteins synthesis such as collagen and will be responsible for liver fibrosis (Wallace, Friedman, & Mann, 2015). Surviving hepatocytes will also compensate for senescent hepatocytes by compensatory proliferation (Gentric, Desdouets, & Celton-Morizur, 2012).

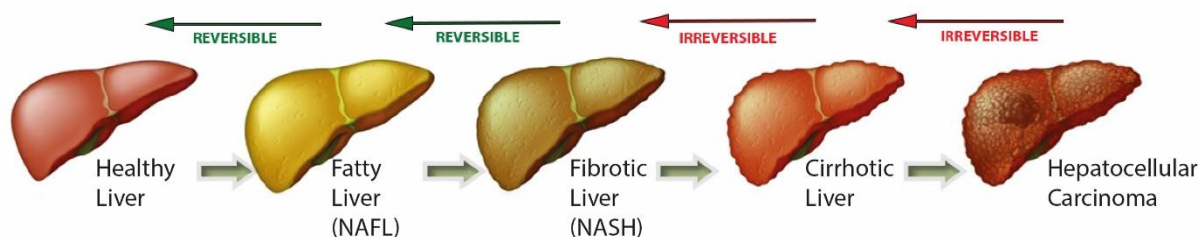


Figure 2: Progression of the NAFLD spectrum.

The first stage of NAFLD is characterized by ectopic lipid accumulation in the liver resulting in hepatic steatosis (NAFL), progressively leading to inflammation and fibrosis (NASH). Ultimately, liver damage becomes more advanced and the majority of hepatocytes enter senescence, inducing liver failure and cirrhosis. In some cases, liver damage leads to hepatocyte transformation and the development of HCC. While NAFL and NASH are partially reversible through diet and drug intervention, cirrhosis and HCC are irreversible conditions with few therapeutic options and poor prognosis. Adapted from (Hardy et al., 2016).

Eventually, the hepatocyte degenerescence will overwhelm the regenerative capacity of the remaining hepatocytes causing massive fibrosis and liver failure defined as liver cirrhosis. Also, the combination of long-term ROS production, endoplasmic reticulum stress and inflammation can cause DNA damage in hepatocytes and lead to transformation, initiating hepatocellular carcinoma (Brunt et al., 2015; Font-Burgada et al., 2016). These two conditions are currently irreversible and pose a major threat for the future generations since no curative treatment is available.

Furthermore, the understanding of the NAFLD progression and the transition between the different stages of the disease are still limited. In particular, the identification of the factors that trigger the inflammation and the transition from NAFL to NASH is not well understood in humans (Schuster et al., 2018). Nuclear receptors (NR) are among the major players in metabolism and are currently studied as potential therapeutic targets for obesity and its complications.

1.2 Nuclear Receptors as regulators of metabolism and drug targets for obesity and NAFLD

1.2.1 The Nuclear receptor family and its role in metabolism

Nuclear receptors are ligand-gated transcription factors that share the unique capacity to bind directly to DNA and regulate the transcription of specific target genes. Nuclear receptors share a particular protein structure with a central DNA binding domain (DBD), a ligand binding domain (LBD) close to the C-terminal part of the protein and transactivation domains in the N-terminal and the LBD domains (Figure 3) (R. M. Evans, 1988). The DBD is composed of a dimerization domain and two highly conserved zinc fingers that set them apart from other DNA-binding proteins (Berg, 1989; Klug & Schwabe, 1995). The DBD can recognize specific DNA sequences known as hormone response elements (HRE) that gives each nuclear receptor a specific binding pattern. Furthermore, the LBD adds another layer of control of the specificity and selectivity of the nuclear receptor action by recognizing specific ligands and shifting the receptor in a transcriptionally active state (D. J. Mangelsdorf et al., 1995). The combination of

the DBD and LBD ensures a spatial and temporal control of the activity of each nuclear receptor.

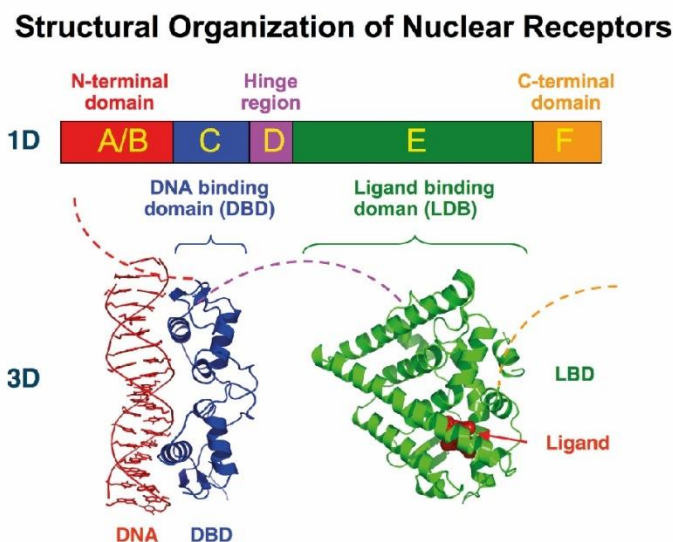


Figure 3: Structural organization of Nuclear Receptors.

Nuclear receptors (NR) are characterized by a DNA binding domain (DBD) that can recognize and bind specific DNA regions and a Ligand binding domain (LBD) that can bind to specific ligands to induce its activity. The DBD (C) contains two zinc fingers and a dimerization domain. The LBD (E) contains an activation function domain (AF-2) whose action depends on the presence of the ligand. The N-terminal domain (A/B) also contains an activation function domain (AF-1) that synergizes and amplifies the action of the AF-2 in presence of ligand. The hinge region (D) works as a connector between C and E and is involved in NR transport through a target peptide sequence. The C-terminal domain (F) is highly variable between different NR. Source of image: Wikipedia.

In humans, the NR family is composed of 48 members (Figure 4). The founding members of the NR family are the glucocorticoid receptor (GR) and the endrogen receptor (ER) since their complete cDNAs were the first to be isolated and cloned in the 1980s (Greene et al., 1986; Hollenberg et al., 1985). These steroid hormone receptors were quickly joined by the mineralocorticoid receptor (MR), the androgen receptor (AR) and the progesterone receptor (PR).

These nuclear receptors were named after the endogenous steroid hormone that they recognize. They bind as homodimers to response elements configured as palindromes composed of two hexad nucleotide sequence separated by three base pairs (Figure 5.A) (Beato, 1991).

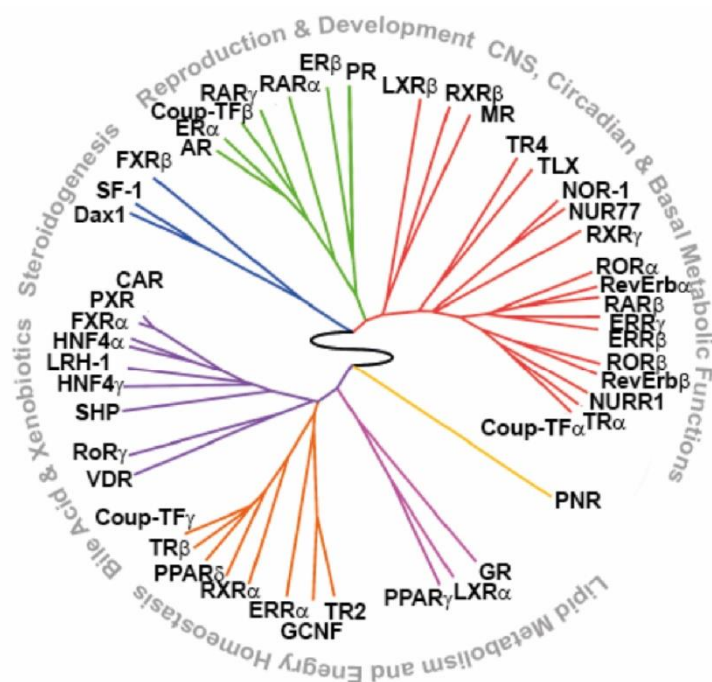


Figure 4: The superfamily of orphan nuclear receptors.

Nuclear hormone receptors were clustered according to tissue distribution revealing the link to physiological pathways, e.g. reproduction, development, lipid and energy homeostasis. Picture adapted from (Bookout et al., 2006).

In addition to these receptors for which the ligands was previously identified, other non-steroidal receptors were discovered and added to the family. Because their ligand was unidentified, these receptors were termed as “orphan receptors” (Giguère, Yang, Segui, & Evans, 1988; Milbrandt, 1988; O'Malley, 1990). Orphan receptors were shown to work either as homo-, heterodimers or both. For example, RXR, TR2 or TR4 can function as homodimers and bind to response elements composed of two repeats of the AGGTCA hexad half-site arranged as tandem repeats separated by one nucleotide called direct-repeat (DR) 1 motifs (Figure 5.B) (Glass, 1994; David J. Mangelsdorf & Evans, 1995). Also, RXR showed a particular place in this class of orphan nuclear receptors. Indeed, it can heterodimerize with multiple partners. Due to the adaptive structure of its LBD, it can bind DR elements with various spacing going from DR1 to DR5 (Figure 5.C) (Chandra et al., 2008; Lou et al., 2014; Perlmann, Rangarajan, Umesono, & Evans, 1993). There are three RXR proteins (RXR α , RXR β , RXR γ) that are functionally interchangeable and at least one of them is expressed in every cell type (David J Mangelsdorf et al., 1992). Two scenarios are possible for RXR heterodimerization. The first one is when the partner was identified to be a hormone receptor with an endocrine ligand such as thyroid receptors (TRs), vitamin-D receptor (VDR) or the retinoic acid receptors (RARs). In that case, the hormone receptor is called non-permissive as it silences RXR activity and only their own ligand will activate the heterodimer (Petkovich, Brand, Krust, & Chambon, 1987; Shulman

& Mangelsdorf, 2005). Permissive partners, on the other hand, allow the presence of both RXR and the partner receptor ligands to bind, creating a synergistic response that goes beyond the activation of only one of the two receptors (Leblanc & Stunnenberg, 1995). Permissive partners of RXR include farnesoid X receptor (FXR), peroxisome proliferator activated receptors (PPARs), liver X receptors (LXRs). They all partner with RXR to bind DR1 response elements except for FXR that is shown to bind an inverted repeat 1 (IR1) asymmetric motif (Chong et al., 2010).

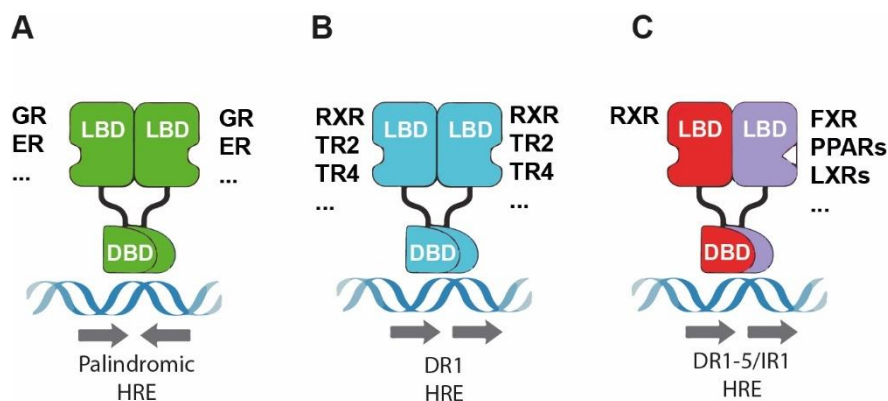


Figure 5: Models of NR mechanism of action.

A: Steroid hormone receptors (GR,ER...) function as homodimers and bind hormone response elements (HRE) configured as palindrome of two hexad nucleotide sequence separated by a 3 base pairs spacer. B: Some non-steroid nuclear receptors function as homodimers and can recognize DR1 hormone response elements arranged as tandem repeats. C: RXR can heterodimerize with non-steroid nuclear receptors such as FXR, PPARs or LXRs and bind IR1 or DR1-5 HRE. Picture adapted from (D. J. Mangelsdorf et al., 1995)

This implies that more than one heterodimer can recognize and interact with a given binding site. This promiscuity of the nature of the binding sites between different RXR heterodimers adds a new layer of complexity in the regulation of individual target genes. Also, in addition to the specificity of the binding site sequence and the ligand, other factors influence the tissue-specific action of a given nuclear receptor. In each cell-type, lineage determining factors will establish a specific chromatin landscape that will determine the future accessibility of enhancer regions for the nuclear receptors (Figure 6) (Dawn & Christopher, 2013; Greulich, Hemmer, Rollins, Rogatsky, & Uhlenhaut, 2016). The nature of the surrounding transcription factors binding in the vicinity and the coregulators recruited to modulate the transcription influence the regulation of genes in a locus-specific manner.

Among orphan nuclear receptors, the retinoid X receptor (RXR) was the first one to be deorphanized: it was shown to be activated by a metabolite of vitamin A, the 9-cis retinoid

acid (Heyman et al., 1992; Levin et al., 1992; David J Mangelsdorf, Ong, Dyck, & Evans, 1990; Petkovich et al., 1987). The list of “adopted” orphan receptors increased over the years and showed that the RXR permissive partners were essential for the regulation of metabolism. For example, peroxisome proliferator-activated receptors (PPARs) and Farnesoid X Receptor (FXR) were identified to be activated by unsaturated fatty acids and bile acids respectively (Gross, Pawlak, Lefebvre, & Staels, 2016; Mi et al., 2003).

Interestingly, for this class of receptors, there is a close link between the nature of the ligands and the biological processes they regulate (Ronald M. Evans & Mangelsdorf, 2014). During starvation, PPAR α is a primary regulator of the adaptive response to caloric depletion. In the liver, PPAR α senses the reversed flux of fatty acids and activates a transcriptional program to convert fatty acids into a usable energy source such as ketone bodies (Contreras, Torres, & Tovar, 2013). Activation of PPAR α also results in the production of the hepatokine FGF21, which sends a signal to white adipose tissue depots to facilitate the liberation of fatty acids in the blood circulation and adapt the body metabolism to an energy-deprived state (Potthoff, Kliewer, & Mangelsdorf, 2012). In sensing the rising levels of fatty acids *via* enhanced free fatty acid uptake from the liver, PPAR α is activated to manage triglyceride and fatty acid metabolism by promoting ATP production through mitochondrial β -oxidation (Montagner et al., 2016). Similarly, in response to bile acids, FXR controls bile acid synthesis and promotes the enterohepatic circulation of bile acids through the small intestine and the liver (Matsubara, Li, & Gonzalez, 2013). Liver FXR is a crucial regulator of cholesterol and bile acid homeostasis (Schmitt et al., 2015). It is also involved in lipid, glucose and xenobiotic metabolism.

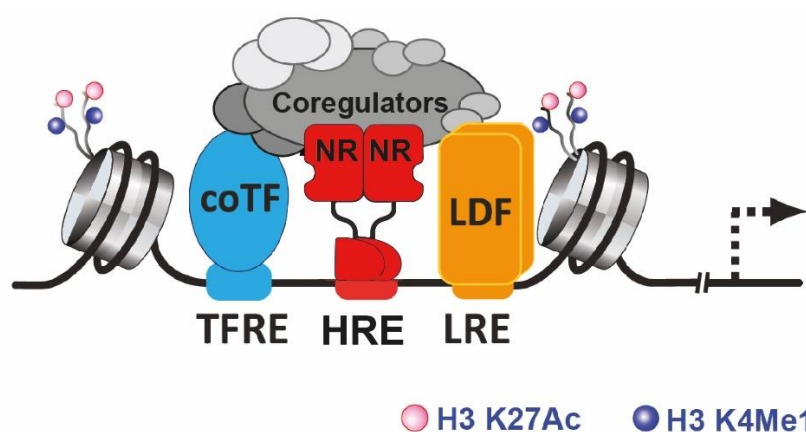


Figure 6: Mechanism of nuclear receptor cell-type specific gene regulation.

The cell-type specificity of a NR is determined by several layers of regulation. As seen before, the structure of the DBD will influence the DNA sequence that the NR is able to recognize (HRE). Its LBD and its ligand will also determine the time and place where the NR is active. Also, lineage-determining factors (LDF) are cell-type specific factors that will establish the chromatin landscape and the accessible enhancers for the NR by recruiting histone modifying enzymes. Finally, other response elements (TFRE) for various transcription factors (coTF) will

influence the assembly of a coregulator complex and the gene regulation of the NR in a locus-specific manner. Picture adapted from (Greulich et al., 2016)

By their inner capacity to bind specific ligands, NRs have proven to be strong therapeutic targets for drug discovery. PPARs are regulating the development and the physiology of liver and adipose tissue and were promising targets for drug development against obesity and NAFLD. However, the first generation of PPAR agonists are associated with severe adverse effects that led to the discontinuation of their development (Gross et al., 2016). Obesity and NAFLD are complex multi-systemic diseases which make them difficult to treat. Understanding the physiopathology and the players involved in the progression of these diseases is more than ever a priority for the development of combinatorial therapies. In addition to increase the knowledge of already known nuclear receptors, uncovering the tissue-specific functions of understudied members of the NR family would give an improved picture of the global knowledge on physiological processes regulating metabolism and their implication in the physiopathology of the metabolic syndrome.

The orphan receptors TR2 and TR4 are involved in several biological processes including metabolism. The next section will review the current knowledge that makes them promising targets in adipocyte and hepatocyte physiology.

1.2.2 Structure of the orphan receptors TR2 and TR4

The testicular nuclear receptor 2 (TR2) and 4 (TR4) form a unique subfamily of orphan receptors within the NR superfamily and are encoded by the *Nr2c1* and *Nr2c2* genes respectively. TR2 was one of the first identified orphan receptor and its cDNA was first cloned in 1989 from human testis libraries based on the strong homology of its DBD with steroid receptors. (C. Chang et al., 1989; C. S. Chang, Kokontis, & Liao, 1988). In 1994, TR4 was cloned from human and rat hypothalamus, prostate, and testes libraries (C. S. Chang et al., 1994). The mouse TR4 open reading frame (ORF) was cloned the same year from a mouse brain cDNA library and was originally named TR2R1 from its resemblance with TR2 (Law, Conneely, & O'Malley, 1994). The two receptors share a 65% identity in their overall structure, with 51% homology in the N-terminus, 82% homology in the DBD, and 65% homology in the ligand-binding domain (LBD) (S.-J. Lin et al., 2017). Although the TR2 DBD shows a certain degree (50%–54%) of homology with several other NRs such as AR, ER, PR, MR and GR, the LBD shows very low homology (<10%) with these same NRs (Y.-F. Lee, Lee, & Chang, 2002).

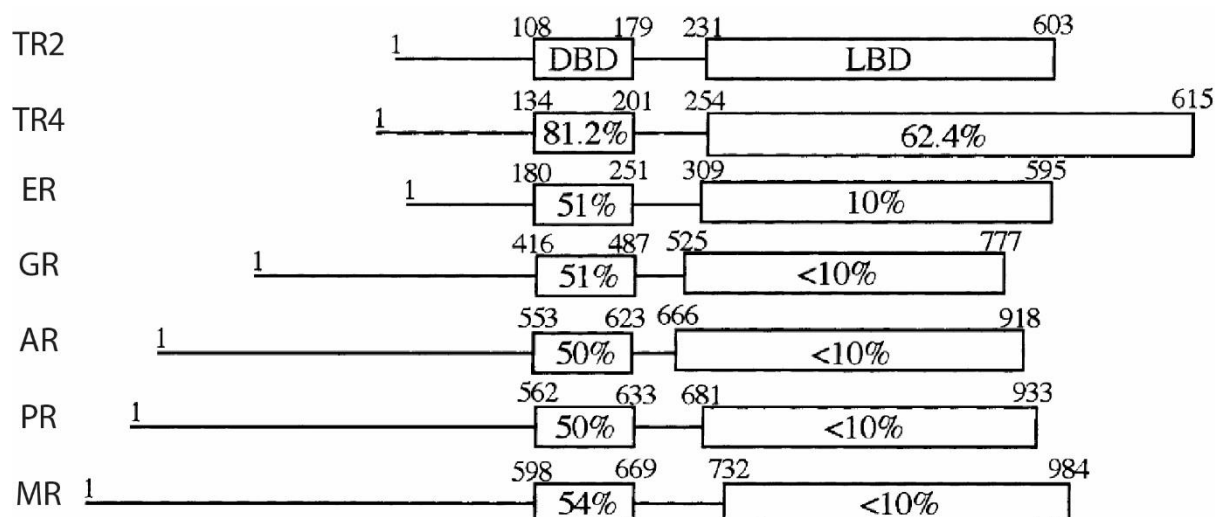


Figure 7: Sequence homology of the LBD and DBD of the human TR2, TR4 and the known steroid receptors.

Picture adapted from (Y.-F. Lee et al., 2002).

The structure of the DBD of TR4 shows high homology with TR2, RXR and COUP-TF/ARP-1. They all share the same type of direct repeat DR1 motifs (Chang et al., 1994). TR2 has four isoforms with calculated molecular weights of 53 (TR2-5), 21 (TR2-7), 51 (TR2-9), and 67 (TR2-11) kDa, while TR4's molecular weight is 67 kDa. TR2 is ubiquitously expressed but predominantly in the prostate, seminal vesicle, and testis. TR4 is expressed widely in the whole body including testis, prostate, ovary, cerebellum, and hippocampus (Bookout et al., 2006; Y.-F. Lee et al., 2002) and is regulated in a circadian rhythmic manner (Yang et al., 2006). TR2 is located on the chromosome 12q22 (D.-L. Lin, Wu, & Chang, 1998) whereas TR4 locates on the chromosome 3p24, which is close to the other NRs including TR β (3p22-24), RAR β (3p24), and PPAR γ (3p25) (Yoshikawa, DuPont, Leach, & Detera-Wadleigh, 1996).

TR2 and TR4 sequences are highly conserved between human and rodents. The DBD of the mouse TR2 shares 97,1% homology with the human while the LBD has 87,7% similarity. For the mouse TR4, the conservation reaches 98,5 and 97,2% respectively with the DBD and LBD of human TR4. The peptide sequence alignment of the two receptors in Figure 8 shows that the overall homology reaches 62% between the two receptors. Notably, the DBD domain reaches 76,3% homology between the mouse TR2 and TR4 while the LBD has 71% conservation. The two zinc finger domains are almost identical with 91,1% homology for the first zinc finger and 80% for the second.

Score	Expect	Method	Identities	Positives	Gaps
725 bits(1872)	0.0	Compositional matrix adjust.	367/594(62%)	449/594(75%)	36/594(6%)
mTR2	15	QMGEIVTEQQTGQKIQIVTALDHSTQGKQ-FILANHEGSTPGKVFLTTPDAAGVNQLFFT			73
mTR4	21	Q +IVT+QQTGQKIQIVTA+D S KQ FIL + +G+ GKV L +P+ + QL FT			80
mTR2	74	SPDLSAP-HLQLLTE-----KSPDQGPNKVFDLCVVCGDKASGRHYGAITCEGCKG			123
mTR4	81	+ D P +Q++T+ K+ Q P +V + CVVCGDKASGRHYGA++CEGCKG			139
mTR2	124	TSDNLVPGRIQIVTDSASVERLLGKADVQRP-QVEYCVVCGDKASGRHYGAVSCEGCKG			183
mTR4	140	FFKRSIRKNLVYSCRGSKDCVINKHHRNRCQYCR LQRCIAFGMKQDSVQCERKPIEVSRE			199
mTR2	184	FFKRS+RKNL YSCR S+DC+INKHHRNRCQ+CR L++C+ GMK +SVQ ERKP +V RE			243
mTR4	200	FFKRSVRKNLTYSCRSSODCIINKHHRNRCQFCRLKKCLEMGMKMEVQSERKPFQVRE			259
mTR2	244	KSSNCAASTEKIYIRKDLRSPLAATPTFVTDSETARSAGLLDSGMFVNIHPSGIKTEPAM			302
mTR4	260	K SNCAASTEKIYIRKDLRSP L ATPTFV D + AR GLLD GM VNI I+ + +			302
mTR2	244	LMAPD-KAESCQDLSTLASVVTSLANL GKAKDL SHCGGDMPVVQSLRNGDTSFGAFHHD			302
mTR4	260	L+A D KAE+ QG L TLA+VVTSLANL +SL NGD S +			302
mTR2	303	LLAADSKAETSQALGTLANVVTSLANLS-----ESLNNGDAS--EMQPE			302
mTR2	303	IQTNGDVSRAFDTLAKALTPGESSACQSP E GME --- GSPHLIAGEPS--FVEKEGPLL			356
mTR4	303	Q+ +++RAFDTLAKAL +S++ S +G++ GS H+I+ + S +E EGPLL			362
mTR2	357	DQSASEITRAFDTLAKALNTTDSASPPSLADGIDASGG GSIHVISRDOSTPIIEVEGPLL			362
mTR2	357	SESHVAFRLTMPSPMPEYLVNHYIGESASRLLF LSMHWALSIPSFQALGQENSISLVKAY			416
mTR4	363	S++HV F+LTMPSPMPEYLVNHYI ESASRLLF LSMHWA SIP+FQALGQ+ + SLV+A			422
mTR2	417	SDTHVTFKL TMPSPMPEYLVNHYICESASRLLF LSMHWARSIPAFQALGQDCNTSLVRAC			422
mTR2	417	WNELFTLGLAQCWQVMNVATILATFVNCLHSSLQQDKMSPERRKSLMEHIFKLQEFNCNM			476
mTR4	423	WNELFTLGLAQ C QVM+++TILA VN L +S+Q+DK+S +R K +MEHI+KLQEFNCNM			482
mTR2	477	WNELFTLGLAQCAQVMSLSTILAAI VNH LQNSIQEDKLSGDR I KQVMEHIWKLQEFNCNM			482
mTR2	477	VKLCIDGHEYAYLKAIVLFSPDHPGLENMELIERFQEKAYVEFQDYITRTYPDDTYRLSR			536
mTR4	483	KL IDG+EYAYLKAIVLFSPDHPGL IE+FQEKA +E QDY+ +TY +DTYRL+R			542
mTR2	537	AKLDIDGHEYAYLKAIVLFSPDHPGLTGTSQIEKFQEKAQMELODYVQKTYSEDTYRLAR			542
mTR2	537	LLLRLPALRLMNATITEELFFKGLIGNVRIDSVIPHILKMEPADYNSQIIGHSL			590
mTR4	543	+L+RLPALRLM++ ITEELFF GLIGNV IDS+IP+ILKME A+YN QI G SL			596
mTR4	543	ILVRLPALRLMSSNITEELFF TGLIGNV SIDSIIPIYILKME TAEYNGQITGASL			596

DBD	76,3% identity (58/76)	Zn Finger I	90,5% identity (19/21)
LBD	71% identity (174/245)	Zn Finger II	80% identity (16/20)

Figure 8: Sequence homology of the peptide composition of the mouse TR2 and TR4 proteins.

The mouse TR2 and TR4 proteins have an overall 62% homology. The DBD is similar at 76,3% between the two receptors with 58 identities out of 76 amino acids. The two zinc fingers reach a 90,5 and 80% homology respectively. The LBD has a 71% identity between the two receptors.

1.2.3 TR2/4 as potential regulators of glucose and lipid metabolism

TR2 and TR4 total knockout mice have been generated and are viable. Interestingly, TR2 -/- TR4 -/- dKO mice die during early embryogenesis due to a loss of differentiation and self-renewal from embryonic stem cells (Shyr et al., 2009). This finding suggests that TR2 and 4 have redundant functions and can partially compensate for each other. For example, TR2 and 4 are involved in erythroid cell maturation and embryonic and fetal globin repression in definitive erythroid cell (Tanabe et al., 2002). Also, forced expression of TR2 and 4 in sickle

cell disease (SCD) mouse models has proven to be beneficial for the production of fetal hemoglobin in the mature erythroid cells and the reduction of hemolysis and SCD complications (Campbell et al., 2011).

Reports on the mechanism of action of TR2 and TR4 show that they can work as homodimers or heterodimerize with each other (Tanabe et al., 2002). Depending on the tissue and the context, they were shown to act as transcriptional activators (metabolic organs) or repressors (blood cells). In erythroid cells, they were shown to be part of the direct repeat erythroid-definitive (DRED) repressing complex. To analyse the binding pattern of TR4 and its potential tissue specific functions, ChIP-Sequencing (ChIP-Seq) analysis for TR4 have been performed in four human cell lines : erythroleukemia cells (K562), liver carcinoma (HepG2), cervical carcinoma (HeLa) and immortalized lymphoblastoma cells (GM12878) (Greene et al., 1986; O'Geen et al., 2010). Interestingly, the majority of the binding sites for TR4 in all cell lines were mapped in the promoter region, near the transcription start site (TSS) of the closest gene (+/- 1kb). While blood cells (K562, HeLa, GM12878) shared most of their binding sites with each other, HepG2 cells showed many unique binding sites, suggesting a lineage and organ specific functions. Motifs analysis of the TR4 binding sites found DR1 elements only in a minority of cases, suggesting that TR4 associates with some partners such as ETS factors like ELK4 which have abundant binding sites in the TSS region. The common binding sites were associated with genes involved in fundamental biological functions such as RNA metabolism and protein translation. In addition, TR4 seems to regulate other functions in HepG2 cells and be involved in lipid and glucose metabolism.

On top of their common targets, TR2 and 4 have specific functions. Indeed, while TR2 *-/-* mice show abnormalities in retinal development (Olivares et al., 2017), TR4 *-/-* mice display a complex phenotype involving multiple biological systems. TR4 *-/-* mice show impaired fertility of both male and female (L.-M. Chen et al., 2008; Mu et al., 2004), impaired osteogenesis and reduced body size (S.-J. Lin et al., 2012) and impaired cerebellar development and locomotor activity (Y.-T. Chen, Collins, Uno, & Chang, 2005).

Furthermore, TR4 *-/-* mice have been characterized after a dietary challenge. Interestingly, after 12 weeks of HFD, those mice show reduced body weight and fat accumulation as well as lower blood glucose and an improved insulin sensitivity (Kang et al., 2011), implying a direct role of TR4 in metabolism. Loss of TR4 has also been shown to be beneficial against atherosclerosis. In macrophages, studies from Xie et al. suggest that TR4 could act as a lipid sensor that modulates foam cell formation by activating directly the expression of *Cd36* and promoting cardiovascular diseases.

Overall, the current knowledge on TR2 and TR4 suggests a functional redundancy between the two receptors and an important role in metabolism. The mechanism of action of these receptors shows overlap of function but the exact gene programs and tissue-specific functions of these receptors in the control of metabolism have not yet been explored.

2. Scope of the thesis

The hypothesis of this PhD thesis was that the orphan nuclear receptors TR2 and TR4 are involved in the pathophysiology of obesity, insulin resistance and NAFLD by regulating adipose tissue and hepatic metabolic programs. To explore the functions of these two orphan receptors, the main aims for this project were :

1. Characterize liver and adipose tissue-specific TR2/4 double knockout mice and liver-specific TR4 overexpressing mice after a nutritional challenge

The functions of TR2 and TR4 in adipose tissue and liver metabolism have not been characterized yet. Adipose tissue specific TR2-4 double knockout (dKO) mice were challenged with HFD to study their response to obesity and insulin resistance. Liver-specific gain and loss of function mice were challenged with HFD or a profibrotic diet (DIAMOND) to study the role of these two receptors in the progression of NAFLD. Liver-specific gain and loss of functions validate a role for TR4 as a driver of hepatic fibrosis.

2. Identify the tissue specific transcriptional program of TR2/4 in response to HFD

To explore the transcriptional program underlying the changes in the response to HFD in our mouse models, ChIP-Sequencing for TR2 and TR4 and RNA-Sequencing were performed to correlate the phenotypic features of our models with gene expression. Combining both methods led to the identification of direct target genes regulated by TR2 and TR4 in response to a dietary challenge.

3. Determine the downstream impact of TR2/4 transcriptional regulation on metabolite composition

To determine the output of the key metabolic enzymes regulated by TR2 and TR4 and bridge it with the NAFLD progression, metabolomic analysis were performed to identify the different classes and species of metabolites that are dependent on TR2 and TR4 activity.

The overall scope of this PhD project was to analyze the physiological and molecular functions of the two orphan receptors TR2 and TR4 in important metabolic organs. These discoveries will open potential drug development for metabolic syndrome by targeting these two receptors.

3. Materials and Methods

3.1 Chemicals, commercial kits, antibodies and primers

Table 1: List of chemicals and reagents.

Chemicals and reagents	Company/provider
Agarose	VWR Chemicals
Bovine serum albumin	Sigma Aldrich
Bradford reagent	Carl Roth GmbH
Chelex	Sigma Aldrich
Complete Mini protease inhibitor	Roche Applied Science
D-(-)-Fructose powder	Sigma Aldrich
D-(+)-Glucose powder	Sigma Aldrich
45% D-(+)-Glucose solution	Sigma Aldrich
dNTP	Thermo Fisher Scientific GmbH
Dynabeads M-280 sheep anti-rabbit IgG-10	Life Technologies GmbH
Dithiothreitol	Serva Electrophoresis GmbH
EDTA	G-Biosciences
Eosin Y	Sigma Aldrich
Eukitt quick hardening mounting medium	Sigma Aldrich
Ethanol	AppliChem GmbH
Formaldehyde (w/v)	Thermo Fisher Scientific GmbH
Formaline	Sigma Aldrich
Glycerol	Carl Roth GmbH
Glycine	Sigma Aldrich
GoTaq Green DNA Polymerase	Promega
Hematoxylin Gill no.3	Sigma Aldrich
HEPES buffer	Carl Roth GmbH
HRP western substrate	Merck Millipore
Igepal (NP-40)	Sigma Aldrich
Insulin	Novo Nordisk Pharma
Magnesium chloride	Carl Roth GmbH
Methanol	Sigma Aldrich
Milk powder	Carl Roth GmbH
Igepal (NP-40)	Sigma Aldrich
Paraformaldehyde	Sigma Aldrich
Penicilin/Streptomycin	Sigma Aldrich
Phosphate-buffered saline (PBS)	Thermo Fisher Scientific GmbH
Phosphatase inhibitor	Thermo Fisher Scientific GmbH
Physiological saline (0.9%)	B-Braun group
Picric acid solution (saturated 1,3%)	Sigma
Potassium chloride	Carl Roth GmbH
Potassium hydroxide	Carl Roth GmbH

Power SYBR Green Master mix	Thermo Fisher Scientific GmbH
Protein G-coupled Dynabeads	Life Technologies GmbH
Proteinase K	Sigma Aldrich
QIAzol Lysis reagent	Qiagen
Rnase A (DNase-free)	AppliChem GmbH
Sepharose protein A/G beads	Biomol GmbH
Sirius Direct Red 80	Sigma Aldrich
0,9% Sodium chloride solution	Sigma Aldrich
Sodium dodecyl sulfate (20%)	Sigma Aldrich
Sodium pyruvate	Sigma Aldrich
Triton-X	AppliChem GmbH
Tween-20	AppliChem GmbH
Xylene	AppliChem GmbH

Table 2: List of commercial kits.

Kits	Company/provider
Ambion DNase Treatment and Removal Kit	Life Technologies GmbH
High Sensitivity DNA Kit	Agilent Technologies
Lab Assay Triglycerides Colorimetric Assay	Wako Chemicals
MinElute PCR Purification Kit	Qiagen
QuantiTect Reverse Transcription Kit	Qiagen
QUBIT dsDNA HS kit	Thermo Fisher Scientific GmbH
RNeasy Extraction Mini Kit	Qiagen
RNA 6000Nano Reagents	Agilent Technologies
KAPA Hyperprep Kit	Kapa Biosystems
KAPA Library Quantification Kit	Kapa Biosystems

Table 3: List of primary and secondary antibodies.

Antibody name	Reference	Provider
rabbit anti-TR2	ab83278	Abcam
rabbit anti-TR4	HPA006313	Sigma
goat anti-TR2 antibody	sc-8617	Santa Cruz
donkey anti-goat HRP-conjugated IgG2a	sc-2033	Santa Cruz
donkey anti-rabbit HRP-conjugated IgG2a	sc-2317	Santa Cruz
rabbit IgG	2729	Cell Signalling Technology

Table 4: Primer sequences for qRT-PCR.

Gene name	Forward primer	Reverse primer
m36B4	AGCGGTTTTGCTTTTTTCATC	TATGGGATTCGGTCTCTTCG
mNr2c1	ATCGTGACAGCACTTGACCA	AATGACGCCCTGATGCTTTG

mNr2c2	GGATCCAGATCGTCACGGATT	TTCACAACCTGACAGCCCCAT
mCwc15	TGAGTGGAAACCCCTCCTCTAAA	CTTGTGAAATTCAGATCGCAGTG
mFam114a2	AGTGTCCACCCGGAAAAGAC	TACAGCCAGTGAAACCTGAGC
mRomo1	CCTTCTCCTGTCTCAGGATCG	GGCCATGAAAGTGCCAAACG
mRps6kc1	GGTTACCGCACGGGTTGTT	TCAATCACCGTCTTGTCTGAAC
mGstp1	CGGCAAATATGTCACCCCTCAT	CAGCAGGTCCAGCAAGTTGT
mGstp2	AGCACTTGATCCCCACTTCT	GTAACCACCTCCTCCTTCCAG
mAkr1c14	GTGTGGTACTAAACGATGGTCAC	CAAATAAGCGGAGTCAAATGGC
mAkr1d1	AAGACAGCTATTGATGAGGGGT	CCTCTTTACCTTCCCTTCTGCTA
mSlc27a5	TCTATGGCCTAAAGTTCAGGCG	CTTGCCGCTCTAAAGCATCC
mFga	CACCTGCCTCATCTTGAGCG	GCATTGACTCTGATGTCTCTCCA
mFgg	GCTGCCTGCTTTTACTGTTCT	GGAAATCTGCGATACCACAGGT
mCdkn1a	CCTGGTGATGTCCGACCTG	CCATGAGCGCATCGCAATC
mMmp2	ACCTGAACACTTTCTATGGCTG	CTTCCGCATGGTCTCGATG
mCol4a1	CCTGGCACAAAAGGGACGA	ACGTGGCCGAGAATTTACC
mMmp1	GCTCATGCTTTTCTGCCAGG	TAGAATGGGAGAGTCCAAGGG
mCyp2b9	ACCAGGACCCCATCCTCTAC	TTTCTTGAAGCTGAATGAAACT
mCyp8b1	TGCAAAGAAGTGGTGCTCAA	CGAACCTTTAGGCCCTAGCAT

Table 5: Primer sequences for ChIP-qPCR.

Gene name	Forward primer	Reverse primer
mFoxl2	GCTGGCAGAATAGCATCCG	TGATGAAGCACTCGTTGAGGC
mCwc15	CCCTAGGCAACGTCATTCCAT	GCTGTGGAGAAGATGGCAAC
mRps6kc1	GCTAGGGCGTAGTAACCACA	GATCTGCTTCCGGATCACCA
mFam114a2	CAGTTTGTGTCCCGGATCGT	AGAGGTGAGTGAATCCGCTG

3.2 Animal experiments

3.2.1 Transgenic mouse lines

All animal procedures were approved by the relevant authorities - regional animal welfare committee of the state of Bavaria (2532-Vet-02-1980 and 1943) - in accordance with Helmholtz Zentrum München – Deutsches Forschungszentrum für Gesundheit und Umwelt (HMGU) guidelines for the care and use of animals. All mice were bred on a C57BL/6 background.

Liver and adipose tissue-specific double knockout mice

Nr2c1 floxed (*Nr2c1^{fl/fl}*) and *Nr2c2* floxed (*Nr2c2^{fl/fl}*) targeting vectors were previously generated and provided by Eucomm (Fig. 9A-B). Embryonic stem cell injection was performed to generate *Nr2c1^{fl/fl}* mice and *Nr2c2^{fl/fl}* mice. LoxP sites flanking exon 4 of *Nr2c1* and exon 5 of *Nr2c2* were

inserted to target the structure of the DNA binding domain of both proteins. After Cre-mediated recombination, exon 4 and exon 5 are excised in the *Nr2c1* and *Nr2c2* genes respectively. The two lines were bred together to generate mice with floxed exons for *Nr2c1* and *Nr2c2* (*Nr2c1^{fl/fl}*-*Nr2c2^{fl/fl}* mice). *Nr2c1^{fl/fl}*-*Nr2c2^{fl/fl}* mice were bred to Albumin (Alb)-Cre mice obtained from JAX (B6.Cg-Tg(Albcre)21Mgn/J) to generate hepatocyte-specific TR2-TR4 double knockout (L-dKO) mice. Adiponectin-Cre (AdipoQ-Cre) mice were bred to *Nr2c1^{fl/fl}*-*Nr2c2^{fl/fl}* mice to generate adipocyte specific TR2-TR4 double knockout (A-dKO) mice. In all groups, Cre-recombinase negative littermates served as controls.

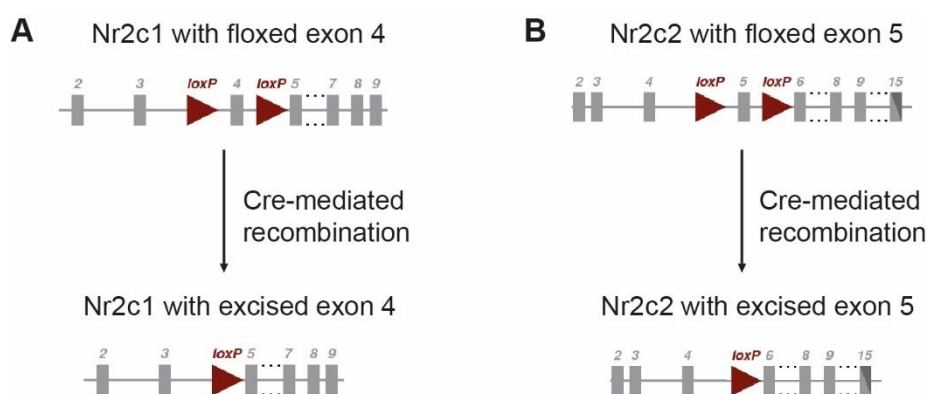


Figure 9: Recombination strategy on *Nr2c1* and *Nr2c2* genes using Cre-LoxP system.

A: Graphical representation of the *Nr2c1* gene with floxed exon 4 generated by Eucomm. After Cre-mediated recombination, exon 4 of *Nr2c1* is excised. B: Graphical representation of the *Nr2c2* gene with floxed exon 5 generated by Eucomm. After Cre-mediated recombination, exon 5 of *Nr2c2* is excised.

Liver-specific TR4 overexpressing mice

We generated HPRT-TR4 mice by inserting a conditional TR4 expressing construct under a CAG promoter in the HPRT locus (Figure 10). The targeting vectors contained a 2.2-kbp *HPRT* 5'-homology region, followed by the ubiquitously expressed CMV early enhancer/chicken β -actin (CAG) promoter, the conditional expression cassette (mouse *Nr2c2* ORF-flag-2A-Venus), and a 5.1-kbp *HPRT* 3'-homology region. The ORF of 3' flag-tagged mouse *Nr2c2* (~1.8kb) was first subcloned 5' to a viral (*Thosea Asigna*) 2A-Venus fusion reporter protein, and then shuttled as 5'-*Swal*-ORF-2A-Venus-*MluI*-3' fragment into the *MluI* and *Swal* sites of the targeting vector. This resulted in a reverse orientation of the ORF, relative to the CAG promoter, avoiding "leaky" expression. After cre-mediated "flipping" and excision events between pairs of *loxP* and *loxM* sequences, the ORF locates in sense direction, directly

downstream of the CAG promoter. The targeting vector was verified by sequencing before linearization and electroporation into *Hprt*-positive SV129 ES cells.

HPRT-TR4 mice were bred to Albumin (Alb)-Cre mice obtained from JAX (B6.Cg-Tg(Albcre)21Mgn/J) to generate hepatocyte-specific TR4 over-expressing mice (L-TR4OE). In all groups, Alb-Cre negative littermates served as controls.

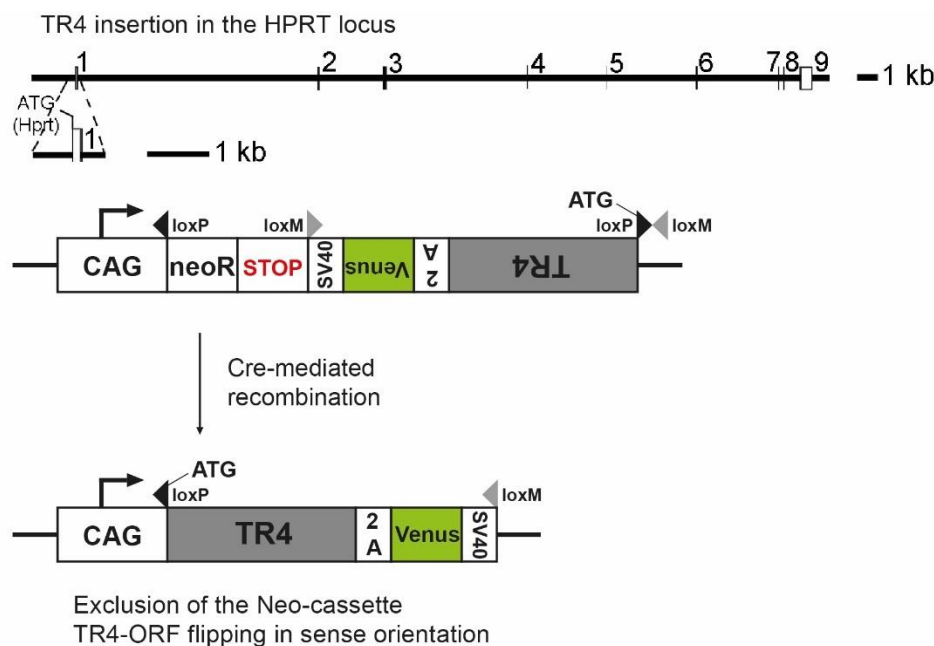


Figure 10: Insertion and recombination strategy of the TR4 sequence under a CAG promoter.

Graphical representation of the targeting vector containing the *Nr2c2* ORF in reverse orientation, coding for the mouse TR4 protein, separated from the CAG promoter by a Neo-cassette and a STOP codon. After Cre-mediated recombination, the Neo-cassette and the STOP codon are excluded and the TR4 ORF sequence is flipped in sense orientation directly downstream of the CAG promoter.

3.2.2 Housing and diets

Mice were housed in a controlled specific-pathogen-free (SPF) facility with a 12 h dark/light cycle in groups of 4 animals per cage. The cages were individually ventilated, and the room was kept at 23°C with constant humidity. After weaning, mice were fed *ad libitum* with a regular chow diet (Altromin GmbH, 1318M diet) until adulthood (12 weeks old).

To induce metabolic syndrome in mouse models, mice were fed with a high fat diet (HFD; 58% kcal fat, Research Diets D12331) for 12 weeks for L-dKO mice and L-TR4OE mice and up to 20 weeks for A-dKO mice.

The Diet Induced Animal Model Of Non-alcoholic fatty liver Disease (DIAMOND) was used to generate western diet-induced liver fibrosis in L-dKO and L-TR4OE mice (Asgharpour et al., 2016). This model consists in the combination of a high fat high carbohydrate diet containing 42% cal from fat and enriched with 0,1% cholesterol (Harlan TD.88137) and drinking water supplemented with 18,9g/L of D-Glucose (G8270, Sigma) and 23,1 g/L of D-Fructose (F0172, Sigma) for 26 weeks.

3.2.3 Animal sacrifice and organ withdrawal

Mice were sacrificed by cervical dislocation at ZT8 and blood was collected from the carotids. Livers and adipose tissues were quickly collected and snap-frozen in liquid nitrogen then stored at -80 °C before further processing. Serum was obtained from coagulated blood after centrifugation at 1500 g for 10 min and stored at -80 °C. Frozen livers were manually crushed into powder using liquid nitrogen cooled mortar and pestle.

3.2.4 Genotyping

Genotyping of A-dKO, L-dKO and L-TR4OE mice was performed on DNA extracted from the skin collected during ear tagging at weaning. Ear punches were digested in 200 µL of 50 mM NaOH solution for 30 min at 95°C and neutralized with 15 µL of 75 mM TRIS. 1µl of this DNA was used as template for the genotyping PCR. The PCR reaction mix contained 12.5 µl GoTaq Green DNA polymerase master mix (Promega), 40 mM MgCl₂ (Carl Roth GmbH), 0.2 µM of each primer and was filled up to 25 µL with H₂O. Table 6 describes the PCR reaction, which was used for all genotyping procedures. Primers were produced by Eurofins Genomics. All PCR products were separated on a 2% agarose gel (VWR Chemicals) and detected with a UV detection chamber (Benchtop 2UV Transilluminator and GelDoc-It TS Imaging System, UVP).

Table 6: Genotyping PCR reaction.

Step	Temperature (°C)	Duration	Cycles
Initiation	95	5 min	1
Denaturation	95	1 min	} 35
Primer annealing	60	1 min	
Elongation	72	1 min	
Final elongation	72	10 min	1

For the A-dKO and L-dKO mouse line, two primer pairs were used to genotype the two LoxP sites surrounding exon 4 of Nr2c1 and exon 5 of Nr2c2 genes:

Nr2c1_Lox1_Fw: TGCCTGAACTAGTCTTACCC

Nr2c1_Lox1_Rv: ACATACCAAACCCCAACTGG

Nr2c1_Lox2_Fw: TAAGACTTTACCTTTCTCTGG

Nr2c1_Lox2_Rv: CAATTCATTTTTCAATGATTCC

Nr2c2_Lox1_Fw: AGTTGTTTTCTCCTAGATGG

Nr2c2_Lox1_Rv: ACCCAGACTTTCCTGATTGG

Nr2c2_Lox2_Fw: TGTTCCAATTGTTTATATGC

Nr2c2_Lox2_Rv: CATAGAAGCTTATCACACAGG

For all reactions, the wildtype (WT) allele makes a product of 150 bp and the floxed allele gives a product of 260 bp, showing the insertion of the LoxP site sequence.

For the L-TR4-OE mouse line, the PCR for the insertion of the TR4 construct in the HPRT locus was detected with the following primer pair:

HprtTR4_Fw: GGATGACGACGATAAGGGCG

HprtTR4_Rv: GCTGAACTTGTGGCCGTTTA

The wildtype allele does not amplify any product whereas the allele with TR4 insertion shows a product of 100 bp.

The Alb-Cre recombinase genotyping was performed with 3 primers in the L-TR2-4-dKO and L-TR4OE mice:

AlbCre_wt_Fw: GTTGTCTTTGTGCTGCTGA

AlbCre_mut_Fw: GAAGCAGAAGCTTAGGAAGATGG

AlbCre_wt_Rv: CCTGCCAGCCATGGATATAA

The wildtype allele shows a 500 bp product whereas the Alb-Cre positive locus amplifies two bands of 400 and 750 bp.

The AdipoQ-Cre recombinase genotyping was performed with the following two primers in the A-dKO:

AdipoQCre_Fw: GCATTACCGGTCGATGCA ACGAGTGATGAG

AdipoQCre_Rv: GAGTGAACGAACCTGGTCGAAATCAGTGCG

The wildtype allele shows a faint 450 bp product whereas the Alb-Cre positive locus shows an intense 450 bp band.

3.2.5 Glucose tolerance test

For a GTT, mice were fasted for 16 hours overnight with free access to water. Glucose (45% D-glucose; Sigma Aldrich) was administered by intraperitoneal injection at a rate of 2g/kg dissolved in sterile physiological 0,9% NaCl (B. Braun) and the injection volume was calculated based on the fasted body weight of each mouse. Blood glucose levels were sampled from the tail vein using a handheld glucometer (AccuCheck Aviva, Roche Diagnostics). Blood glucose was measured prior to injection (time = 0) and at time = 15, 30, 60, 90 and 120 min after intraperitoneal injection.

3.2.6 Insulin tolerance test

For an ITT, mice were fasted for 5 hours during the light phase with free access to drinking water. Fresh insulin solution was prepared by diluting the 100 U/mL insulin (Sigma) in 0,9% NaCl sterile physiological serum (B. Braun). Mice fed on chow diet received an intra-peritoneal injection equivalent to 0,75 U/kg of insulin (Insulin Novorapid, Novo Nordisk Pharma) whereas high-fat diet mice were injected with a volume corresponding to 1,5 U/kg. Blood glucose levels were sampled from the tail vein using a handheld glucometer (AccuCheck Aviva, Roche Diagnostics). Blood glucose was measured prior to injection (time = 0) and at time = 15, 30, 60, 90 and 120 min after intraperitoneal injection.

3.2.7 Pyruvate tolerance test

For a PTT, mice were fasted for 5 hours during the light phase. Sodium pyruvate (P5280, Sigma Aldrich) was dissolved in sterile physiological 0,9% NaCl and administered by intraperitoneal injection at 2g/kg. The injection volume was calculated based on the fasted body weight of each mouse. Blood glucose levels were determined from the tail vein using a handheld glucometer (AccuCheck Aviva, Roche Diagnostics). Blood glucose was measured prior to injection (time = 0) and at time = 15, 30, 60, 90 and 120 min after intraperitoneal injection.

3.2.8 Body fat composition using Echo-MRI

Body composition in fat and lean mass was measured using quantitative nuclear magnetic resonance technology (EchoMRI 900, Echo Medical Systems, Houston, USA) after HFD feeding. For the measurement, each mouse was placed in a cylindrical holder without anesthesia inside the machine for approximately 1 min.

3.2.9 Indirect calorimetry, food intake and locomotor activity

Mice were single-housed for one week prior to the experiment and placed in the calorimetric cages (Labmaster, TSE Systems GmbH, Bad Homburg, Germany) for one week. The first two days were used for acclimation and the actual measurements were carried on for 5 days. Oxygen consumption (VO_2), carbon dioxide production (VCO_2), energy expenditure (EE), locomotor activity and food intake were measured every 15 minutes for each mouse over the course of the experiment. Respiratory exchange ratio ($RER = VCO_2/VO_2$) was calculated to determine the preferential energy substrate over time and the overall contribution of lipids and carbohydrates in the energy production. A RER of 1 indicates exclusive glucose consumption whereas a value of 0,7 corresponds to exclusive lipid oxidation. EE was calculated following Weir's equation that connects ATP consumption and gaseous exchanges (Weir, 1949). Access to food and water was *ad libitum* for the whole experiment. Food intake was measured with automated sensors connected to the food dispensers calibrated before the start of the experiment. Locomotor activity was measured using a three-dimensional automated infrared beam grid surrounding each cage.

3.3 Molecular biology techniques

3.3.1 RNA isolation from tissue

Livers and adipose tissues were harvested as described in 3.2.3 and 25-50 mg of frozen tissue was used for extraction. For liver tissue, total RNA from tissue was isolated using the RNeasy Mini kit (Qiagen) according to manufacturer's instructions. For adipose tissues, RNA was extracted using the QIAzol lysis reagent (Qiagen) according to the manufacturer's instructions.

3.3.2 cDNA synthesis

Total RNA from tissue was reverse transcribed into cDNA (complementary DNA) with the

QuantiTect Reverse Transcription Kit (Qiagen) according to manufacturer's instructions. The total amount of RNA used for reverse-transcription was 1 µg.

3.3.3 Real-time quantitative polymerase chain reaction

Real-time quantitative polymerase chain reaction (RT-qPCR) was performed using Power SYBR Green Master Mix (Life Technologies GmbH) in a ViiA 7 Real-Time PCR System (Thermo Fischer Scientific GmbH). The qPCR reaction contained 5 µl SYBR Green Master Mix, 0.8 µl H₂O, 0.2 µl primer mix (1 µM) and 4 µl of diluted cDNA. Each sample was run as a technical triplicate in a 384-well plate format. The relative expression levels of each gene were normalized to the housekeeping gene *U36b4*. RT-qPCR primers were produced by Eurofins and are listed in Table 4.

3.3.4 Nuclear protein extraction from liver

Complete cell lysis of 100mg of liver tissue was performed using a tissue lyser (Qiagen) for 2 minutes at 30 Hz with 5mm steel beads (Qiagen) in cold cell lysis buffer (10 mM Hepes-KOH at pH 7.9, 1.5 mM MgCl₂, 10 mM KCl, 0.5 mM DTT, 0.15% NP-40) containing complete mini protease inhibitors (Roche Applied Science) and phosphatase inhibitors (Thermo Fisher Scientific).

Cytosolic and nuclear fractions were separated by centrifugation for 20 min at 2700g at 4°C and the nuclear fraction was washed once with PBS. Nuclear lysis was performed in nuclear lysis buffer (420 mM NaCl, 20 mM Hepes-KOH at H 7.9, 2 mM MgCl₂, 0.2 mM EDTA, 0.5 mM DTT, 0.1% NP-40, 20% glycerol, complete protease and phosphatase inhibitors) and passed through an insulin syringe for complete lysis. After incubation for 1 h at 4°C with rotation, nuclear extracts were obtained by centrifugation at 21000 g for 45min. Protein concentration was measured by using Bradford reagent (Bio Rad) according to manufacturer's instructions.

3.3.5 Western Blot analysis

Western blots (WB) for nuclear localization of TR2 and TR4 were performed using nuclear extracts of livers from WT, L-TR2/4-dKO and L-TR4-OE mice. For each sample, 10 µg of nuclear protein extracts were diluted in Laemmli buffer and boiled for 5 min at 95°C before loading and separation on a 4-12% Bis-Tris gel (Invitrogen). After transfer to a PDVF membrane (Merck Millipore), amido-black staining was performed to control for equal

balancing and transfer of all samples to be compared. Membranes were then blocked for 1 h at room temperature in 10% milk/TBS-T (50 mM Tris-Cl, 150 mM NaCl, pH 7.6 supplemented with 1% Tween20 (AppliChem GmbH)) and then incubated overnight at 4°C with either a rabbit anti-TR4 antibody (1:1000 in 10% milk/TBS-T; HPA006313, Sigma) or a goat anti-TR2 antibody (1:500 in 10% milk/TBS-T; sc-8617, Santa Cruz).

Membranes were washed with TBS-T and incubated for 1 h at room temperature with either a donkey anti-rabbit or a donkey anti-goat HRP-conjugated IgG2a secondary antibody (1:10000 in 10% Milk/TBS-T; sc-2317 and sc-2033, Santa Cruz) used to conjugate the primary anti-TR4 and anti-TR2 antibodies respectively. After TBS-T washes, peroxidase activity was measured using HRP Western substrate (Merck Millipore) and visualized using X-ray films (CEA X-ray) by chemiluminescence detection of proteins.

3.4 Tissue assays

3.4.1 Triglyceride measurement in serum and liver

Plasma and livers were collected as described in 3.2.3 and 100 mg of liver powder were used for lipid extraction. Liver samples were digested at 60°C for 6 hours in fresh alcoholic KOH consisting of 2/3 of 100% EtOH + 1/3 of 30% potassium hydroxide. Digested sample volume was measured and mixed with 1,08 volume of 1M MgCl₂ and incubated on ice for 10 min followed by centrifugation in a cold table-top centrifuge for 30 min at 14000 rpm for separation. The supernatant containing extracted lipids was transferred to a new tube. Triglycerides were measured in liver and serum samples by colorimetric assay (#290-63701, Wako Chemicals) according to the manufacturer's instructions.

3.4.2 Paraffin embedding of liver and adipose tissues

The right median lobe of livers and pieces of sub-cutaneous, visceral and brown inter-scapular adipose tissues were collected and immediately fixed in 10% formaline (Sigma-Aldrich) overnight at 4°C. Before dehydration, formaline-fixed tissues were washed 3 times with PBS pH 7,4 then placed in 70% EtOH overnight at 4°C. The next day, further dehydration was carried out by incubating the samples in increasing percentages of EtOH for 1 hour each (80%, 90% and 2 times 100%). To remove the ethanol from the tissue, the samples were incubated 3 times for 10 minutes in Xylene (AppliChem GmbH). Samples were placed in 3 successive melted paraffin baths at 65°C. The next day, the samples were embedded in paraffin blocks

using a paraffin embedding station (Leica EG1150). Liver and adipose tissues were cut with a microtome (Leica RM255) in 6 µm thick sections and dried overnight before staining.

3.4.3 Hematoxylin and Eosin staining

For hematoxylin and eosin (H&E) staining, slides were first deparaffinized in xylene and rehydrated through baths of decreasing concentration of ethanol (100%, 96%, 70%) and deionized water. Incubation with hematoxylin gill no.3 (GHS332, Sigma Aldrich) and eosin Y (HT110216, Sigma Aldrich) was performed for 30s-1min followed by rapid washes in tap water. Stained slides were quickly dehydrated again in increasing concentrations of ethanol and cleared in xylene. Stained slides were mounted with quick-hardening mounting medium (03989, Sigma Aldrich). Brightfield capturing was performed with a Nikon Eclipse Ci-L microscope.

3.4.4 Sirius Red staining

The Sirius Red staining solution was obtained by dissolving Sirius Direct Red 80 (365548, Sigma Aldrich) in saturated 1,3% saturated picric acid solution (P6744, Sigma). Slides were first deparaffinized in xylene and rehydrated as described in 3.4.3 then stained in the Sirius red solution for one hour. Stained slides were quickly dehydrated and cleared in xylene. Stained slides were mounted in quick-hardening mounting medium (03989, Sigma Aldrich). Brightfield capturing was performed with a Nikon Eclipse Ci-L microscope.

3.5 Next generation sequencing techniques

3.5.1 ChIP-Sequencing

The protocol for ChIP-Seq was performed using described methods in (Mir et al., 2019). For pellet preparation, 200 mg of frozen liver tissue was homogenized in lysis buffer (10mM Hepes-KOH, 10mM KCl, 5mM MgCl₂, 0.5mM DTT) containing complete proteinase inhibitors (Roche Applied Science) using a TissueLyser (Qiagen) at 30 Hz for 2 min with 5 mm steel beads. Lysates were passed through a 70 µm cell strainer (Falcon) and cross-linked in 1% formaldehyde for 15 min followed by quenching with 0.2M glycine solution for 5 min and final washing with PBS.

Pellets were resuspended three times with IP buffer (150 mM NaCl, 5 mM EDTA at pH 7.5, 5 mM Tris at pH 7.5, 1% Triton X-100, 0.5% NP40, complete protease inhibitors) and

passed through a 24G syringe. The chromatin was sonicated in shearing buffer (50 mM Tris at pH8, 10 mM EDTA at pH8, 1% SDS, complete mini protease inhibitors) into 0.1-1kb DNA fragments using a Bioruptor (Diagenode). Sonicated chromatin was centrifuged at 12.000 rpm at 4°C for 10 min. Chromatin immunoprecipitation (IP) was set up in dilution buffer (167 mM NaCl, 16.7 mM Tris at pH 8, 1.2 mM EDTA at pH 8, 1.1% Triton X-100, 0.01% SDS, complete mini protease inhibitors) overnight at 4°C with rotation.

For each IP, 8 µg of the following antibodies were used: rabbit anti-TR2 antibody (ab83278, Abcam), rabbit anti-TR4 antibody (HPA006313, Sigma). Sheared chromatin was kept as input control at -20°C overnight. The next day, chromatin was cleared by centrifugation at 3500 rpm for 20 min at 4°C. 90% of each IP samples were incubated with Dynabeads M-280 (Invitrogen) blocked overnight in 0,5% BSA for 6 h at 4°C with rotation. Coupled Dynabeads M-280 were washed six times with washing buffer (150 mM NaCl, 5 mM EDTA at pH 7.5, 5 mM Tris at pH 7.5, 1% Triton X-100, 0.5% NP40) and once with TE-Buffer. Elution of IP samples from the beads was performed with elution buffer (105 mM NaHCo3, 1% SDS in H₂O) for 15 min at 1000 rpm at room temperature. For DNA-protein decrosslinking, 200mM NaCl was added to the ChIPed chromatin as well as the input control and incubated at 65°C overnight. Next day, samples were treated with 0.05 µg of RNase A (AppliChem GmbH) at 37°C for 30 min followed by Proteinase K digestion (0.05 µg Proteinase K, 10mM EDTA at pH 8, 40 mM Tris at pH 7.5) for 2 hrs at 45°C. ChIP DNA and input were isolated with MinElute PCR Purification Kit (QIAGEN). DNA concentration was determined using QUBIT dsDNA HS kit (Thermo Fisher Scientific).

Libraries were prepared using the KAPA Hyperprep Kit (#KK8504, Kapa Biosystems). Illumina compatible adapters were synthesized by IDT (Integrated DNA Technologies) and used at a final concentration of 68nM. Size-selection (360-610bp) of adapter-ligated libraries was performed using 2% dye free gels (CDF2010, Sage Science) in a Pippin Gel size selection station (Sage Science). qPCR was performed to estimate library concentrations with the KAPA Library Quantification Kit (#KK4873, Kapa Biosystems). Library quality was verified using the Agilent High Sensitivity DNA Kit (Agilent) in a 2100 Bioanalyzer (Agilent).

3.5.2 ChIP qPCR

Sonication of chromatin and immunoprecipitation was performed as described in 2.5.1. For each IP, 3 µg of the following antibodies were used: rabbit IgG (2729, Cell Signalling Technologies), rabbit anti-TR2 antibody (ab83278, Abcam), rabbit anti-TR4 antibody (HPA006313, Sigma). Sheared chromatin was kept as input control and precipitated in 3

volumes of EtOH at -20°C overnight. The next day, chromatin was cleared by centrifugation at 12.000 rpm for 10 min at 4°C. 90% of each IP sample was incubated with 0.5% BSA-blocked Sepharose Protein A/G beads (Rockland Inc.) for 3 h at 4°C with rotation. Coupled Sepharose Protein A/G beads were washed four times with wash buffer (150 mM NaCl, 5 mM EDTA at pH 7.5, 5 mM Tris at pH 7.5, 1% Triton X-100, 0.5% NP40) by centrifugation at 500 rpm at 4°C. For isolation, 100 µl of 10% Chelex (Sigma Aldrich) was added to the washed sepharose beads and vortexed.

After boiling for 10 min, proteinase K is added, and the beads are incubated for 30 min at 55°C while shaking, followed by another round of boiling for 10 min. For elution, the bead suspension is centrifuged and the supernatant is collected twice after addition of another 100 µl water. Precipitated input was centrifuged at maximum speed for 10 min and the pellet was dried and processed the same way. The ChIPed DNA and input DNA was purified using the MinElute PCR purification kit according to manufacturer's instructions.

ChIP-DNA was diluted accordingly and served as template for qPCR using Power SYBR Green Master Mix (Life Technologies) in a ViiA 7 Real-Time PCR System (Thermo Fischer Scientific). Each sample was run in technical triplicates on a 384-well plate.

Fold enrichment was calculated over IgG using the raw Ct values: $(Ct\ IP) - (Ct\ IgG) = \text{double delta Ct}$ ($d\Delta Ct$) = $2^{-d\Delta Ct}$. This normalization method divides the ChIP signal by the mock-antibody signal, representing the ChIP signal as the fold increases relative to the background signal. Primers for ChIP qPCR are listed in Table 5.

3.5.3 RNA-Sequencing

RNA-Sequencing (RNA-Seq) was performed in liver samples. RNA was extracted using the RNeasy minikit (Qiagen) according to manufacturer's instructions. All samples for RNA-Sequencing were DNase-treated using the Ambion DNase I kit (Thermo Fisher Scientific) according to manufacturer's instructions. The quality of the RNA was verified using an Agilent 2100 Bioanalyzer with RNA 6000Nano Reagents (Agilent Technologies). Library preparation and rRNA depletion was performed using the Illumina TruSeq stranded/unstranded mRNA Library Prep Kit v2 chemistry in an automated system (Agilent Bravo liquid handling platform) starting with 1µg total RNA for each sample.

3.6 NGS data analysis

3.6.1 ChIP-Sequencing

Libraries were subjected to NGS on an Illumina HiSeq4000 in paired end mode. Reads were aligned to the mouse mm10 reference genome using BWA-MEM version 0.7.13 (H. Li & Durbin, 2010) and duplicates were removed using Picard Tools version 2.8.3 (<http://picard.sourceforge.net/>). Reads were filtered for uniquely mapped read pairs with samtools version 1.8 (H. Li et al., 2009) To visualize the tracks, mapped reads were converted to converted to bigwig files merging 10 bp per bin using bamCoverage from the Deeptools package version 3.0.2-1 (Nowlan, 2016) and visualized with IGB.

Peaks were called using MACS2 version 2.1.1.20160309 (FDR<0.05) (Yong Zhang et al., 2008). Called peaks for TR2 and TR4 were defined as overlapping if 50% of chromosomal peak position was intersecting. Gene Ontology analysis was performed with GREAT (McLean et al., 2010). Motif enrichment and read distribution analyses were conducted with HOMER version 4.0 (Heinz et al., 2010).

3.6.2 RNA-Sequencing

Libraries were sequenced on the Illumina HiSeq2500 or HiSeq4000. Sequencing quality was assessed with FastQC (<http://www.bioinformatics.babraham.ac.uk/projects/fastqc/>). Gene-level quantification was performed with Salmon version 0.10.2 (<https://combine-lab.github.io/salmon/>). Settings were: -libType A, -gcBias, -biasSpeedSamp 5 using the mm10 (GRCm38.p6) reference transcriptome provided by Ensembl. Gene count normalization and differential expression analysis was performed using DESeq2 (Love, Huber, & Anders, 2014). For gene annotation, biomaRt was used (Durinck, Spellman, Birney, & Huber, 2009). Functional enrichment according to gene ontology was carried out using Gorilla (Eden, Navon, Steinfeld, Lipson, & Yakhini, 2009).

3.6.3 Metabolite profiling, data processing and analysis

Metabolite profiling, peak identification, and curation were performed by Metabolon. Briefly, the non-targeted metabolic profiling platform used by Metabolon combines 3 independent platforms: UHPLC/MS/MS optimized for basic species, UHPLC/MS/MS optimized for acidic species, and GC/MS. The analysis of 100 mg of frozen liver tissue was performed from 7 L-

dKO mice and 5 L-TR4OE mice fed with HFD for 12 weeks and corresponding numbers of wildtype littermates.

The data were first normalized according to raw area counts and processed according to (S.-Y. Shin et al., 2014). Run day correction was performed for each metabolite by setting the run day medians equal to 1. We removed metabolites with more than 50% missing values and transformed data to log₁₀. Data points outside 4 times the standard deviation for each metabolite were considered as outliers and removed. Missing data were imputed by k-nearest-neighbor algorithm.

3.6.4 Statistical analysis

All tests were performed using statistical tools in Graph Prism 7 (GraphPad Software, San Diego, CA USA). For difference between two groups, unpaired two-tailed Student's t-test was performed. Differences between more than two groups were assessed by 2-way ANOVA followed by Bonferroni's multiple comparison test. All results are given as mean ± SEM unless otherwise specified. A p-value <0.05 was considered significant.

3.7 Contributions from collaborators

Evaluation and scoring of fibrosis in liver sections was performed by Dr. med. Carolin Mogler (Technische Universität München, Munich, Germany). Dr. Franziska Greulich performed NGS data analysis of ChIP-Seq and RNA-Seq samples (IDC, Helmholtz Zentrum München, Munich, Germany). Metabolomic statistical analysis were performed with the help of Dr. Dominik Lutter (IDO, Helmholtz Zentrum München, Munich, Germany) and Dr. Kenneth Allen Dyar (IDC, Helmholtz Zentrum München, Munich, Germany). Dr. Kenneth Allen Dyar was also involved in generating the genetically modified mice.

4. Results

4.1 Characterization of adipose tissue-specific TR2/4 dKO mice

4.1.1 Generation of adipose-tissue specific TR2/4 dKO mice

TR2 *fl/fl* – TR4 *fl/fl* were generated by breeding mice with floxed alleles on the 4th exon of TR2 with mice with floxed alleles on the 5th exon of TR4 for two generations. These TR2 *fl/fl* – TR4 *fl/fl* mice were bred with Adiponectin-Cre mice that specifically express the Cre recombinase in adipocytes under the control of the Adiponectin promoter to generate a first generation of AdipoQ-Cre TR2 *wt/fl* – TR4 *wt/fl* males (Fig. 11A). To generate adipose-tissue specific TR2/4 dKO mice, these males were bred again with TR2 *fl/fl* – TR4 *fl/fl* females. We verified the efficient recombination and exclusion of the exon 4 of TR2 and the exon 5 of TR4 by PCR in BAT and SCAT respectively (Fig. 11B&C). In Cre-positive mice, a short band of 250 bp consistent with exclusion of the floxed exon was detected in addition to the 1 kb wildtype unrecombined band from the extra cell types composing the adipose tissue (endothelial cells, macrophages...).

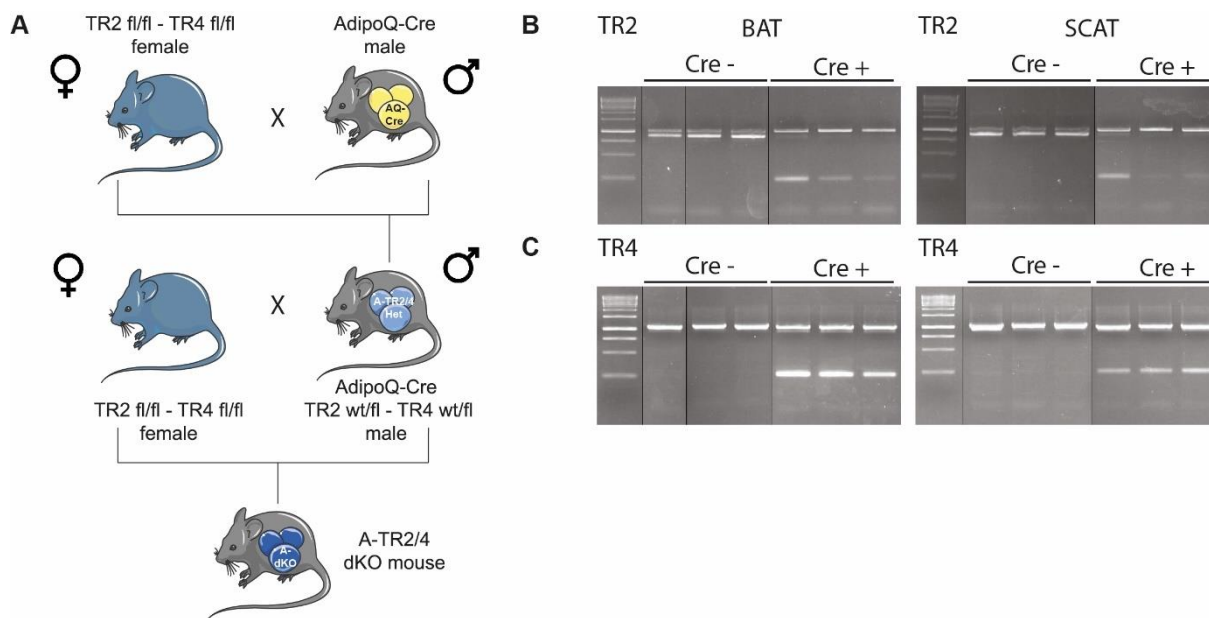


Figure 11: Generation and validation of adipose-tissue specific TR2/4 dKO mice (A-dKO mice).

A: Breeding strategy by crossing TR2 *fl/fl* – TR4 *fl/fl* females with AdipoQ-Cre males to generate AdipoQ-Cre TR2 *wt/fl* – TR4 *wt/fl* males. Those males were bred again to TR2 *fl/fl* – TR4 *fl/fl* females to generate adipose tissue specific TR2/4 dKO mice. B-C: Agarose gels of PCR products from exon 4 of *Nr2c1* (B) and exon 5 of *Nr2c2* (C) genes showing recombined

exons in brown (BAT) and sub-cutaneous (SCAT) adipose tissues. The 1kb band corresponds to the unrecombined allele, the 250 bp corresponds to the recombined allele with excision of the floxed exon.

4.1.2 TR2/4 deletion in adipose tissue does not affect glucose metabolism after HFD

To mimic a diet-induced obese phenotype and its complications, A-dKO mice and wildtype littermates were fed a high-fat high-sucrose diet (HFD) for 12 weeks. In both groups, the diet induces an intolerance to glucose during a GTT without visible differences between the two genotypes (Fig. 12A). Also, these mice showed a mild and comparable insulin resistance in both groups during an ITT (Fig. 12B). In order to challenge glucose and insulin signaling further, the exposure to HFD was increased up to 20 weeks. In both wildtype and A-dKO mice, the glucose intolerance and the insulin resistance were increased but without noticeable differences between the groups (Fig. 12C&D). From these experiments, the conclusion is that TR2 and TR4 function in adipose tissues don't affect the global glucose tolerance and insulin sensitivity.

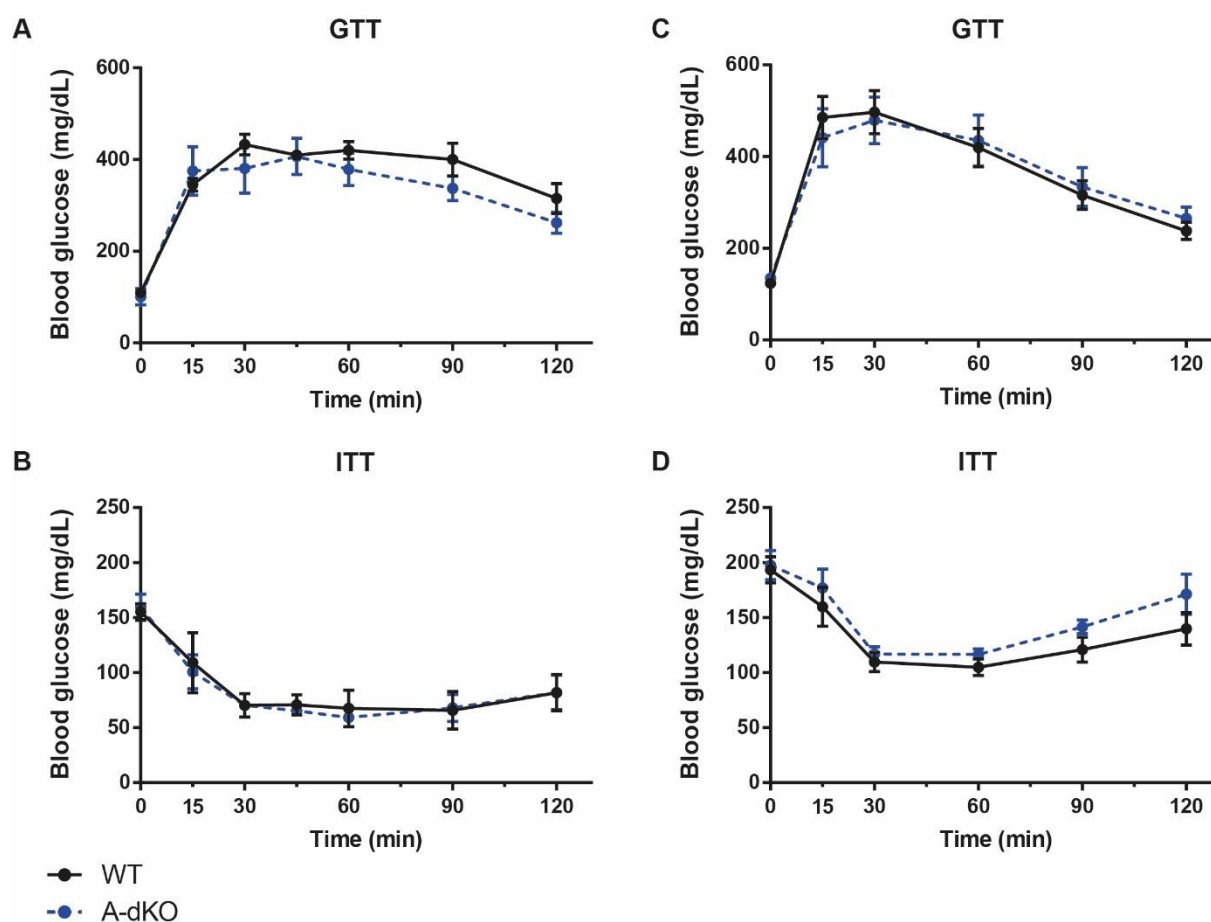


Figure 12: A-dKO mice show no differences in glucose and insulin tolerance after 12 and 20 weeks of HFD.

A-B: Intra-peritoneal Glucose tolerance test (GTT) (A) and insulin tolerance test (ITT) (B) in wildtype and A-dKO mice after 12 weeks of HFD. Statistical analysis by ANOVA and Bonferroni's multiple comparison test, n=4 per group. C-D: Intra-peritoneal Glucose tolerance test (GTT) (C) and insulin tolerance test (ITT) (D) in wildtype and A-dKO mice after 20 weeks of HFD. Statistical analysis by ANOVA and Bonferroni's multiple comparison test, n=6 per group.

4.1.3 TR2/4 deletion in adipose tissue does not affect adipose tissue morphology after HFD

After 20 weeks of HFD, mice from both genotypes had similar body weight after the diet and their body composition in fat and lean body mass was equivalent (Fig. 13A&B). Wildtype and A-dKO mice showed lipid accumulation in the various adipose tissues. In BAT, enlarged macro- and microvesicular lipid vacuoles were visible on H&E staining and consistent with BAT inactivation (Fig. 13C). In SCAT and VAT, wildtype and A-dKO mice showed no differences in their lipid accumulation in response to the diet (Fig. 13D&E). Body weight, body composition, lipid accumulation and adipocyte morphology were similar between wildtype and A-dKO mice, suggesting that TR2 and TR4 do not affect adipose tissue morphology.

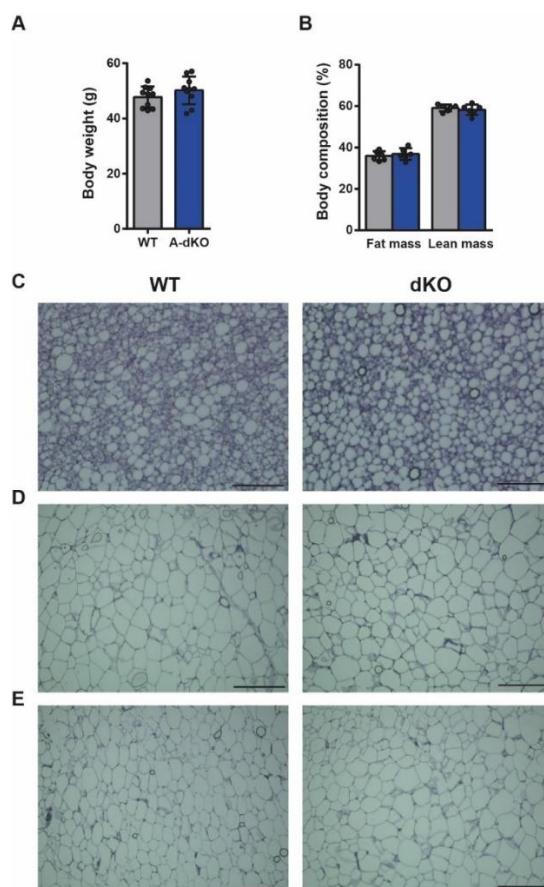


Figure 13: A-dKO mice show no differences in body weight and composition and adipose tissue morphology after 20 weeks of HFD.

A: Body weight of WT and A-dKO mice after 20 weeks of HFD, $n = 10$ per group. Data are mean \pm SEM. B: Body composition of WT and A-dKO mice after 20 weeks of HFD, $n = 6$ per group. Data are mean \pm SEM. C-E: H&E stainings of BAT (C), SCAT (D) and VAT (E) paraffin embedded sections from WT (left panel) and A-dKO (right panel) mice after 20 weeks of HFD. Representative images from $n=6$ per group, scale bars = 100 μm .

4.1.4 TR2/4 deletion in adipose tissue does not affect food intake, activity and calorimetric parameters.

Indirect calorimetry, food intake and locomotor activity of 4 wildtype and 4 A-dKO mice fed with HFD for 12 weeks were measured hourly during 4 consecutive days at 23°C and 12h light – 12 h dark daily cycle. Data shown is the average of the 4 days of measurement of all animals from each group.

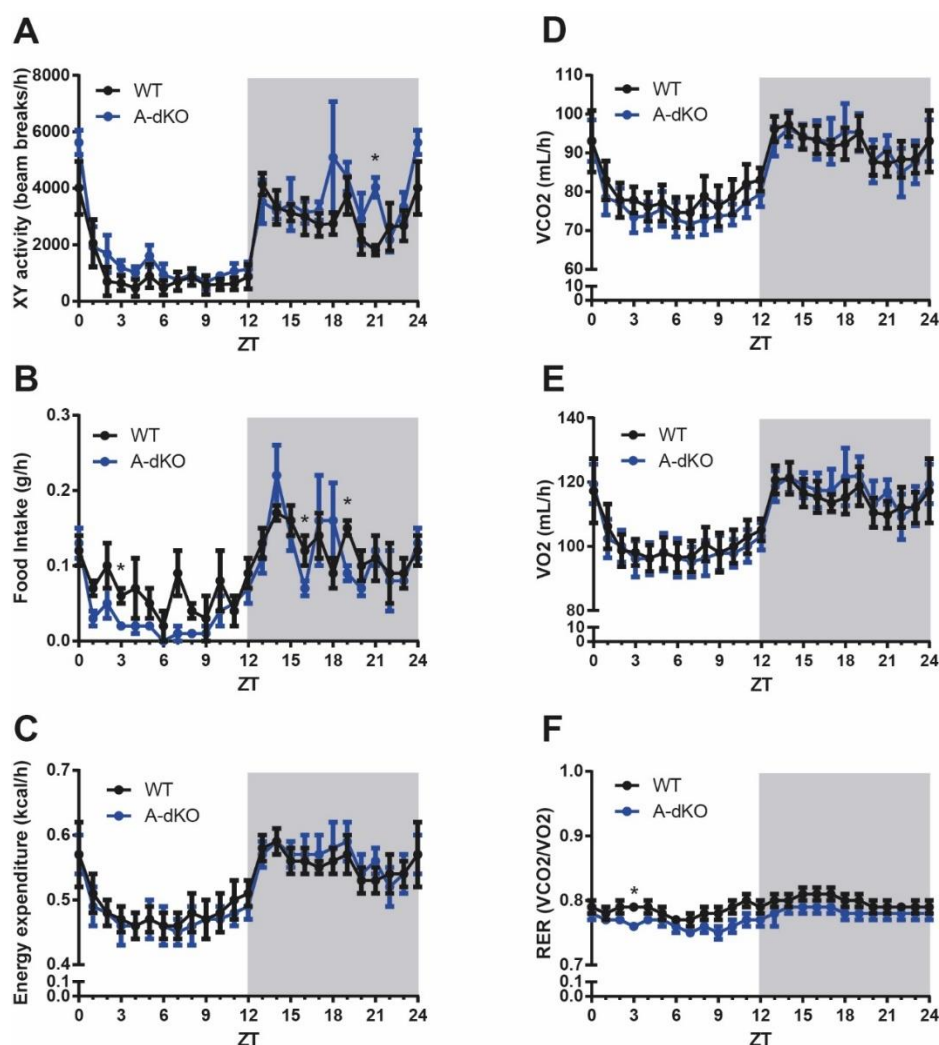


Figure 14: A-dKO mice show mild differences in food intake, activity and calorimetric parameters after 12 weeks of HFD.

A: Hourly locomotor activity on the XY axis measured in beam breaks per hour. B: Hourly food intake measured in gram per hour. C: Hourly EE measured in kcal per hour. D-E : Hourly

volume of CO₂ production (D) and O₂ consumption (E) measured in mL per hour. F : Hourly respiratory exchange ratio calculated as the ratio between VCO₂ and VO₂. Data are mean ± SEM, (*) P < 0.05, Student's t-test, n=4 per group, all data represent the average of hourly measurements performed over a total period of 4 days.

A-dKO mice showed slightly increased locomotor activity at ZT21 compared to wildtype mice but without a significant impact on the total activity (Fig. 14A). Slight changes in the food intake occurred with a decrease of food intake from the A-dKO mice at ZT16 and ZT19 during the dark phase and at ZT3 during the light phase (Fig. 14B). However, these changes didn't affect significantly the total food intake of the A-dKO mice over the 24h cycle. EE was strictly comparable between A-dKO and wildtype mice (Fig. 14C). CO₂ production and O₂ consumption was following similar patterns between the two groups (Fig. 14D-E). The RER was slightly decreased at ZT3 for A-dKO mice but this change did not significantly impact the overall RER of the mice which was comprised between 0,77 and 0,80, indicating a preferential oxidation of lipids as a direct consequence of the high-fat content of the diet (Fig. 14F).

4.2 Characterization of liver-specific TR2/4 dKO mice and TR4 OE mice

4.2.1 Generation of liver-specific TR2/4 dKO mice

TR2 *fl/fl* – TR4 *fl/fl* mice were bred with Alb-Cre mice that specifically express the Cre recombinase in hepatocytes under the control of the Albumin promoter to generate a first generation of Alb-Cre TR2 *wt/fl* – TR4 *wt/fl* males (Fig. 11A). To generate liver specific TR2/4 dKO mice, these males were bred again with TR2 *fl/fl* – TR4 *fl/fl* females. We verified the efficient recombination and exclusion of the exon 4 of TR2 and the exon 5 of TR4 by PCR in liver (Fig. 15 B&C). In Cre-positive mice, a short band of 250 bp consistent with exclusion of the floxed exon was detected. By qRT-PCR, a ten-fold reduction of the *Nr2c1* and *Nr2c2* transcripts in the Albumin-Cre positive mice validated the loss of function in the liver (Fig. 15D&E). Also, TR2 and TR4 proteins were not detected on western blots performed on nuclear extracts, validating the specific deletion of the two proteins in hepatocytes (Fig. 15F-G).

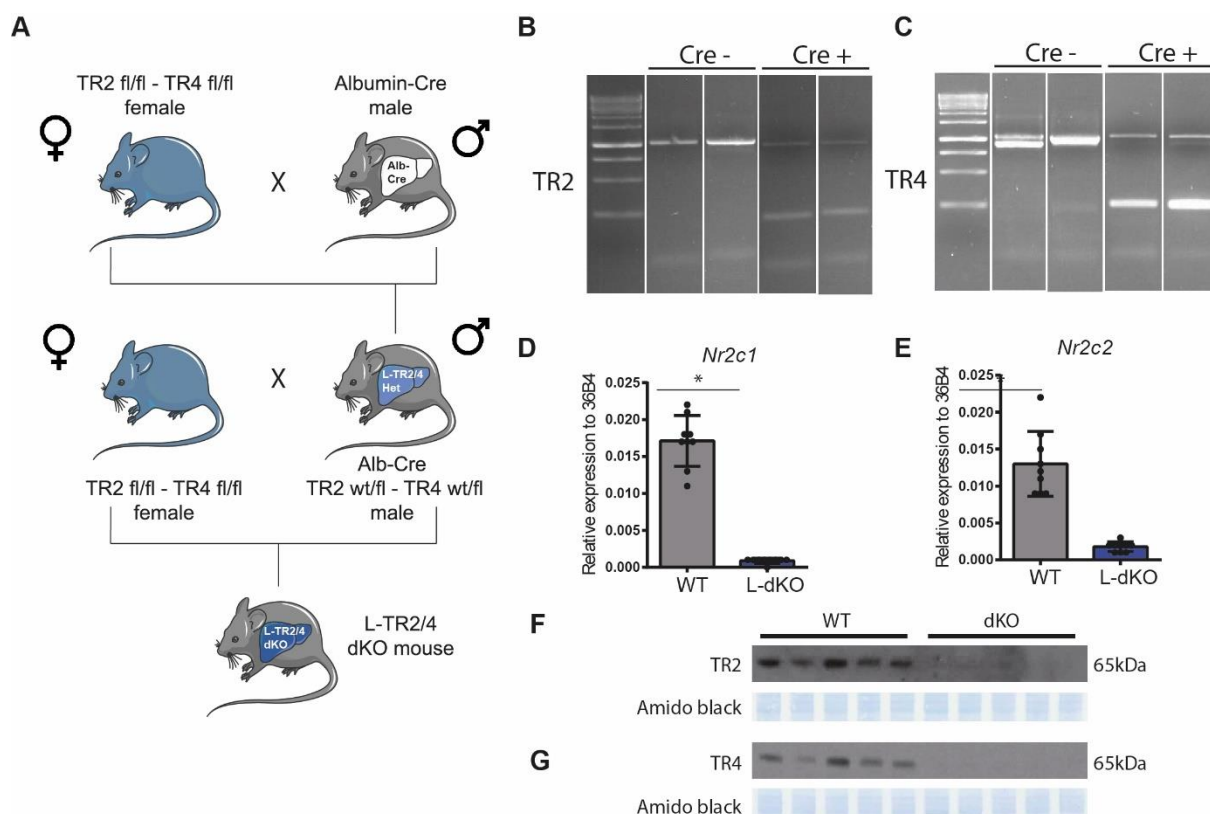


Figure 15: Generation and validation of liver-specific TR2/4 dKO mice (L-dKO mice).

A: Breeding strategy by crossing TR2 *fl/fl* – TR4 *fl/fl* females with Alb-Cre males to generate Alb-Cre TR2 *wt/fl* – TR4 *wt/fl* males. Those males were bred again to TR2 *fl/fl* – TR4 *fl/fl* females to generate liver specific TR2/4 dKO mice. B-C: Agarose gels of PCR products from exon 4 of *Nr2c1* (B) and exon 5 of *Nr2c2* (C) genes showing recombined exons in liver. The 1kb band corresponds to the unrecombined allele, the 250 bp corresponds to the recombined allele with excision of the floxed exon. D-E: qRT-PCR for *Nr2c1* (D) and *Nr2c2* (E) genes normalized to *u36b4*. Data are mean \pm SEM, (*) $P < 0.05$, Student's t-test, $n=9$ per group. F-G: Western blotting of for TR2 (F) and TR4 (G) protein on nuclear protein extracts from livers of wildtype and L-dKO mice. $n=5$ per group, amido black stained membranes serve as loading control.

4.2.2 Generation of liver-specific TR4 OE mice

To create a conditional TR4 over-expressing mouse, a construct containing the full TR4 ORF in antisense under a CAG promoter was inserted in the HPRT locus. By breeding female mice to Albumin-Cre males, the Cre recombinase excludes the stop codon and the neo-cassette downstream of the CAG promoter and translocates the TR4 ORF in sense direction directly downstream of the CAG promoter, generating a liver-specific TR4 OE mouse (Fig. 16A). By qRT-PCR, over-expression of the *Nr2c2* gene was confirmed by a ten-fold factor (Fig. 16C) while the expression of *Nr2c1* remained unchanged (Fig. 16B). The TR4 protein was increased

on western blots performed on nuclear extracts, validating the specific over-expression of the TR4 protein in hepatocytes (Fig. 16D).

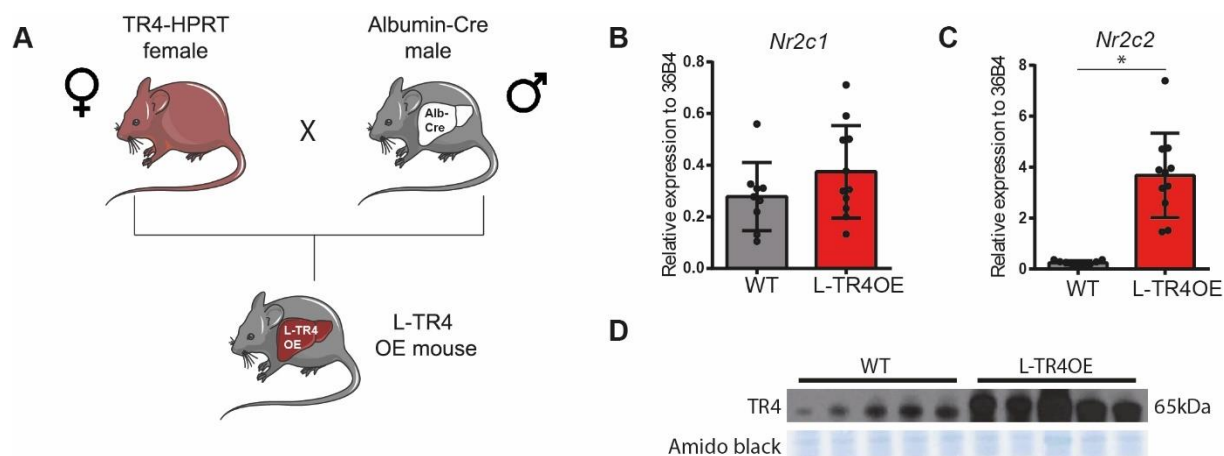


Figure 16: Generation and validation of liver-specific TR4 OE mice (L-TR4OE mice).

A: Breeding strategy by crossing TR4-HPRT mice with Alb-Cre mice to generate liver-specific TR4 OE mice. B-C: qRT-PCR for *Nr2c1* (B) and *Nr2c2* (C) genes normalized to *u36b4*. Data are mean \pm SEM, (*) $P < 0.05$, Student's t-test, $n=9$ for WT and 11 for L-TR4OE mice. D: Western blotting of for TR4 protein on nuclear protein extracts from livers of wildtype and L-TR4OE mice. $N=5$ per group, amido black stained membranes serve as loading control.

4.2.3 TR2/4 deletion in liver does not affect glucose metabolism before and after HFD

In wildtype and L-dKO mice, glucose tolerance, insulin sensitivity and pyruvate-induced gluconeogenesis were similar in tolerance tests performed on chow-fed mice (Fig. 17A-C). After 12 weeks of HFD, mice became glucose intolerant in both wildtype and L-dKO genotypes without differences between the two groups (Fig. 17D). L-dKO showed slight increase in insulin sensitivity during the first 15 minutes of the ITT but the difference with wildtype mice was resorbed after 30 minutes (Fig. 17E). Both wildtype and L-dKO mice showed slightly increased glucose production during PTT without differences between groups (Fig. 17F). Overall, the loss of TR2 and TR4 in liver does not affect glucose metabolism in response to HFD.

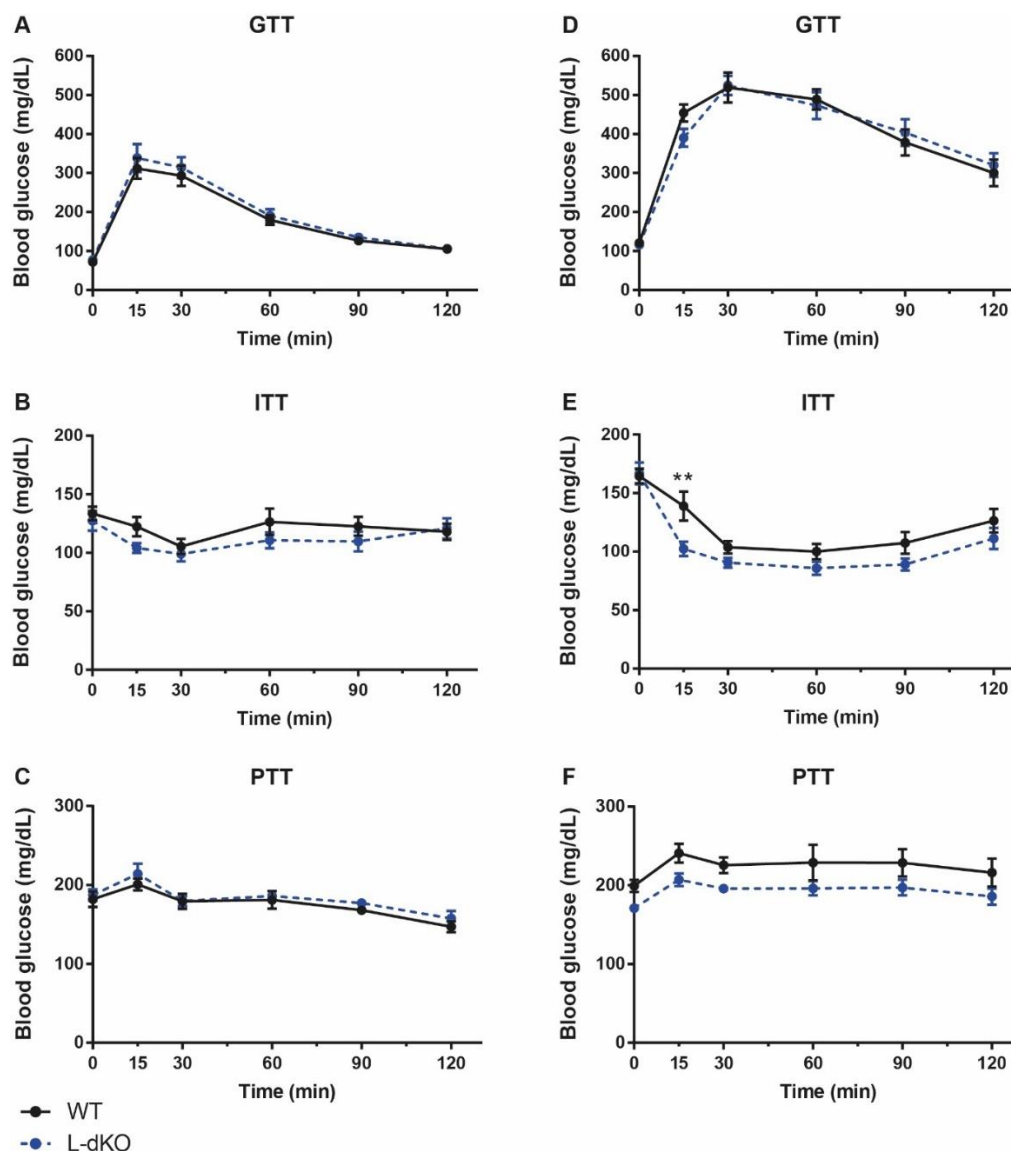


Figure 17: L-dKO mice show no differences in glucose, insulin and pyruvate tolerance on chow diet or after 12 weeks of HFD.

A & D: Intra-peritoneal Glucose tolerance test (GTT) in wildtype and L-dKO mice on chow diet (A) and after 12 weeks of HFD (D). $n= 15$ WT & 12 L-dKO for (A) and 14 WT & 13 L-dKO for (D). B & E: Intra-peritoneal Insulin tolerance test (ITT) in wildtype and L-dKO mice on chow diet (B) and after 12 weeks of HFD (E). $n= 15$ WT & 13 L-dKO for (B) and 13 WT & 12 L-dKO for (E). C-F : Intra-peritoneal Pyruvate tolerance test (PTT) in wildtype and L-dKO mice on chow diet (C) and after 12 weeks of HFD (F). $n= 5$ WT & 4 L-dKO for (C) and 12 WT & 13 L-dKO for (F). Statistical analysis by ANOVA and Bonferroni's multiple comparison test.

4.2.4 TR4 overexpression in liver does not affect glucose metabolism before and after HFD

In wildtype and L-TR4OE mice, glucose tolerance, insulin sensitivity and pyruvate-induced gluconeogenesis were similar in tolerance tests performed on chow-fed mice (Fig. 18A-C). After 12 weeks of HFD, mice became glucose intolerant in both wildtype and L-TR4OE

genotypes with no differential effect between groups (Fig. 18D). L-TR4OE and wildtype mice showed similar insulin resistance on ITT (Fig. 18E). Both wildtype and L-dKO mice showed slightly increased glucose production during PTT without differences between groups (Fig. 18F). Overexpression of TR4 in the liver had no significant impact on glucose metabolism.

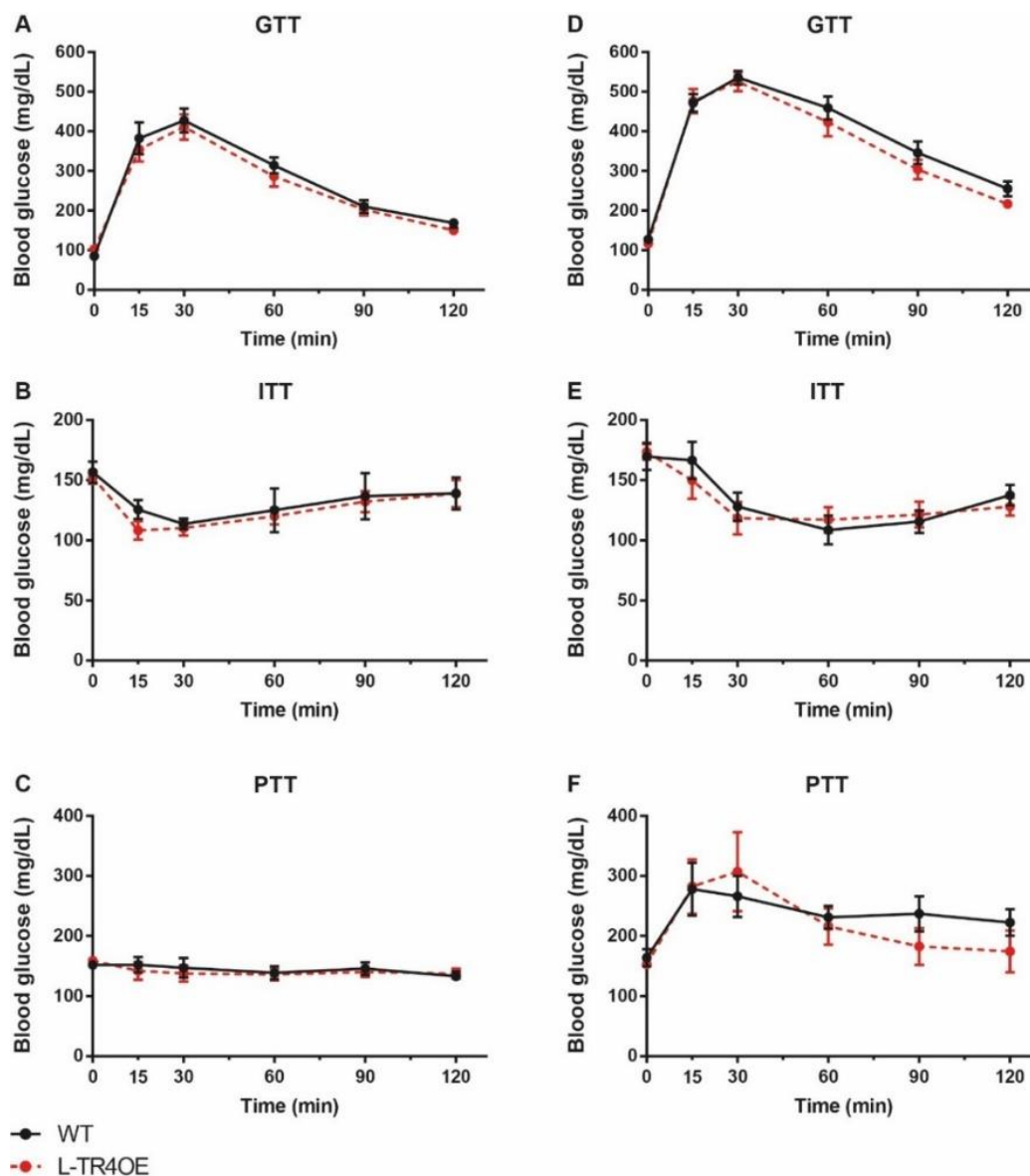


Figure 18: L-TR4OE mice show no differences in glucose, insulin and pyruvate tolerance on chow diet or after 12 weeks of HFD.

A & D: Intra-peritoneal Glucose tolerance test (GTT) in wildtype and L-TR4OE mice on chow diet (A) and after 12 weeks of HFD (D). $n = 6$ (WT) & 9 (L-TR4OE) for (A) and 9 (WT) & 11 (L-dKO) for (D). B & E: Intra-peritoneal Insulin tolerance test (ITT) in wildtype and L-dKO mice on chow diet (B) and after 12 weeks of HFD (E). $n = 3$ (WT) & 5 (L-dKO) for (B) and 6 (WT) & 8 (L-TR4OE) for (E). C-F : Intra-peritoneal Pyruvate tolerance test (PTT) in wildtype and L-dKO mice on chow diet (C) and after 12 weeks of HFD (F). $n = 6$ (WT) & 9 (L-TR4OE) for (C) and 4 (WT) & 6 (L-dKO) for (F). Statistical analysis by ANOVA and Bonferroni's multiple comparison test.

4.2.5 L-dKO mice show microvesicular storage of lipids in the liver

After 12 weeks of HFD, livers from WT, L-dKO and L-TR4OE mice were collected and H&E stainings were performed to evaluate the architecture of the cellular components. Wildtype and L-TR4OE mice have macrovesicular steatosis characterized by large lipid vacuoles in the hepatocyte lumen. On the contrary, L-dKO display a predominant microvesicular form of steatosis with small lipid droplets inside the cytoplasm of hepatocytes (Fig. 19A). Interestingly, genetic modification of the expression of TR2 and TR4 in the liver does not affect the body weight of the mice before or after HFD (Fig. 19B-C). This is a major difference with the TR4^{-/-} mice that showed reduced body size and weight (Kang et al., 2011) and was an important confounding effect for metabolic fitness. This L-dKO model offers a context with stable size and body weight where changes in liver physiology can be directly linked to TR2 and TR4 and not as an indirect effect of body size or other metabolic organ. Furthermore, triglyceride content in the liver and circulating triglycerides in the serum is identical in all groups (Fig. 19D-G). This change in lipid storage in the L-dKO mice is independent of the amount of lipids accumulated but might be related to the way hepatocytes are handling and storing lipids, indicating a possible change in lipid storage and trafficking machinery in the L-dKO. The structural impact of lipid droplets differences and their function in hepatocytes are still unknown but we hypothesize that such differences in storage might have an impact on lipotoxicity.

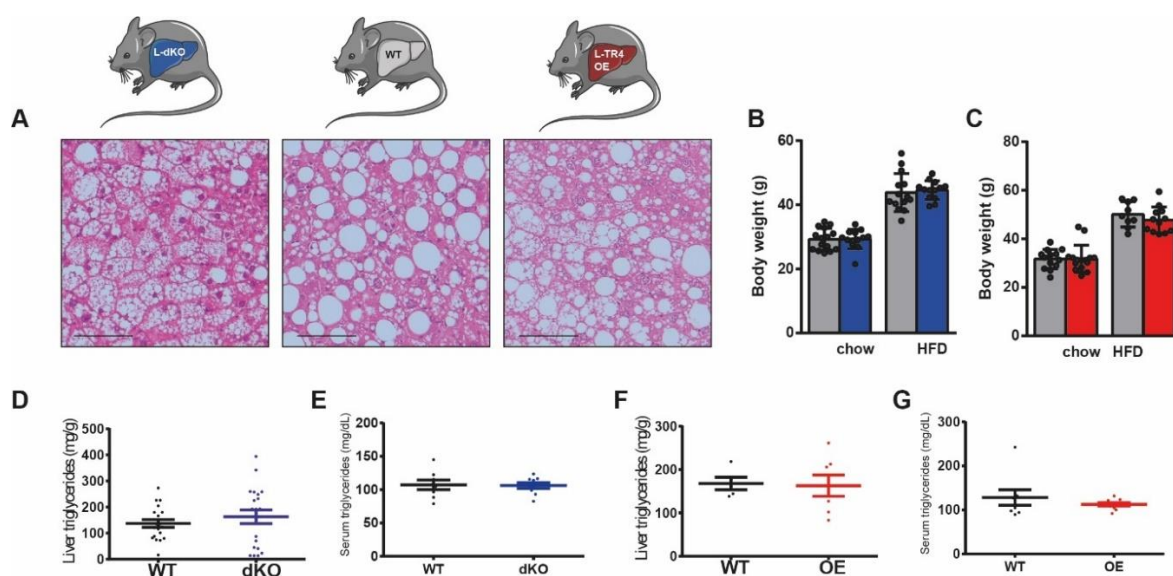


Figure 19: L-dKO and L-TR4OE mice become obese and have hepatic steatosis on HFD.

A: Liver staining with H&E after 12 weeks of HFD. Magnification 10x, representative image from n=16 WT, 11 L-dKO and 11 L-TR4OE. B: Body weight of WT and L-dKO mice before and after HFD, n=15 on chow and 14 on HFD for WT and 13 on both diets for L-dKO. Data are mean \pm SEM. C: Body weight of WT and L-TR4OE mice before and after HFD, n=13 on chow and 9 on HFD for WT and 15 on chow and 12 on HFD for L-TR4OE. Data are mean \pm SEM. D-E: Liver (D) and serum (E) triglyceride measurements in WT and L-dKO mice after HFD. Data are mean \pm SEM, n=19 WT and 20 L-dKO in (D), n=8 WT and 9 L-dKO in (E). F-G: Liver (F) and serum (G) triglyceride measurements in WT and L-TR4OE mice after HFD. Data are mean \pm SEM, n=5 WT and 7 L-TR4OE in (F), n=8 WT and 10 L-TR4OE in (G).

4.2.6 L-TR4OE mice show early fibrosis on HFD

Hepatic steatosis is the first stage of NAFLD and lipid accumulation and lipotoxicity ultimately lead to NASH, hepatocyte degeneration and liver fibrosis. To evaluate liver fibrosis, Sirius Red staining were performed to quantify collagen deposition in the liver. While WT and L-dKO mice exhibit minimal collagen depots in the liver after 12 weeks of HFD, we saw that L-TR4OE mice have already pronounced liver fibrosis suggesting a faster progression of NAFLD in these animals where TR4 activity is increased in the liver (Fig. 20A). Systematic blind scoring of fibrosis showed that none of the L-dKO mice had fibrosis at this stage, 20% of WT mice showed mild fibrosis with a score of 0.5 and more than half of the L-TR4OE mice showed a score of 1 or higher, with an average of 0.86, significantly higher than in WT and L-dKO mice (Fig. 20B-C). High-fat diet is usually not sufficient to induce liver fibrosis unless used for extensive periods of time (Febbraio et al., 2019). This result indicates a predisposition of L-TR4OE for NASH and that TR4 seems to play an important role in the transition between steatotic liver and liver fibrosis. The next step was to challenge those mice with a stronger profibrotic dietary challenge.

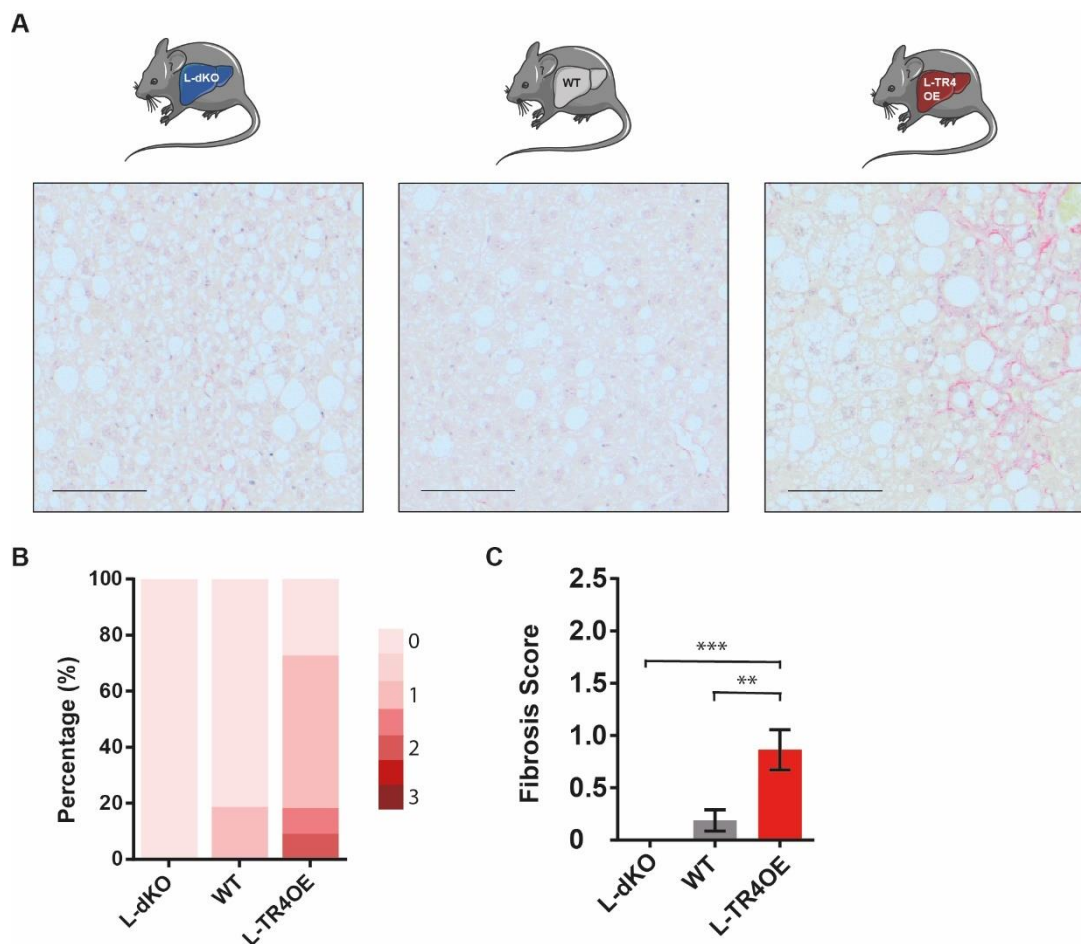


Figure 20: L-TR4OE mice show early liver fibrosis after HFD.

A: Liver stainings with Sirius Red after 12 weeks of HFD. Magnification 10x, representative image from n=16 WT, 11 L-dKO and 11 L-TR4OE. B: Fibrosis score distribution in WT, L-dKO and L-TR4OE mice. n=16 WT, 11 L-dKO and 11 L-TR4OE. C: Average fibrosis score in WT, L-dKO and L-TR4OE mice. n=16 WT, 11 L-dKO and 11 L-TR4OE, data are mean \pm SEM, (**) $P < 0.01$, (***) $P < 0.001$ Student's t-test.

4.2.7 L-TR4OE mice progress faster into NAFLD on a pro-fibrotic diet

To put the mice on a stronger dietary profibrotic challenge, we used the DIAMOND diet for 26 weeks. With high cholesterol and high fructose levels in addition to high fat and glucose content, the DIAMOND model induces liver inflammation and fibrosis after a period of 16 weeks and can trigger HCC if prolonged for up to 52 weeks (Asgharpour et al., 2016). H&E staining were performed and show massive mixed hepatic steatosis in all mice with even distribution between micro- and macrovesicular steatosis (Fig. 21A). Sirius Red staining showed increased fibrosis in all genotypes compared to HFD (Fig. 21B). While WT mice have an average fibrosis score of 0.93, L-TR4OE mice show the same tendency as on HFD with a significant increase in liver fibrosis with an average score of 1,72. L-dKO mice have a tendency towards reduced liver fibrosis compared to WT with an average score of 0.55 but this difference is not significant.

However, more than half of the L-dKO mice have a fibrosis score of 0.5 or lower while more than half of the WT mice have a score of 1 or higher (Fig. 21C&D). Interestingly, mRNA expression for TR2 and TR4 was upregulated in wildtype mice after DIAMOND diet compared to chow and HFD, suggesting a correlation between TR2/4 expression and transition into liver fibrosis and NASH (Fig. 21E). These results confirm the importance of TR2/4 in the response to a pro-fibrotic dietary challenge and the progression into the NAFLD spectrum. In order to identify the processes regulated by these two receptors in the onset of liver fibrosis, the next step was to determine their respective cistromes in the liver.

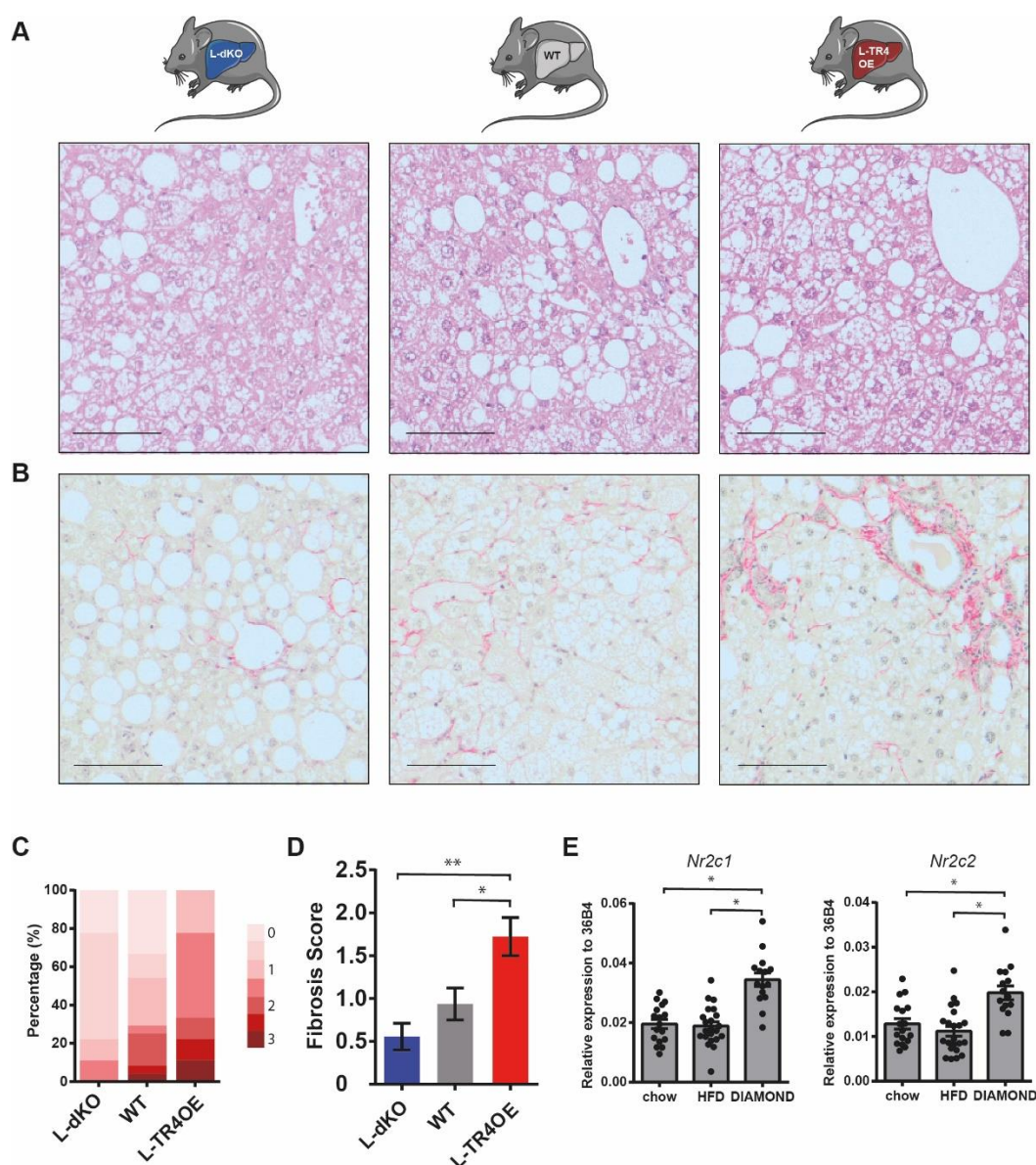


Figure 21: L-TR4OE mice are prone to liver fibrosis and L-dKO mice are protected against liver fibrosis on DIAMOND diet.

A: Liver stainings with H&E after 24 weeks of DIAMOND diet. Magnification 10x, representative image from n=24 WT, 9 L-dKO and 9 L-TR4OE. B: Liver stainings with Sirius Red after 26 weeks of DIAMOND diet. Magnification 10x, representative image from n=24 WT, 9 L-dKO

and 9 L-TR4OE. C: Fibrosis score distribution in WT, L-dKO and L-TR4OE mice. n=24 WT, 9 L-dKO and 9 L-TR4OE. D: Average fibrosis score in WT, L-dKO and L-TR4OE mice. n=24 WT, 9 L-dKO and 9 L-TR4OE, data are mean \pm SEM, (*) P < 0.05, (**) P < 0.01 Student's t-test. E: RT-qPCR for *Nr2c1* and *Nr2c2* in wildtype mice after chow, HFD or DIAMOND diet. (n= 15-20 mice/diet, * : p-value < 0.05)

4.3 Genomic binding of TR2 and TR4 in the liver

4.3.1 TR2 and TR4 cistromes partially overlap in liver and control mRNA maturation, protein synthesis and degradation and lipid metabolism.

TR2 and TR4 cell-type specific mechanism of action and target genes in metabolic organs remain largely unknown. ChIP-Seq has become a standard method to identify the genome-wide binding patterns of transcription factors and nuclear receptors.

ChIP-Seq was performed in livers collected from WT mice sacked at ZT8. After alignment to the mouse mm10 reference genome and peak calling using MACS2, 10 013 reproducible peaks for TR4 and 3989 reproducible peaks for TR2 were identified from 2 biological replicates. Interestingly, more than half (64%) of the TR2 cistrome is shared with TR4 with an overlap of 2551 binding sites, suggesting a redundancy in some functions shared by both receptors (Fig. 22A).

The overlap between TR2 and TR4 is almost exclusively located at the promoter region of the closest genes of the binding sites suggesting a tight regulation in accessible regions for the two receptors at common DNA binding sites (Fig. 22B). TR2 specific peaks are also located almost exclusively at the promoter region whereas TR4 specific peaks are more evenly distributed between promoter, intragenic and enhancer regions.

HOMER motif analysis showed that the TR2/TR4 overlap is enriched for consensus sequences of various factors such as YY1, an ubiquitous transcriptional repressor, E26 transformation specific factors (ETS) which are known to bind at promoter regions and PPAR α , another DR1 nuclear receptor involved in lipid metabolism and inflammation, in addition to the TR4 motif (Fig. 22E). For the TR2 specific peaks, the motif analysis reveals binding sites for similar factors, including NFY, an important pioneer factor for promoter selection (Fig. 22D) (Oldfield et al., 2014). Due to a broader range of binding sites, TR4 specific peak motif analysis shows enrichment for sequences corresponding to DR1 nuclear receptors important in liver physiology such as HNF4 α , PPAR α and FXR (Fig. 22C).

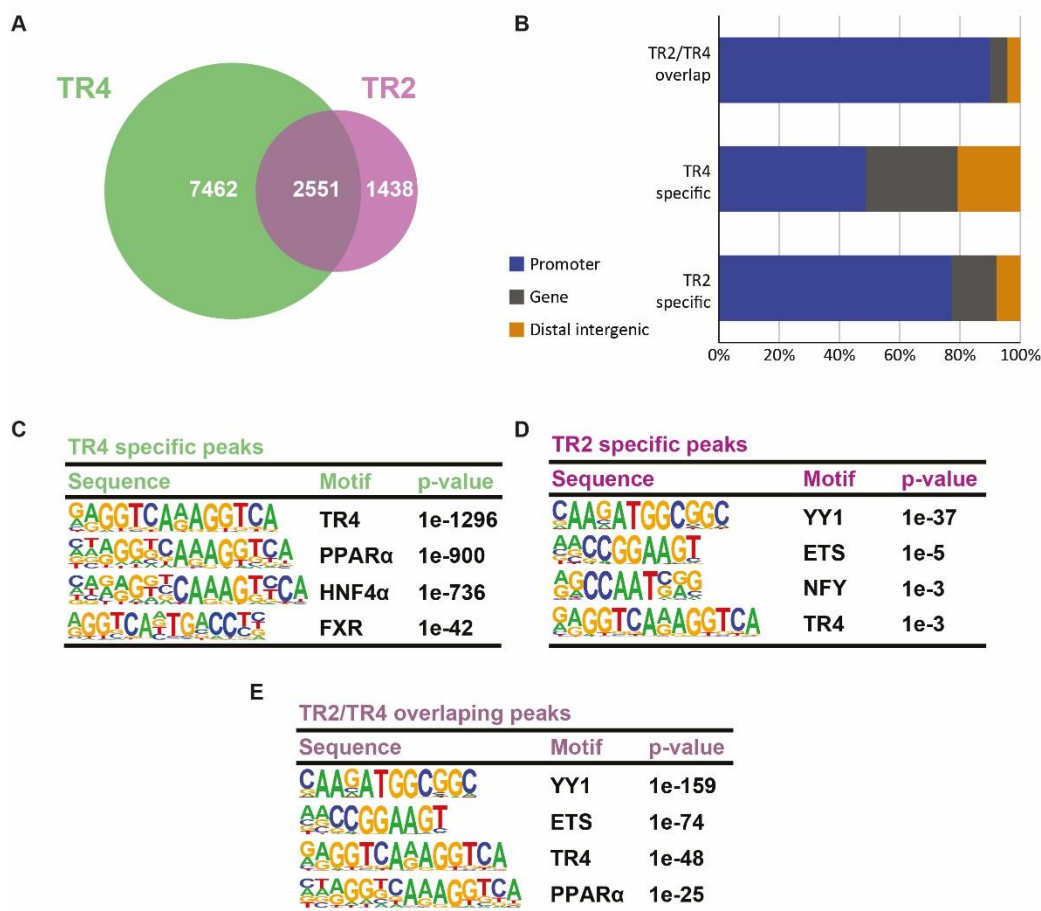


Figure 22: TR2 and TR4 share a strong overlap in the liver and specific binding for TR4.

A: Area-proportional Venn diagram illustrating the cistrome of TR2 and TR4 and their overlapping binding sites. Numbers correspond to the number of peaks identified in both biological replicates. B: Peak distribution of the overlap and the TR2 and TR4 specific binding regions. Binding sites are split in 3 groups: gene (intragenic regions: exons, introns), promoter (within 1 kb of the TSS of the closest gene) and enhancer (more than 1kb from the TSS). C-E: HOMER motif analysis of TR4 (C) and TR2 (D) specific peaks and their overlapping binding regions (E). For each factor, the consensus binding site recognized is shown and ordered by p-value.

KEGG pathway annotation of the common and the specific peaks for TR2 and TR4 show that TR2 and TR4 share binding sites in the vicinity of genes involved in fundamental biological processes such as autophagy, mRNA maturation, protein processing in the endoplasmic reticulum and amino acid synthesis and degradation (Figure 23). They also share binding sites close to metabolic genes involved in peroxisome function, lipid metabolism, glyoxylate and dicarboxylate metabolism and PPAR signaling.

In addition, TR4 specific binding sites cover additional functions such as cholesterol metabolism and a signature of genes involved in hepatocellular carcinoma, adherens junction and apoptosis.

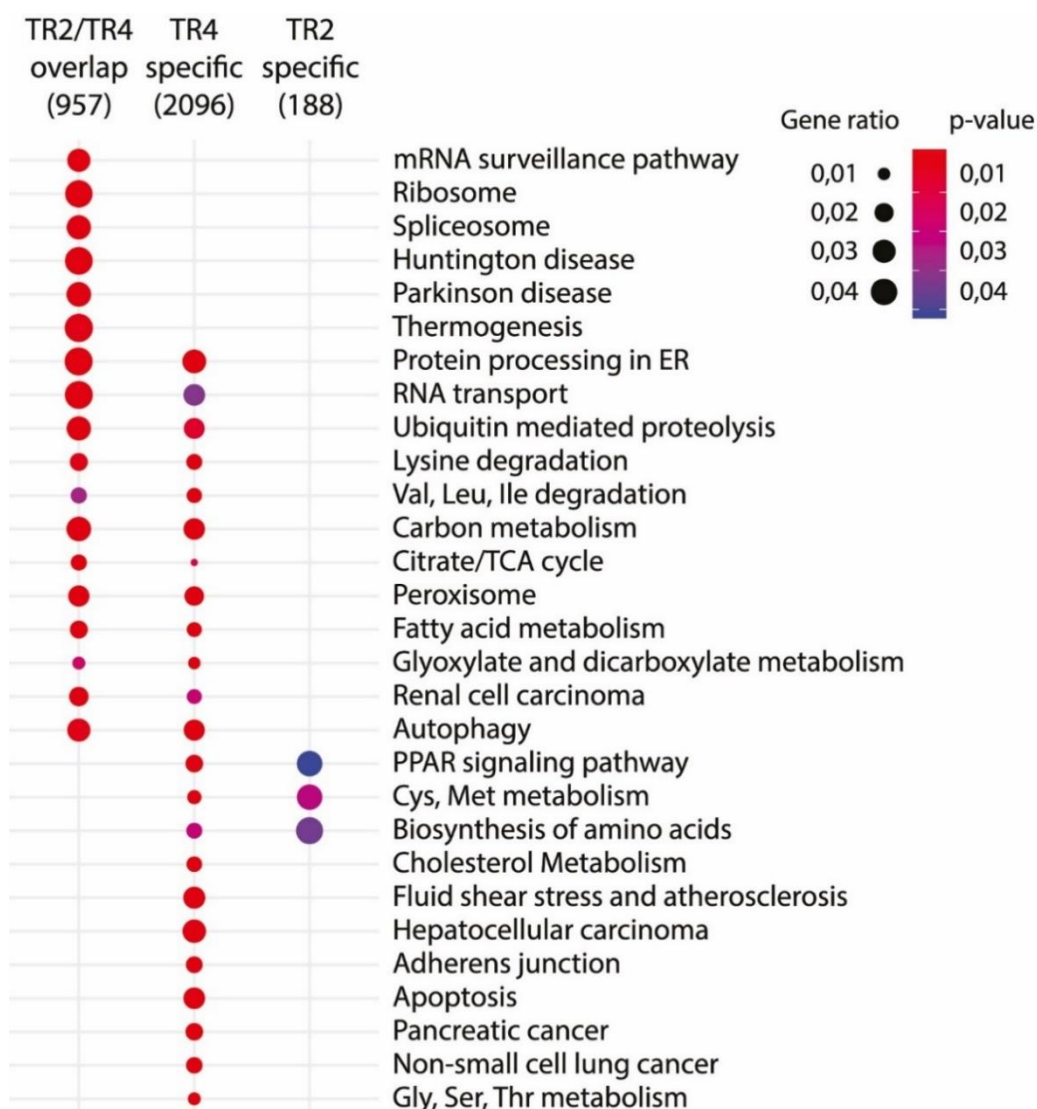


Figure 23: KEGG pathway annotation of TR2 and TR4 cistromes in WT livers.

Scatter plot of KEGG enriched pathways in TR2 and TR4 specific peaks and in the overlap between TR2 and TR4.

4.3.2 TR4 overexpression in the liver increases the number and the amplitude of TR4 binding sites with similar functionality.

To evaluate the impact of the TR4 overexpression in the liver of L-TR4OE mice, ChIP-Seq was performed in livers collected from L-TR4OE mice sacked at ZT8. After alignment to the mouse mm10 reference genome and peak calling using MACS2, we compared the 9992 reproducible

peaks for TR4 in WT with the 23 360 reproducible peaks for TR4 in L-TR4OE livers from 2 biological replicates.

Unsurprisingly, more than 90% of the WT peaks were also identified in the TR4OE ChIP-Seq with an overlap of 9027 peaks (Fig. 24A). In addition, the TR4OE ChIP-Seq analysis identified 14 333 newly bound peaks. Half of the overlap between TR4 in WT and TR4OE livers bind to promoter regions and the other half is equally distributed between gene bodies and enhancers regions. The TR4 WT specific peaks follow the same binding pattern as the overlap. Interestingly, the additional binding sites for TR4 in the OE are located in majority in intragenic or distant enhancer regions (Fig. 24B). Due to the increased amount of TR4 in this context, the additional protein can get access and bind to more distant sites with lower affinity that are not bound in the normal context.

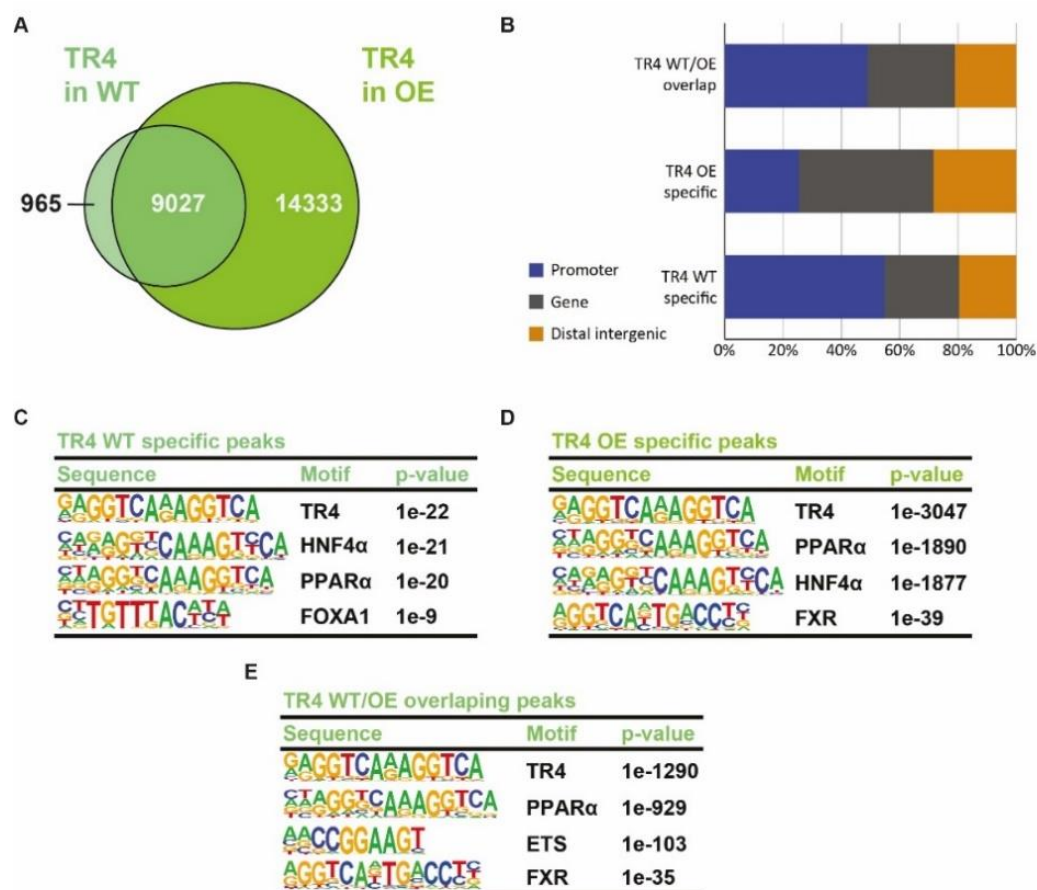


Figure 24: TR4 binds extra DNA regions in the liver of L-TR4OE mice compared to WT mice.

A: Area-proportional Venn diagram illustrating the cistrome of TR4 in WT and L-TR4OE livers and their overlapping binding sites. Numbers correspond to the number of peaks identified in both biological replicates. B: Peak distribution of the overlap and the TR4 specific binding regions in WT and L-TR4OE livers. Binding sites are split in 3 groups: gene (intragenic regions: exons, introns), promoter (within 1 kb of the TSS of the closest gene) and enhancer (more than

1kb from the TSS). C-E: HOMER motif analysis of the TR4 in WT (C) and in L-TR4OE (D) specific peaks and their overlap of binding regions (E). For each factor, the consensus binding site recognized is shown and ordered by p-value.

HOMER motif analysis showed that the TR4 WT/OE overlap is enriched for consensus sequences of ETS factors as seen previously for the TR2/TR4 overlap along with motifs for PPAR α and FXR (Fig. 24E). Consensus sequences for TR4, PPAR α and HNF4 α are found in the TR4 WT and OE specific peaks (Fig. 24C-D). In addition, the TR4 WT specific peaks are also enriched for the FOXA1 motif and the FXR IR1 motif in the TR4OE specific peaks.

KEGG pathway annotation of the common and the specific peaks for TR4 WT and TR4 OE show as previously that TR4 is involved in lipid and cholesterol metabolism, peroxisome function, glyoxylate cycle, autophagy, and hepatocellular carcinoma (Figure 25). The vast majority of the new TR4 binding sites in the OE analysis are involved in the same biological processes, suggesting that TR4 OE expands the binding capacity of TR4 in new regions close to genes involved in similar biological processes.

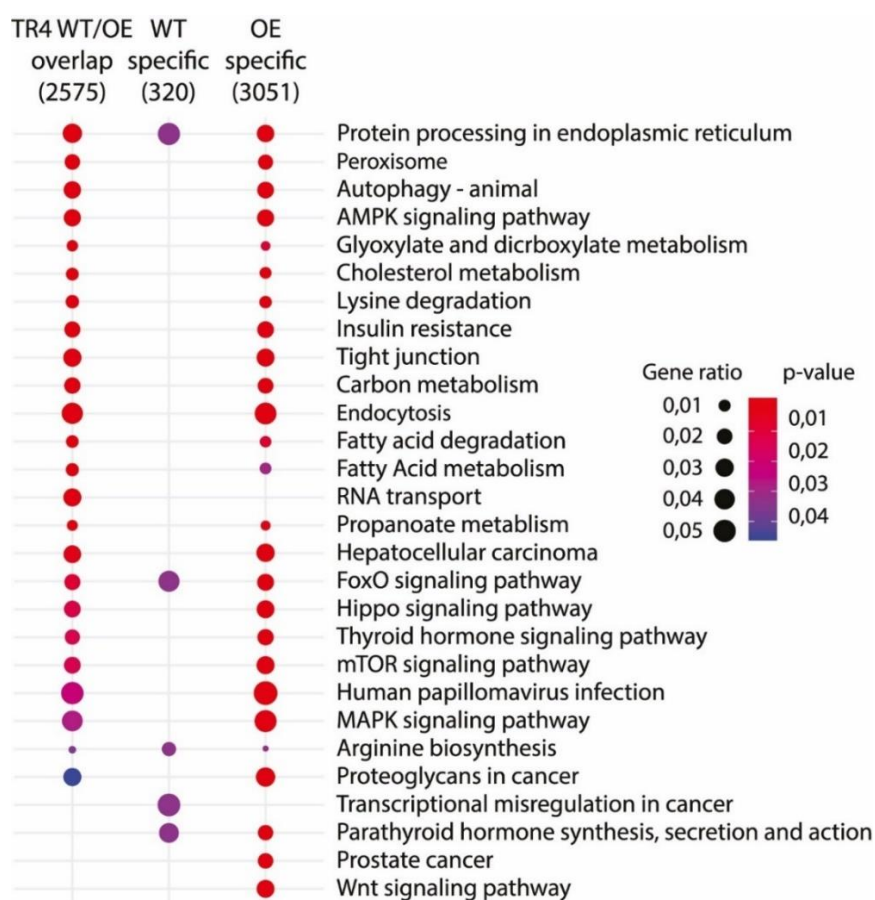


Figure 25: KEGG pathway annotation of TR4 cistromes in WT and L-TR4OE livers. Scatter plot of KEGG enriched pathways in TR4 WT and L-TR4OE liver cistromes and their overlap.

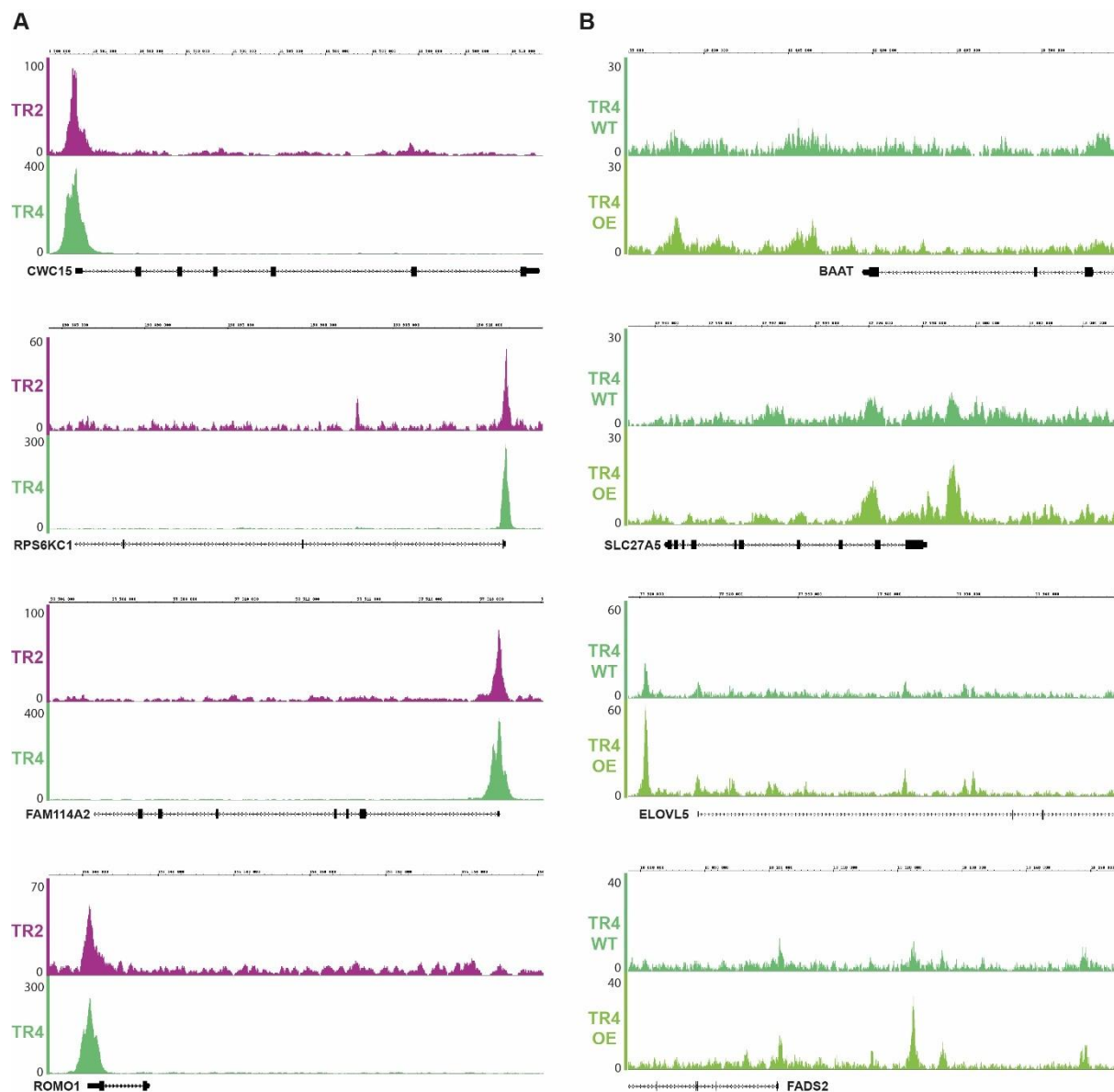


Figure 26: TR2 and TR4 bind in the promoter region of common genes while TR4 binds enhancers in lipid and bile acid metabolic genes.

A: Example tracks for TR2 and TR4 overlapping peaks in the promoter regions of *Cwc15*, *Rps6kc1*, *Fam114a2* and *Romo1*. B: Example tracks for TR4 overlapping regions in WT and L-TR4OE livers with higher binding in the L-TR4OE at promoter and enhancer regions close to *Baat*, *Slc27a5*, *Elovl5*, *Fads2*.

Overall, most of the binding sites and the functions of TR2 seem to be also covered by TR4. As seen on the example tracks of promoter regions for *Cwc15*, *Rps6kc1*, *Fam114a2* and *Romo1*, TR2 and TR4 binding overlap preferentially in the promoter region of the genes they bind together (Fig. 26A, Suppl. Tables 1&2). The functions regulated by both receptors in promoter regions involve fundamental biological processes such as protein and mRNA maturation and degradation for which both receptors probably can compensate for each other.

The functions of TR4 apart from these housekeeping processes involve lipid and cholesterol metabolism. Example tracks of lipid and cholesterol/bile acid metabolic genes for *Baat*, *Slc27a5*, *Elovl5*, *Fads2* show that TR4 binds the promoter region and some enhancer regions close to those genes in the WT liver. TR4 overexpression increases the amplitude of binding of TR4 in promoter and enhancers regions which will probably potentiate the transcriptional regulation of TR4 in the OE compared to the WT (Fig. 26B, Suppl. Tables 2&3).

To evaluate the transcriptional effect of the loss of function of TR2/4 and the gain of function of TR4 in the liver, RNA-Seq was performed on chow and HFD-fed mice to identify the differentially expressed target genes responsible for the susceptibility to liver fibrosis.

4.4 Transcriptional reprogramming of the livers from L-dKO and L-TR4OE mice

4.4.1 L-dKO and L-TR4OE mice have minor changes in transcriptional regulation on chow diet.

To have an insight in the basal effect of the loss of TR2 and TR4 or TR4 overexpression in the liver, gene expression profiles of livers from L-dKO and L-TR4OE mice fed on chow diet were analyzed by RNA-Seq. Reads were mapped to the mouse genome mm10 and differential expression analysis was performed using DESeq2.

L-dKO mice showed a very small number of differentially expressed genes with 28 repressed genes and 11 activated genes in the liver of mice fed with chow diet (Fig. 27A, Suppl. Table 4). Gene Ontology (GO) analysis showed no enrichment for any biological process. *Gstp2* and *Cyp2b9* were detected among the activated genes. *Gstp2* is important for drug and xenobiotic catabolism while *Cyp2b9* is a sexual dimorphic target of GR and growth hormone involved in steroid hormone synthesis (Abril, Ruiz-Laguna, & Pueyo, 2012; Sakuma et al., 2004). Genes with ChIP-Seq peaks for TR2 and TR4 such as *Cwc15*, *Fam114a2*, *Romo1* or *Rps6kc1* were repressed in the absence of the two receptors (Fig. 27B). Binding sites for TR4 were previously identified in human cell lines (O'Geen et al., 2010) but their biological functions in the liver are not yet known. The repression of those genes was confirmed by RT-qPCR (Fig. 27C). Overall, the loss of TR2 and TR4 in the liver has minimal impact on gene regulation in absence of a nutritional challenge.

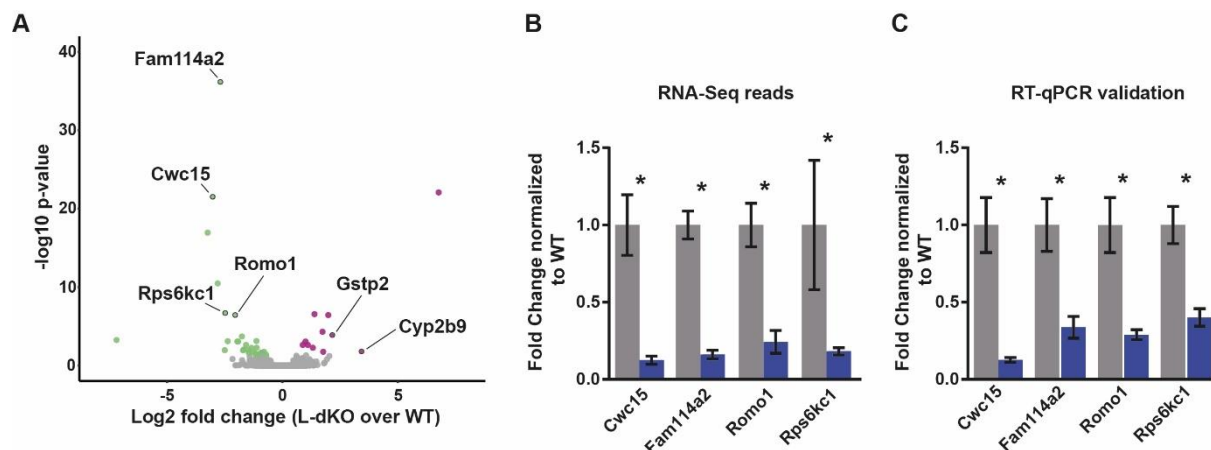


Figure 27: Livers from L-dKO mice show minimal transcriptional reprogramming on chow diet.

A : RNA-Seq of livers from chow-fed WT and L-dKO mice (n = 4 per group, green = 28 repressed genes, purple = 11 activated genes, log₂(fold change) < -0.58 and > 0.58 respectively, adjusted p-value < 0.05) B : Average transcript per million (TPM) count of example repressed target genes normalized to WT average. (n= 4 per group, * : adjp-value < 0.05) C: RT-qPCR in liver for example repressed target genes normalized to WT average. (n=9 WT and 10 L-dKO, * : p-value < 0.05)

L-TR4OE mice had 51 activated genes and 11 repressed genes in the liver on chow diet (Fig. 28A, Suppl. Table 5). GO Biological process analysis showed no enrichment for repressed genes but identified enriched terms involved in sterol and catecholamine synthesis as well as lipid metabolism for the up-regulated genes (Fig. 28B). Enzymes such as *Aacs*, *Akr1b3*, *Acat2*, *Cyp51*, *Hmgcr* and *Mvd* were significantly activated in L-TR4OE mice (Fig. 28C). *Hmgcr* and *Cyp51* are involved in sterol synthesis, *Aacs*, *Acat2* and *Akr1b3* in lipid and catecholamine synthesis, and *Mvd* in alcohol synthesis. However, these changes had no noticeable impact on the physiology and the phenotype of the livers of these mice.

These RNA-Seq analysis in the livers of L-dKO and L-TR4OE mice showed that the gain and loss of function had a minor impact on gene expression in the liver in a healthy liver on chow diet.

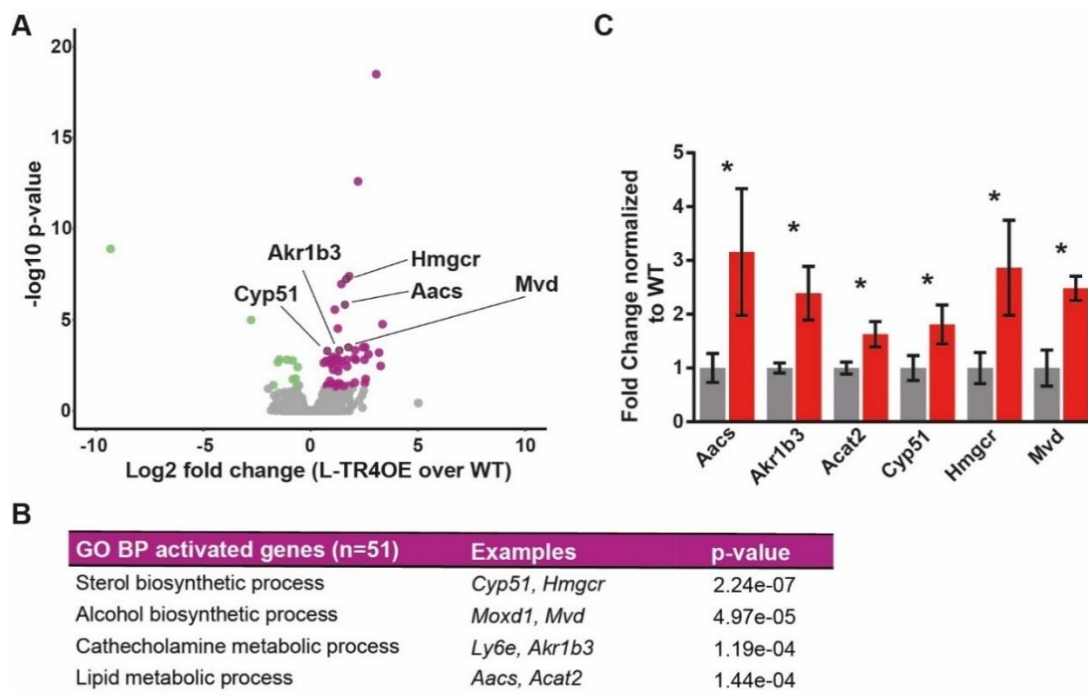
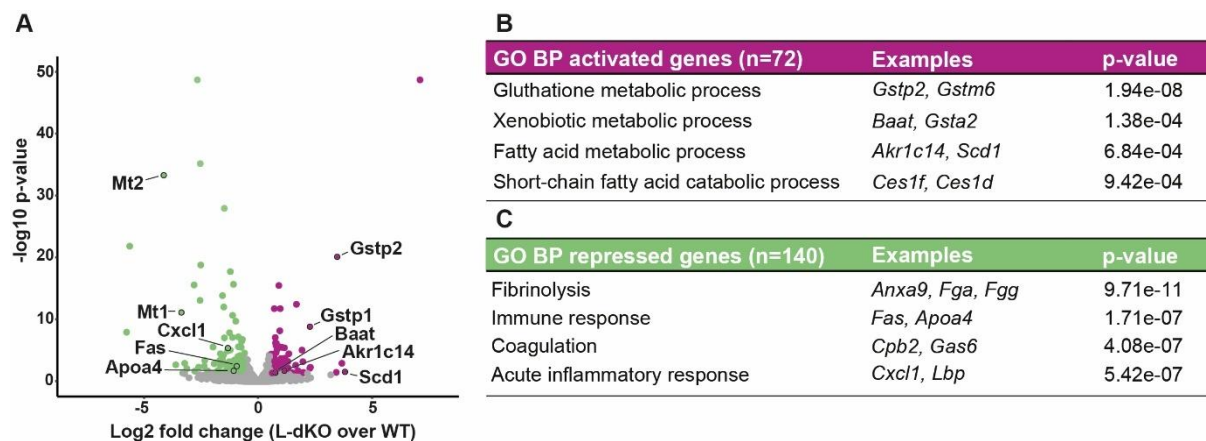


Figure 28: Livers from L-TR4OE mice show activation of sterol and lipid metabolic genes on chow diet.

A: RNA-Seq of livers from chow-fed WT and L-TR4OE mice (n = 3 per group, green = 11 repressed genes, purple = 51 activated genes, $\log_2(\text{fold change}) < -0.58$ and > 0.58 respectively, adjusted p-value < 0.05) B: Gene ontology biological process of the 51 activated genes. C: Average transcript per million (TPM) count of example activated target genes normalized to WT average. (n= 3 per group, * : adjp-value < 0.05)

4.4.2 L-dKO mice show reduced inflammation and immune response and increased xenobiotic and lipid metabolism upon HFD.

To understand the response of the L-dKO mice to HFD and their protection against fibrosis on DIAMOND diet, RNA-Seq analysis of the transcriptome of HFD fed mice was analyzed to identify the changes in transcription of the livers of those mice upon metabolic stress.



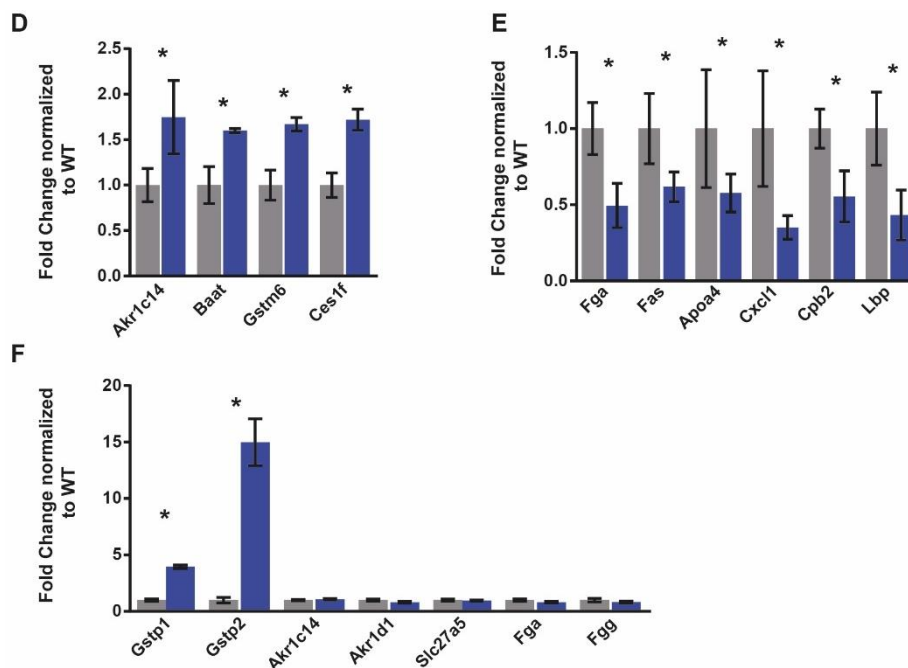


Figure 29: L-dKO mice show up-regulation of lipid and xenobiotic metabolism and down regulation of immune response and inflammation upon HFD.

A: RNA-Seq of livers from HFD-fed WT and L-dKO mice (n = 3 per group, green = 140 repressed genes, purple = 72 activated genes, $\log_2(\text{fold change}) < -0.58$ and > 0.58 respectively, adjusted p-value < 0.05) B: Gene ontology biological process of the 72 activated genes. C: Gene ontology biological process of the 140 repressed genes. D: Average transcript per million (TPM) count of example activated target genes normalized to WT average. (n= 3 per group, * : adjp-value < 0.05) E: Average transcript per million (TPM) count of example repressed target genes normalized to WT average. (n= 3 per group, * : adjp-value < 0.05) F: RT-qPCR of example activated and repressed genes normalized to WT average. (n= 12 WT and 14 L-dKO, * : p-value < 0.05)

On HFD, 140 genes were repressed and 72 activated in L-dKO mouse livers with a minimal fold-change of 1,5 (Fig. 29A, Suppl. Table 6). GO BP analysis of up-regulated genes were associated with glutathione, xenobiotic and lipid metabolism suggesting an improvement in the capacity of the liver of these mice for detoxification and protection against lipotoxicity (Fig. 29B). GO BP for down-regulated genes are linked to immune and inflammatory response as well as fibrinolysis and coagulation, two processes for which the liver secretome is of prime importance and that are disturbed by nutritional challenge (Fig. 29C). Genes such as *Akr1c14*, a member of the Aldo-keto reductase family, *Baat*, the key enzyme for bile acid amidation, *Gstm6*, a membre of the glutathione S-transferase family, and *Cesf1*, an enzyme involved in xenobiotic hydrolyzation, are significantly activated in the L-dKO mouse liver (Fig. 29D). Examples of down-regulated genes include *Fas*, an apoptosis receptor, *Cxcl1*, a macrophage marker, *Lbp*, the lipopolysaccharide binding protein and *Apoa4* involved in lipid transport in hepatocytes and immune cells, indicating a marked reduction in immune response and

inflammation (Fig. 29E). As in the chow diet fed L-dKO mice, *Gstp2* was activated as well as *Gstp1* and this difference was validated by RT-qPCR (Fig. 29F).

Overall, the RNA-Seq data from the livers of L-dKO mice suggest that they have an increased capacity to handle lipotoxicity as well as immune response and inflammation usually related with HFD. On a larger scale, these characteristics could explain why L-dKO mice are protected against fibrosis on DIAMOND diet.

4.4.3 L-TR4OE mice show increased collagen synthesis and fibroblast maturation and reduced drug and lipid metabolism upon HFD.

L-TR4OE mice are prone to fibrosis on HFD and DIAMOND diet. Therefore, RNA-Seq was performed to analyze the transcriptome of HFD fed L-TR4OE mice and identify the pathways involved in this susceptibility to metabolic challenges.

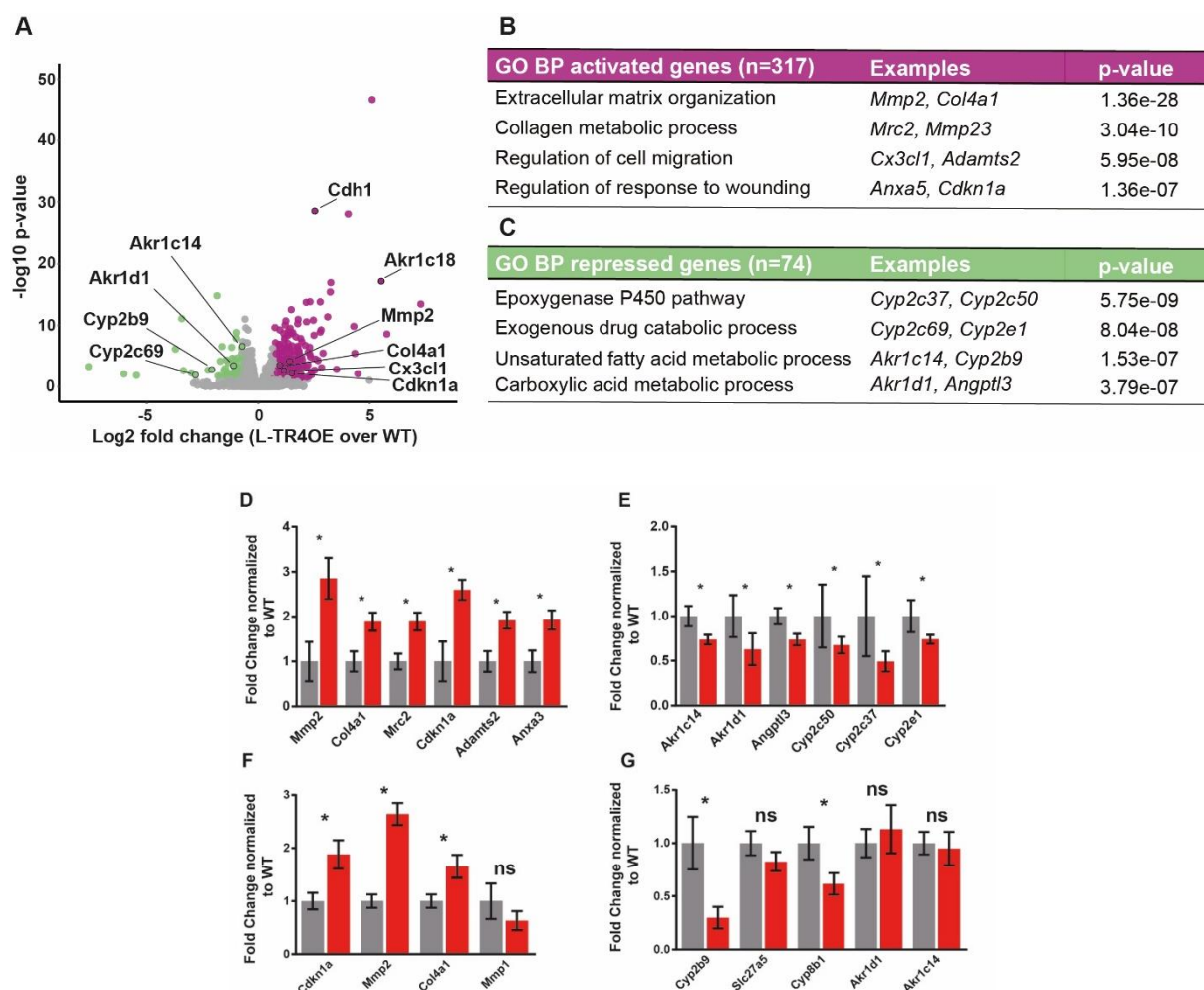


Figure 30: L-TR4OE mice show up-regulation of collagen and fibroblast production and down regulation of xenobiotic and lipid metabolism upon HFD.

A: RNA-Seq of livers from HFD-fed WT and L-TR4OE mice (n = 3 per group, blue = 74 down-regulated genes, red = 317 up-regulated genes, $\log_2(\text{fold change}) < -0.58$ and > 0.58 respectively, adjusted p-value < 0.05) B: Gene ontology biological process of the 317 up-regulated genes. C: Gene ontology biological process of the 74 down-regulated genes. D: Average transcript per million (TPM) count of example up-regulated target genes normalized to WT average. (n= 3 per group, * : adjp-value < 0.05) E: Average transcript per million (TPM) count of example down-regulated target genes normalized to WT average. (n= 3 per group, * : adjp-value < 0.05) F: RT-qPCR of example activated genes normalized to WT average. (n= 8 WT and 13 L-TR4OE, * : p-value < 0.05) G: RT-qPCR of example repressed genes normalized to WT average. (n= 8 WT and 13 L-TR4OE, * : p-value < 0.05)

The analysis identified 317 activated genes and 74 repressed genes in L-TR4OE mouse livers (Fig. 30A, Suppl. Table 7). GO BP analysis of up-regulated genes was enriched with extracellular matrix organization, collagen metabolism and response to wounding which is relevant with the state of increased fibrosis reflecting hepatocyte degeneration and fibroblast compensation (Fig. 30B). GO BP for down-regulated genes are linked to epoxygenase P450 pathway, drug catabolic process and lipid metabolism (Fig. 30C). Up-regulation of genes such as *Mmp2*, a collagenase involved in cell migration, *Col4a1*, a subunit of collagen and *Cdkn1a*, a cell arrest gene involved in apoptosis is consistent with fibrosis associated with cellular stress, hepatocyte death and renewal and fibroblast differentiation (Fig. 30D). This increase in gene expression was validated by RT-qPCR (Fig. 30F).

Examples of down-regulated genes include *Akr1c14* and *Akr1d1*, involved in lipid and bile acid synthesis, *Angptl3*, a lipoprotein lipase inhibitor, and *Cyp* family members involved in lipid and xenobiotic hydrolyzation and oxidation indicating a decrease in the capacity of the livers to respond to the lipid and oxidative overload associated with HFD (Fig. 30E). Repression of *Cyp2b9* and *Cyp8b1* was validated by RT-qPCR but not for *Akr1c14* and *Akr1d* (Fig. 30G). Overall, the RNA-Seq data from the livers of L-TR4OE mice is consistent with the accelerated progression towards fibrosis on HFD with increased inflammation and fibrogenesis and reduced capacity to handle the lipid overload induced by the diet.

4.5 Metabolite profiling identify a role in PUFA and bile acid synthesis for TR2 and TR4.

4.5.1 TR2/4 deletion and TR4 overexpression affect PUFA and bile acid metabolism.

To identify the impact of the loss of TR2/4 or the overexpression of TR4 on metabolite composition and the link between metabolic changes and susceptibility to liver fibrosis and degeneration, untargeted metabolomic analysis on L-dKO and L-TR4OE mouse livers after HFD was performed.

Out of the 661 metabolites detected in the L-dKO samples and WT littermates, 80 metabolites were differentially represented between the two groups with a minimum fold-change of 1.5 up or down. Orthogonal-orthogonal projections to latent structures discriminant analysis (OPLS-DA) of all biological replicates showed a clear separation between the two genotypes (Fig. 31A). SMPDB Pathway-associated metabolite sets enrichment reveal that the differentially represented metabolites are predominantly bile acid and poly unsaturated fatty acid species (Fig. 31B).

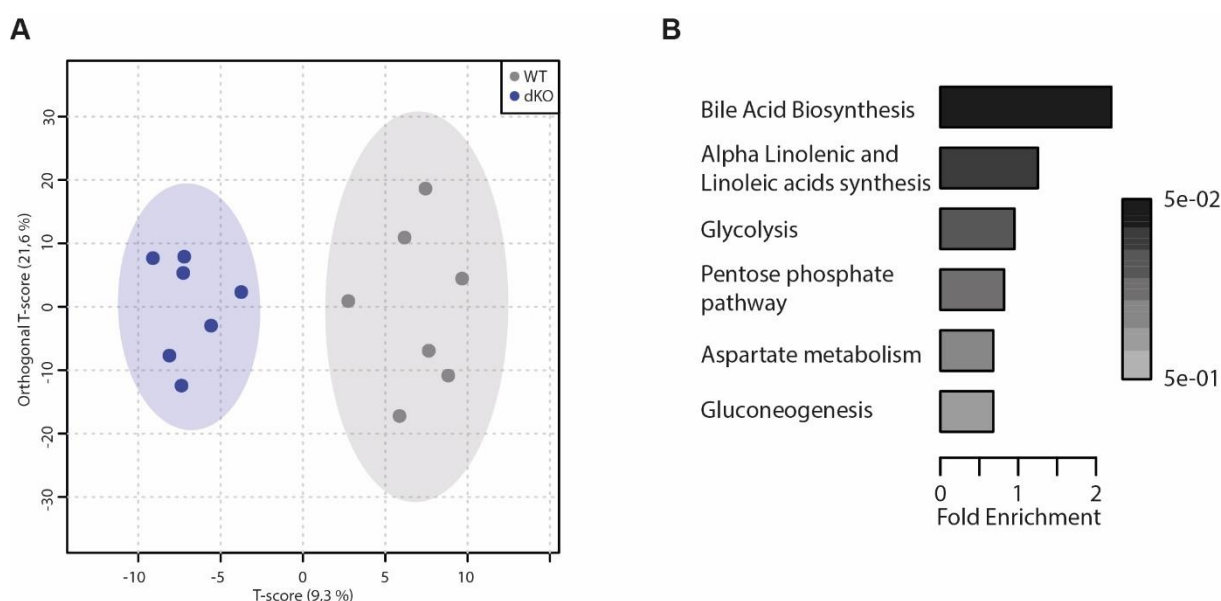


Figure 31: Livers of L-dKO mice have changes in their composition of bile acid species and PUFAs upon HFD.

A: Orthogonal-orthogonal projections to latent structures discriminant analysis (OPLS-DA) of all metabolite features from 661 metabolites detected in WT and L-dKO mouse livers (n= 7 per group). B: SMPDB Pathway-associated metabolite sets enrichment from the 80 metabolites with a 1.5 fold-change up or down-regulation in the L-dKO mouse livers.

The same analysis was performed on L-TR4OE mouse livers and detected 648 metabolites, 112 of which were differentially represented compared to WT littermate livers. The OPLS-DA showed a tight clustering between the biological replicates of each genotype (Fig. 32A). As in the L-dKO mice, the top terms for the SMPDB Pathway-associated metabolite sets enrichment showed involvement in long chain fatty acid metabolism and bile acid synthesis (Fig. 32B). Therefore, further analysis was performed on these two class of metabolites.

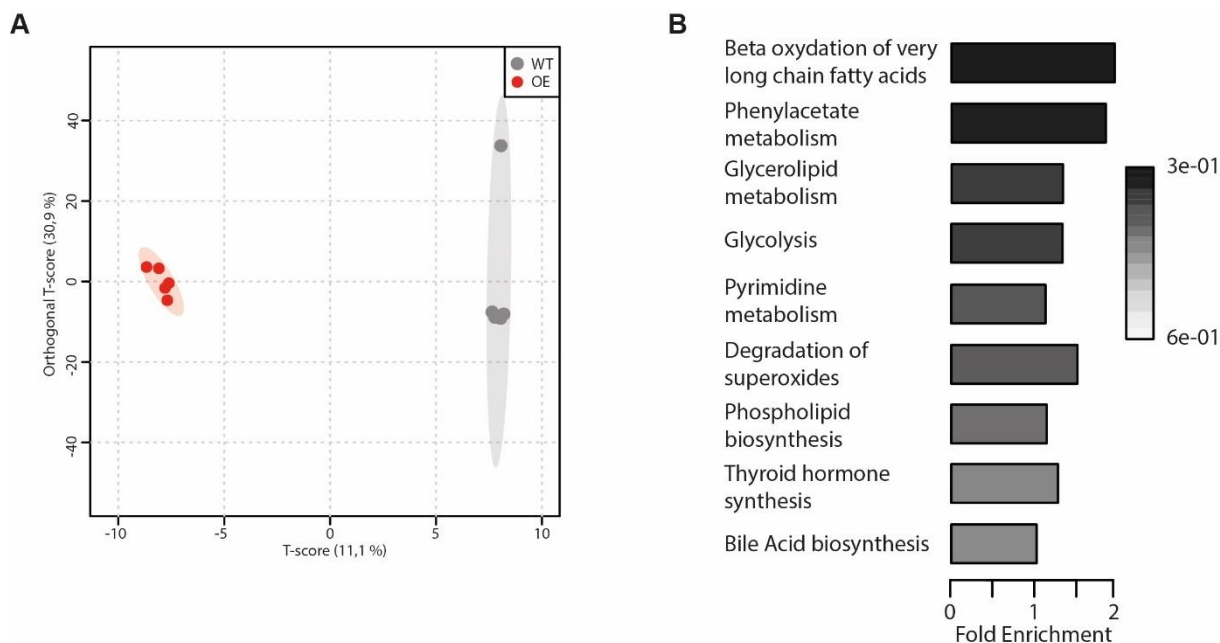


Figure 32: Livers of L-TR4OE mice have changes in their composition of fatty acid and bile acid species upon HFD.

A: Orthogonal-orthogonal projections to latent structures discriminant analysis (OPLS-DA) of all metabolite features from 648 metabolites detected in WT and L-TR4OE mouse livers (n= 5 per group). B: SMPDB Pathway-associated metabolite sets enrichment from the 112 metabolites with a 1.5 fold-change up or down-regulation in the L-TR4OE mouse livers.

4.5.2 L-dKO mice have increased amidated bile acids and n-6 PUFA species in the liver.

All detected primary and secondary bile acid values in L-dKO livers were calculated and plotted in Figure 33. There is a significant increase of the amidated form of bile acids coming from the alternative pathway of bile acid synthesis and deriving from the chenodeoxycholic acid (CDCA). Tauro-CDCA, tauro- β -muricholate and tauro-ursodeoxycholate (T-UDCA) are up-regulated in L-dKO mouse livers (Fig. 33A&C, Suppl. Table 8). As seen previously in the RNA-Seq data, this increase is concomitant with an increase of the transcript of the bile acid amino acid N-acyltransferase (*Baat*). Also, TR4 showed DNA binding sites in the vicinity of the *Baat* gene, suggesting a direct regulation of the gene. This enzyme is responsible for bile acid hydrolyzation through amidation by addition of glycine or taurine (Fig. 33B). This step occurs after the bile acid synthesis and is of prime importance for solubilization of bile acids and facilitating their secretion in the bile canaliculi and into the small intestine. The anion transporter *Sico1a4* involved in the secretion of amidated bile acids was also up-regulated in L-dKO mice. Amidation of CDCA and β -muricholate occur after primary bile acid synthesis whereas UDCA amidation occurs after secretion and reabsorption as a secondary bile acid. T-UDCA has been shown to promote BA enterohepatic circulation (Yunjing Zhang et al., 2019). Oxolithocholate is increased in the L-dKO livers and is a secondary bile acid coming from the degradation of

tauro-CDCA by the microbiome (Fig. 33C). This increase in BA transporter combined with BA amidation and secondary BA suggest that L-dKO mouse livers have an improved potential for BA solubilization and secretion and induction of the BA enterohepatic circulation which was suggested by the transcriptomic profiles showing an improved xenobiotic handling.

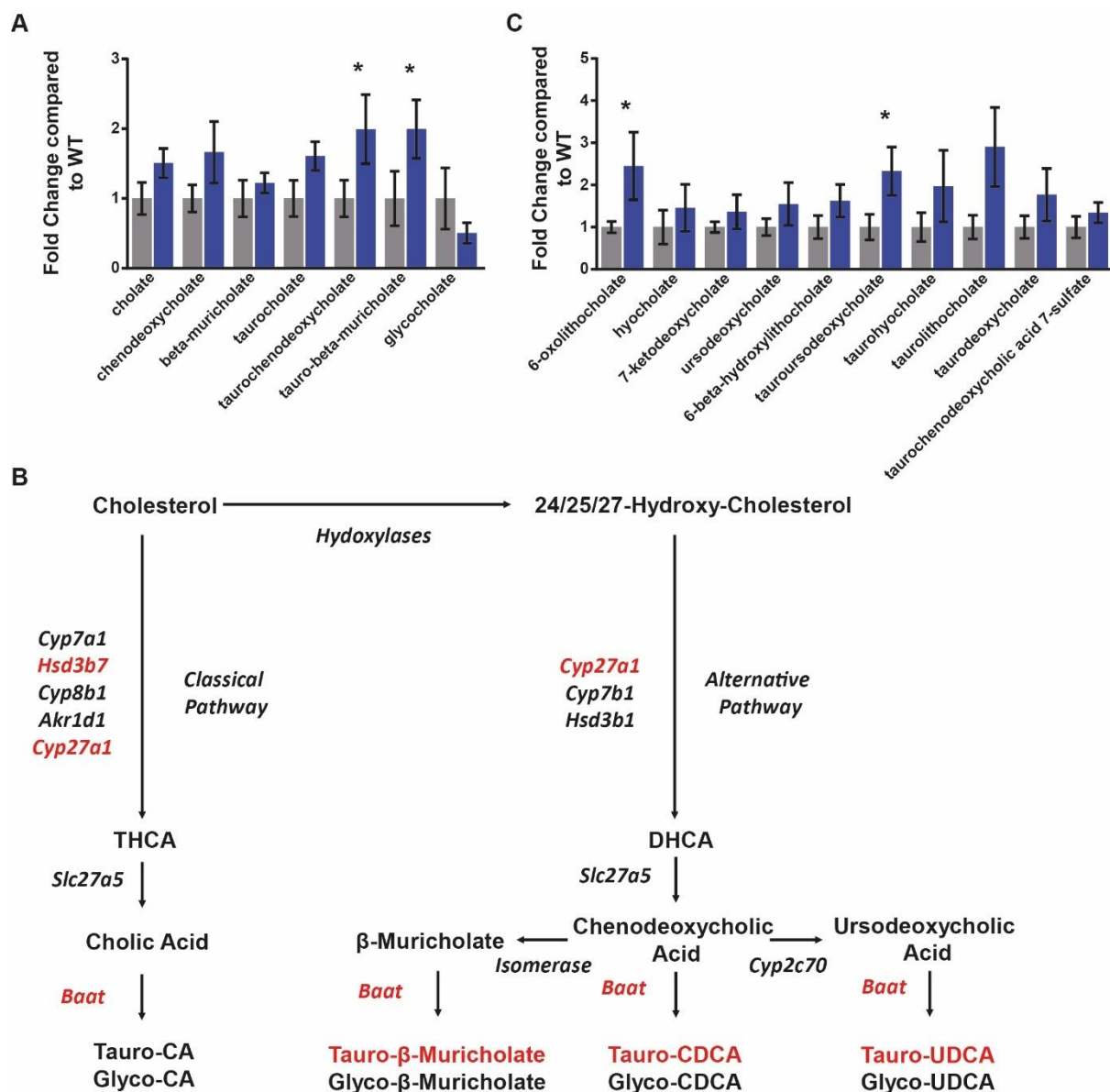


Figure 33: L-dKO mice have increased amidated primary bile acids from the alternative pathway in the liver after HFD.

A: Average fold change of primary bile acids of L-dKO mouse livers compared to WT littermates. *: adjp-value < 0.05, n=7 per group. B: Integrative view of genes and metabolites involved in primary bile acid synthesis. The metabolites and genes more/less expressed in the L-dKO are represented in red/green. C: Average fold change of secondary bile acids of L-dKO mouse livers compared to WT littermates. *: adjp-value < 0.05, n= 7 per group.

Concerning PUFA, L-dKO mouse livers showed an increase in two n-6 long chain PUFAs coming from the elongation and desaturation of linoleic acid: docosatrienoic acid (22:3 n-6) and docosapentaenoic acid (22:5 n-6) (Fig.34A, Suppl. Table 8). This increase correlates with the increase seen in Elov12 and 5 on Fads2 on the RNA-Seq data from those livers that would promote PUFA elongation and desaturation (Fig. 34B&C). Those genes also had response elements for TR4 suggesting direct regulation. These mild changes in PUFA composition is difficult to interpret since the role of these specific species are not well studied yet.

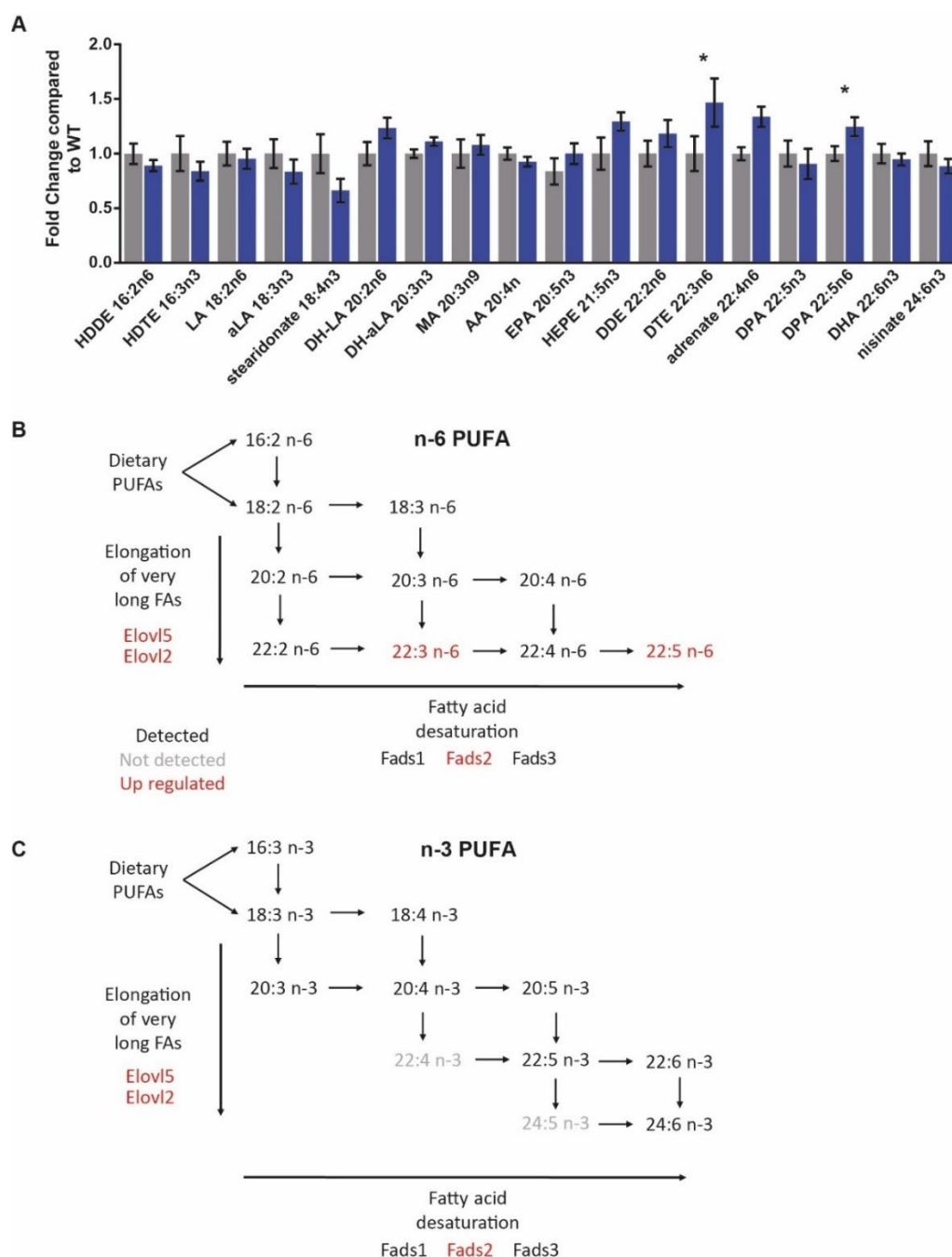


Figure 34: L-dKO mice have an increase in some long-chain n-6 PUFA species in the liver after HFD.

A: Average fold change of n-3 and n-6 PUFAs of L-dKO mouse livers compared to WT littermates. *: adjp-value < 0.05, n=7 per group. B: Integrative view of genes and metabolites

involved in n-6 and n-3 PUFA synthesis. The metabolites and genes more/less expressed in the L-dKO are represented in red/green.

4.5.3 L-TR4OE mice have accumulation of alternative bile acids and reduced PUFA species in the liver.

L-TR4OE mouse livers have an increased accumulation of the primary BA CDCA and β -muricholate as well as their amidated forms tauro-CDCA and tauro- β -muricholate (Fig. 35A Suppl. Table 9). The decrease of the enzymes of the classical pathway of BA synthesis suggests a shunt towards the alternative pathway even though the levels of cholic acid does not seem affected (Fig. 35B). The accumulation of CDCA and β -muricholate is likely caused by a reduction in the *Baat* enzyme that decreases the capacity of the liver for primary BA amidation and solubilization. This delay seems to be partially compensated post-transcriptionally since high levels of tauro-CDCA and tauro- β -muricholate are also detected but this accumulation could also be attributable to a delay in secretion of solubilized BA. Indeed, the anion transporter *Sico1a4* involved in the secretion of amidated bile acids was repressed in L-TR4OE mice. Also, a decrease of the secondary BA oxolithocholate deriving from tauro-CDCA suggests that the pool of secreted tauro-CDCA is reduced and the enterohepatic circulation of BA is slowed down resulting in a longer residence time of BA in hepatocytes before being secreted. Reduced solubilization and increased time in the cytoplasm of hepatocytes can affect the intracellular toxicity of BA on the liver and induce cholestasis (Marschall & Beuers, 2013).

This decrease in BA transporter combined with conjugated and unconjugated primary BA accumulation and reduction in secondary BA suggest that L-TR4OE mouse livers have a deficit in BA excretion and an increased residence time that can cause liver damage and would be consistent with susceptibility to fibrosis.

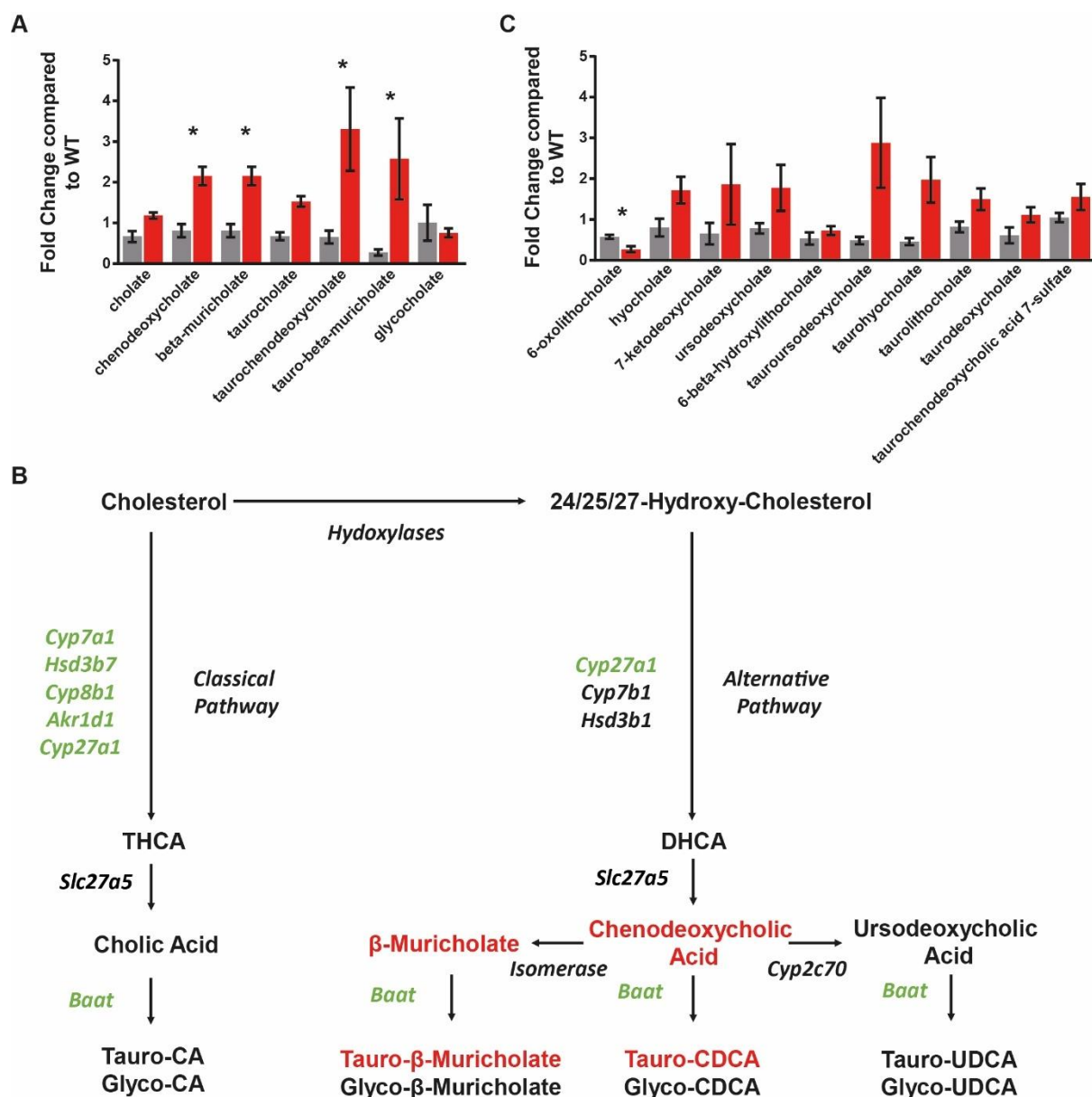


Figure 35: L-TR4OE mice have accumulation of primary bile acids from the alternative pathway in the liver after HFD.

A: Average fold change of primary bile acids of L-TR4OE mouse livers compared to WT littermates. *: adjp-value < 0.05, n=5 per group. B: Integrative view of genes and metabolites involved in primary bile acid synthesis. The metabolites and genes more/less expressed in the L-TR4OE are represented in red/green. C: Average fold change of secondary bile acids of L-TR4OE mouse livers compared to WT littermates. *: adjp-value < 0.05, n=5 per group.

Regarding PUFA composition, L-TR4OE mouse livers show decrease in n-6 and n-3 PUFA content : hexadecadi- and trienoate (HDDE and HDTE), dihomo-gamma-linolenate (DH-gLA), arachidonic acid (AA) and docoshexaenoate (DHA) are all reduced (Fig. 36A, Suppl. Table 9). HDDE and HDTE are two dietary PUFA derived from linoleic acid and have beneficial effects on atherosclerosis and inflammation (Müller et al., 2005). DH-gLA and AA have known anti-

inflammatory effects (Fan & Chapkin, 1998). Overall, this decrease in anti-inflammatory PUFA could play an important role in the onset of liver fibrosis in L-TR4OE mice (Fig. 36B&C).

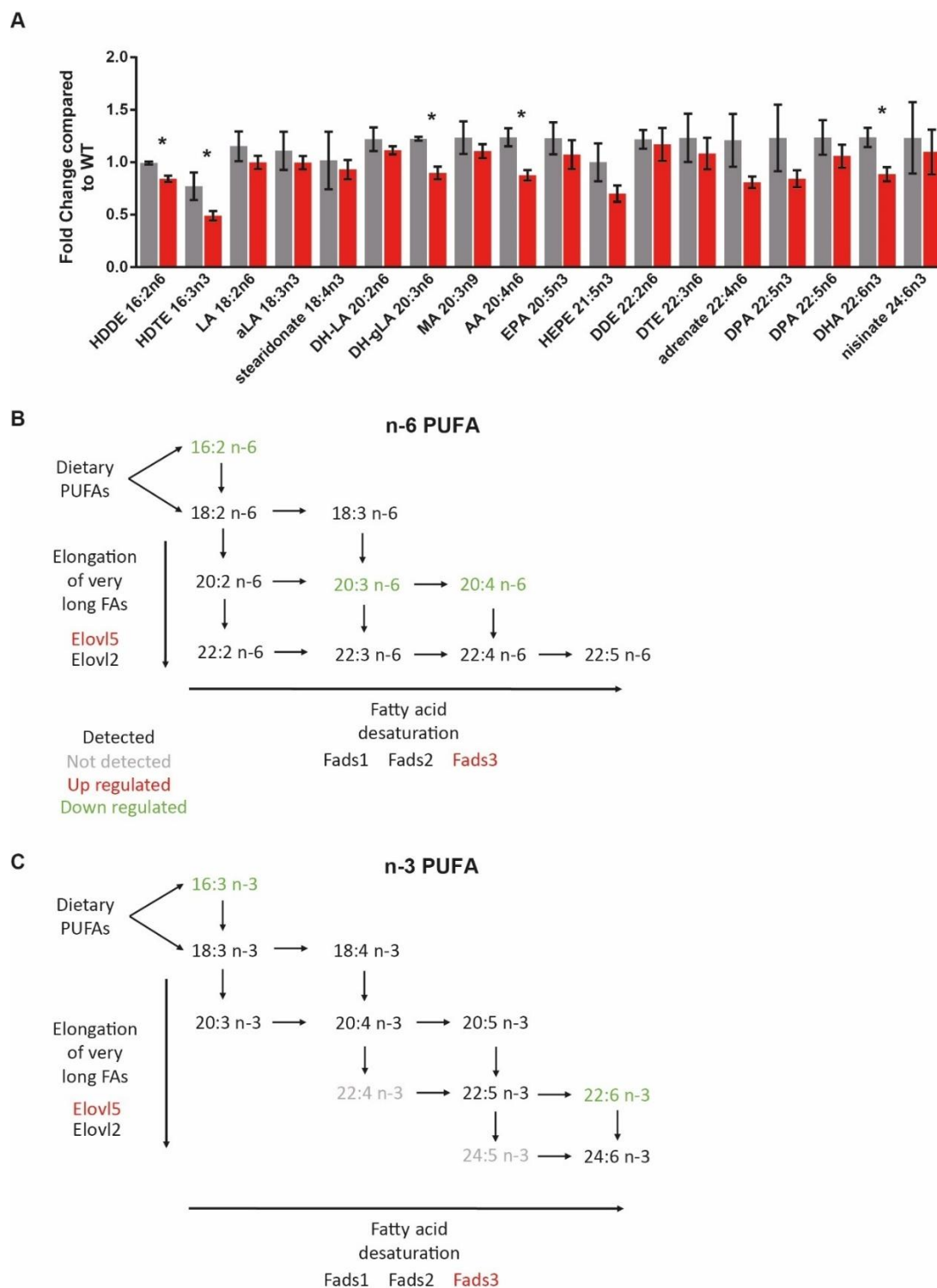


Figure 36: L-TR4OE mice have a decrease in dietary and long chain PUFAs in the liver after HFD.

A: Average fold change of n-3 and n-6 PUFAs of L-TR4OE mouse livers compared to WT littermates. *: adjp-value < 0.05, n=5 per group. B: Integrative view of genes and metabolites

involved in n-6 and n-3 PUFA synthesis. The metabolites and genes more/less expressed in the L-dKO are represented in red/green.

In total, this study identified an important role for TR2 and TR4 in the progression of NAFLD and the transition between hepatic steatosis and liver fibrosis. By binding close to genes involved in lipid and bile acid metabolism and inflammation in the vicinity of FXR and PPAR α binding sites, TR2/4 are modulating the transcriptional response to HFD and the effects of lipotoxicity. They control PUFA and BA synthesis key enzymes such as *Baat*, *Scd2* and *Elov15*. Studies on liver-specific gain and loss of function mouse models showed TR2/4 activity promotes inflammation and fibrogenesis and is detrimental for the progression of NAFLD under a profibrotic nutritional challenge.

5. Discussion

5.1 Hepatic TR2 and TR4 regulate inflammation and fibrogenesis and control the transition between NAFL and NASH.

The work conducted in this thesis describes the role of the orphan nuclear receptors TR2 and TR4 in adipose tissue and liver.

Metabolic characterization of adipose tissue specific TR2/4 dKO mice showed that the main parameters regarding glucose and lipid metabolism were unchanged. Body weight and fat mass composition were identical after 20 weeks of HFD. By histology, no differences in lipid accumulation or adipose tissue structure was detected. A-dKO mice showed similar glucose tolerance and insulin sensitivity than their wildtype littermates. Furthermore, no differences in food intake, EE and RER were observed while monitored in calorimetric cages.

While the action of TR2/4 in adipose tissue physiology seemed negligible, an important role for these receptors in the hepatic response to calory rich diets and in the progression of NAFLD was identified. The loss of both receptors specifically in the liver had a protective effect against the development of liver fibrosis in response to DIAMOND diet while the overexpression of TR4 in the liver potently induced liver fibrosis on both HFD and DIAMOND diet. These results suggest that TR2/4 have a detrimental effect on hepatocyte function and survival when they are subject to a nutritional stress and lipotoxicity. In those models, the triglyceride accumulation and the degree of steatosis of the L-dKO and L-TR4OE livers was comparable to wildtype mice on HFD. The difference between the genotypes relied on the capacity of the hepatocytes to handle this lipid accumulation and lipotoxicity and those processes seemed dependent on TR2 and TR4.

One of the biggest challenges with the NAFLD epidemic is the capacity to predict the evolution of the disease for the patient and to prevent the transition between fatty liver and NASH. The identification of the factors triggering inflammation in the patients suffering from hepatic steatosis to advance into NASH still remain unclear (Schuster et al., 2018). In this context, this study offers a unique characterization of TR2/4 as potential regulators linking lipotoxicity, inflammation and fibrogenesis in the liver. The implication of this finding is that the protection against NASH in the L-dKO mice and the susceptibility to NASH in the L-TR4OE mice are probably translated respectively in a lower/higher risk for HCC. Long exposure to HFD or DIAMOND diet or other nutritional challenges such as choline-deficient HFD are available options to study the advanced stages of NAFLD (Febbraio et al., 2019).

To determine the biological processes regulated by the two receptors, ChIP-Seq was performed for TR2 and TR4 in wildtype livers. The regions co-bound by TR2 and TR4 are primarily promoter regions that are associated with genes related to fundamental biological functions such as mRNA maturation and splicing and protein processing in the endoplasmic reticulum. Similar binding pattern for these biological processes was identified in other cell types such as erythroid cells (Shi et al., 2014). This tight regulation of DR1 motifs in the promoter region of these genes suggests that these functions are the core functions shared by TR2 and TR4 in multiple cell types. Those common functions are fundamental and are probably the cause for early embryonic lethality in the TR2 $-/-$ TR4 $-/-$ embryos (Shyr et al., 2009). Furthermore, the two receptors share binding close to fatty acid metabolism genes showing a tissue-specific function of both receptors. Motifs for ETS factors, YY1 and PPAR α are found in the vicinity of the TR4 DR1 motifs. The ETS factor family is composed of transcription activators and repressors involved in essential processes such as human adult and embryonic development, cell cycle, apoptosis (Hsing, Wang, Rennie, Cox, & Cherkasov, 2019). Aberrant expression of these factors has also been described in many cancer types which makes them prominent target for cancer treatment (Gutierrez-Hartmann, Duval, & Bradford, 2007; Sizemore, Pitarresi, Balakrishnan, & Ostrowski, 2017). YY1 is an ubiquitously expressed factor involved in transcription regulation of genes involved in proliferation, differentiation and apoptosis. It binds enhancers and promoters, forming loops as a dimer to regulate transcription regulation (Weintraub et al., 2017). Interestingly, it was shown to be involved in hepatic steatosis, liver fibrogenesis and hepatocarcinogenesis partially by regulating the expression and activity of PPAR γ and FXR (H. Liu et al., 2019; Lu et al., 2014; M. Zhang et al., 2017). The presence of PPAR α motif in the overlap of TR2 and TR4 suggests that those receptors are regulating common target genes with RXR heterodimers.

This pattern was even more pronounced in the TR4 specific binding sites in the liver. As seen in erythroid cells, TR4 ChIP-Seq also identified more distant regions that are not shared with TR2 that bind in the vicinity of genes involved in cholesterol metabolism, apoptosis and hepatocellular carcinoma, revealing the cell-specific function of TR4 in hepatocytes. In L-TR4OE mice, the cistrome of TR4 was expanded with an increase in the amplitude of binding and a wider number of low affinity DNA binding sites. However, gained peak by TR4 overexpression were involved in similar processes than in the wildtype liver situation. Genes involved in lipid and bile acid metabolism such as *Baat*, *Slc27a5*, *Elovl5* or *Fads2* have multiple binding sites for TR4 in promoter and enhancer regions. Motif analysis identified enrichment for DR1 factors including HNF4 α and PPAR α . FXR IR1 motif was also enriched. Both TR2 and TR4 binding sites and the functions of their associated closest genes indicate a spatial and functional proximity between these receptors and the known functions of RXR heterodimers.

It was previously established that the transcriptional regulation through DR motifs opened a new paradigm of regulation for class II nuclear receptors where several RXR heterodimers could target the same binding sites (Ronald M. Evans & Mangelsdorf, 2014). In particular, the regulation of lipid metabolism by the liver offers a typical example where the action of multiple factors is integrated to adjust the ever changing energetic needs throughout the day (Boergesen et al., 2012). For example, LXRs, PPARs and RXRs have an extensive and complex crosstalk on shared binding sites. Our data suggests that TR2/4 are part of this regulatory nexus and add another layer of regulation on these fine-tuned metabolic genes.

To identify direct targets of TR2/4, RNA-Seq was performed to show the transcriptional changes in L-dKO mice and L-TR4OE mice. In the L-dKO mice, transcriptional changes were minimal in the absence of a nutritional challenge. L-TR4OE mice showed basal activation in some genes involved in steroid hormone synthesis. L-dKO mice showed predominantly repression of genes whereas L-TR4OE mice had mainly activation of genes as expected since these receptors are thought to act mainly as transcriptional activators in metabolic organs. More drastic changes appeared after a HFD challenge. The loss of TR2 and TR4 effectively reduced the inflammatory response in the livers. Also, lipid metabolic genes and genes involved in xenobiotic metabolism, i.e. drug, metabolite and bile acid metabolism were induced in those livers, participating in the protection against lipotoxicity. Overexpression of TR4 had opposite effects with activation of inflammation and fibrogenesis as well as inhibition of lipid and drug metabolism, consistent with the increase in liver fibrosis. Taken together, CHIP-Seq and RNA-Seq analysis reveal an important role of TR2 and TR4 in lipid, bile acid and xenobiotic metabolism and their connection to liver inflammation and fibrosis.

Metabolomics analysis showed that the main effect on metabolism in the liver-specific mouse models concerned the bile acid synthesis and amidation pathways as well as bile acid secretion. Bile acid synthesis from cholesterol is restricted to the liver and represents the major catabolic pathway of cholesterol responsible for about 90% of its breakdown. Bile acid synthesis requires 17 enzymatic reactions in different subcellular compartments of the hepatocyte and its key enzymatic steps are tightly regulated by nuclear hormone receptors, other transcription factors, and posttranscriptional signaling chains. The end products are glycine- and taurine-conjugated bile acids, which are effectively secreted into bile with <2% of bile acids remaining in the unconjugated form (Marschall & Beuers, 2013). In the L-dKO mice, increased taurine amidation of primary bile acids from the alternative pathway (CDCA and derivatives) was consistent with activation of *Baat* expression, the enzyme catalyzing the amidation of BA. Also, increased levels of secondary BA suggested an increase in secretion of primary BA after amidation and acceleration of the recapture of these secondary BA. In the

L-TR4OE mice, non-amidated and taurine amidated primary BA were increased with a down regulation of *Baat*, suggesting a delay in amidation of primary BA and an increase in the residence time of BA before secretion. Bile acids are the endogenous ligands identified to activate FXR, PXR and CAR activity (D.-J. Shin & Wang, 2019). Combined with the ChIP-Seq and RNA-Seq analysis, these changes in bile acid composition suggest that TR2/4 can bind close to known FXR target genes controlling bile acid metabolism and secretion.

The PUFA composition was also altered in both L-dKO and L-TR4OE mice. L-dKO mice showed an increase in long chain n-6 anti-inflammatory PUFA consistent with protection against inflammation. On the other hand, L-TR4OE mice showed a defect in dietary n-3 and n-6 PUFA and reduction of anti-inflammatory long chain PUFA consistent with increased inflammation and fibrosis. PUFAs are known to be the natural ligands of the PPARs (Gross et al., 2016). In the liver, PPAR α is the predominant isoform and controls lipid oxidation as well as repression of pro-inflammatory pathways. PPAR α motif is very similar to TR4 motif and was enriched in the TR2/4 ChIP-Seq, suggesting that they bind on common target genes. This crosstalk can explain the transcriptional changes seen in lipid metabolism and inflammatory and pro-fibrogenic pathways. Furthermore, TR2/4 could control the activity of PPAR α by modulating the amount and availability of its natural ligands.

Whether the regulation of inflammation and fibrogenesis on one side and lipid and bile acid metabolism on the other side happen as independent events or are connected remains an open question. The data suggest that there's direct regulation of inflammatory and fibrogenic genes by TR2/4 happening in parallel of the regulation of bile acids and PUFAs pathways and that these various effects could be controlled through separate crosstalk with FXR and PPAR α .

Overall, this study showed that TR2 and TR4 are involved in the progression of NAFLD in response to a dietary challenge. Both receptors, TR4 in particular, bind close to genes involved in inflammation, fibrogenesis, PUFA and bile acid metabolism and regulate their transcription. Their transcriptional program influences the BA enterohepatic cycle and the PUFA composition, affecting cellular stress, inflammation and fibrogenesis. Their transcriptional programs overlap with known FXR and PPAR α target genes and impact the composition of their ligands in the liver. This suggests a possible regulation of RXR partners in metabolic control through genomic and ligand-dependent mechanisms. Increased activity of the two receptors on HFD is detrimental for the transition between hepatic steatosis and liver fibrosis.

5.2 TR2/4 and FXR as regulators of bile acid metabolism

Bile acids are detergent molecules synthesized from cholesterol exclusively in the liver (T. Li & Chiang, 2014; Russell & Setchell, 1992). Under physiological conditions, most bile acids exist as glycine or taurine conjugates and are referred to as bile salts. Bile acids have several important functions in the liver. Conversion of cholesterol into bile acids in the liver accounts for a major fraction of daily cholesterol turnover in humans (Chiang, 2009). Biliary bile acid secretion generates bile flow and facilitates hepatobiliary secretion of various endogenous metabolites and xenobiotics (Trauner & Boyer, 2003). In the gallbladder, bile acids form mixed micelles with phospholipids and cholesterol to increase cholesterol solubility and decrease bile acid toxicity. Once released into the small intestine, bile acids facilitate the intestinal digestion and absorption of dietary cholesterol, fat, and other lipophilic nutrients. In addition, bile acids are signaling molecules that activate several nuclear receptors to regulate various cellular processes ranging from lipid and glucose metabolism, drug metabolism to immunity (T. Li & Chiang, 2014). They have been identified as the endogenous ligands for FXR which is one of the main drivers of bile acid homeostasis and enterohepatic circulation (Matsubara et al., 2013; H. Wang, Chen, Hollister, Sowers, & Forman, 1999). FXR is particularly sensitive to cholic acid, deoxycholic acid, chenodeoxycholic acid and lithocholic acid (H. Wang et al., 1999).

Hepatic bile acid levels are maintained by the control of uptake, synthesis, metabolism and export. In response to an excess of bile acid, FXR will promote bile acid secretion and amidation and regulate the enterohepatic excretion of BA. FXR is also involved in lipid and drug metabolism and the total knockout for FXR induces hepatic steatosis and cholestasis (Sinal et al., 2000). This effect is potentiated by HFD with ectopic localization of FXR in new genomic loci and increased transcription activation of its target genes in presence of its synthetic ligand (J. Lee et al., 2012). It was shown to promote the final step of bile acid synthesis by bile acid-CoA synthetase (BACS encoded by *Slc27a5*) and bile acid amidation by bile acid-CoA:aminoacid N-transferase (BAAT) in the liver (Pircher et al., 2003).

In our mouse models, L-dKO mice had induction of *Baat* which resembles FXR activation whereas *Baat* was down-regulated in the L-TR4OE mice which would be consistent with repression of FXR activity. The bile acid composition also follows the same trend : L-dKO mice have increased tauro-amidated bile acid content consistent with increased amidation. On the other hand, L-TR4OE mice show accumulation of non-amidated bile acids due to reduction of amidation through repression of *Baat*.

In addition to promoting BA amidation, FXR is regulating amidated BA secretion in the bile ducts by regulating ATP-binding cassette (ABC) transporters. Bile salt exporting pump (BSEP, also termed ABCB11), is a major efflux transporter of bile acids from liver to gallbladder. BSEP deficiencies are associated with several forms of cholestasis (Stieger, Meier, & Meier, 2007). *Fxr*-null mice fed CA-supplement diet showed intrahepatic cholestasis, similar with that of the human BSEP deficiency. Reporter gene assays showed that the *BSEP* promoter was positively controlled by FXR and bile acids (Plass et al., 2002). In *Fxr*-null mice, BSEP expression was significantly reduced and the FXR agonist GW4064 cannot induce the expression of *Bsep* gene thus confirming that FXR controls BSEP expression (Moschetta, Bookout, & Mangelsdorf, 2004). Expression of another ABC transporter ABCB4 is significantly reduced in *Fxr*-null mice, where GW4064-induced *Abcb4* expression is not observed. FXR activates bile acid secretion by increasing *Abcb11* and *Abcb4* expression. In the RNA-Seq data of livers from HFD-fed mice, there is a slight but non-significant up-regulation of *Abcb11* in L-dKO mice and down-regulation in L-TR4OE mice on HFD. *Abcb4* shows no change in expression in those models. This change in *Abcb11* expression follow the trend towards FXR signaling potentiation in the L-dKO livers with increased BA secretion and repression of FXR activity in L-TR4OE with amidated bile acid accumulation.

Also, FXR has an indirect inhibitory effect on bile acid synthesis and reabsorption by activating the expression of SHP, a transcriptional co-regulator expressed mainly in the liver and the gallbladder (Goodwin et al., 2000; D.-J. Shin & Wang, 2019). SHP has been shown to repress bile acid synthesis enzymes *Cyp7a1* and *Cyp8b1* (Kerr et al., 2002; L. Wang et al., 2002). These genes are unchanged in L-dKO mice and repressed in L-TR4OE, indicating a probable compensation of the defective BA amidation and secretion by reducing BA synthesis. This suggests a direct interaction between TR4 and FXR on a subset of FXR activated genes where TR4 is disrupting FXR function in the L-TR4OE mice. In response, FXR tries to compensate indirectly through SHP by increasing repression of BA synthesis in the L-TR4OE mice.

The same principle applies to BA uptake with the regulation of the genes coding for basolateral BA transporters. Na⁺-taurocholate cotransporting polypeptide (NTCP, also termed solute carrier 10A1; SLC10A1) and organic anion-transporting peptides (OATPs, also named SLCO family) are the major bile acid transporters in the hepatocellular basolateral membrane for the uptake of bile acids and organic solutes from portal vein to liver (T. Li & Chiang, 2014). NTCP is responsible for the uptake of conjugated bile acids, whereas the OATPs are largely involved in the uptake of unconjugated bile acids. Hepatic NTCP expression is repressed by SHP that is induced by FXR upon bile acid activation (Denson et al., 2001). FXR activation controls basolateral bile acid reabsorption in hepatocyte by repressing the OATP proteins encoded by the *Slco* gene family through SHP (Matsubara et al., 2013; Trauner & Boyer, 2003). Those

proteins are involved in the transport of xenobiotic compounds such as bile acids, bilirubin, steroid hormone conjugates etc. (Martin, Juliane, Katrin, Walter, & Theresia, 2011). Cholic acid treatment activated *Slco1a4* and repressed *Slco1a1* in the mouse livers (Maeda et al., 2004). RNA-Seq results showed non-significant trends in the expression of NTCP and OATP transporters in the L-dKO and L-TR4OE livers after HFD. L-dKO mice showed increased expression of *Slco1a1* and *Slco1a4* while L-TR4OE showed decreased expression for the same transporters and no changes in NTCP expression. Those changes are consistent with the increased hepatic uptake of secondary BA such as tauro-oxolithocholate in the L-dKO mice and reduced uptake of the same bile acid in L-TR4OE mice.

In total, L-dKO mice show increased expression of *Baat*, amidation of primary BA and expression of bile duct transporters suggesting an improved BA secretion. This effect seems predominant compared to the increase in bile acid basolateral uptake transporters in the protective effect against fibrosis. On the other hand, L-TR4OE mice have unconjugated primary BA accumulation due to decreased *Baat* expression as well as amidated primary BA accumulation due to reduction in *Abcb11*. Compensatory events involving repression of BA synthesis and uptake are probably modulated by SHP through FXR activation but are not sufficient to prevent liver fibrosis. Our data suggest that TR2/4 and FXR have opposite effects on the regulation of bile acid metabolism. The nature of this antagonism would need further study but a direct competition for the regulation of those FXR activated genes is likely. FXR IR1 motif were enriched in the vicinity of TR4 binding sites. Also, in the L-TR4OE where primary bile acids are increased, FXR fails to activate some target genes in a context of high ligand content. The high expression of TR4 in this context suggests that its increased availability and binding capacity is blocking the accessibility for FXR to bind its target genes. Overall, TR2/4 and FXR/SHP functions appear to be intertwined in the regulation of the BA enterohepatic circulation. The proposed model of regulation for TR2/4 with FXR is shown in Figure 37. Further investigation will be necessary to characterize precisely the crosstalk and possible competition between TR2/4 and FXR in the regulation of cholesterol and bile acid metabolism.

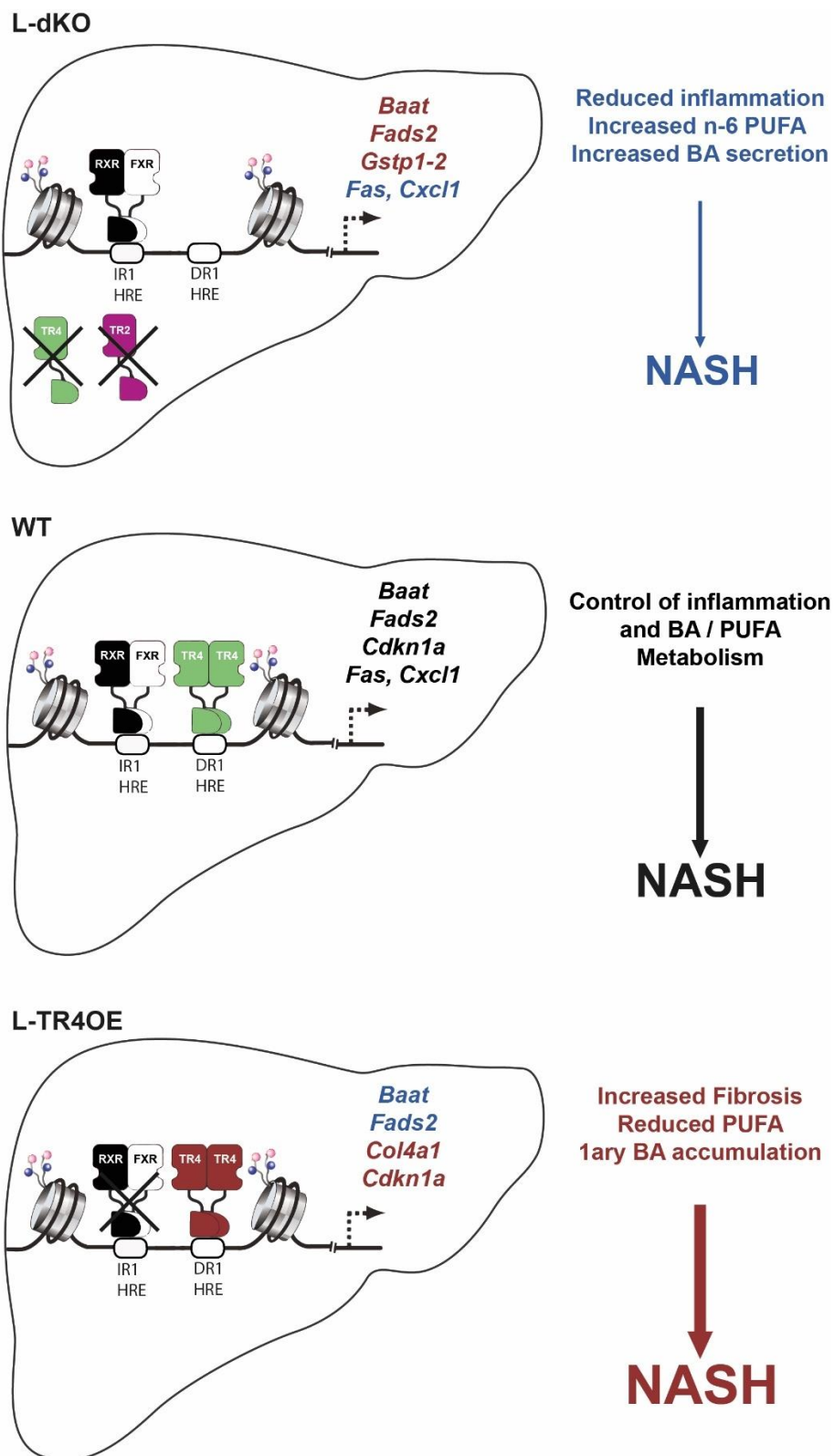


Figure 37: Regulation of NASH progression by TR2 and TR4.

In wildtype livers, TR2 and TR4 participate in the progression of hepatic steatosis towards NASH by promoting inflammation and lipotoxicity on HFD. In the L-dKO mice, the absence of TR2 and TR4 reduces liver inflammation and promotes long chain PUFA synthesis and amidation and secretion of primary bile acids which have a protective effect against NASH. On the other hand, L-TR4OE mice suffer from early fibrosis on HFD with reduced PUFA content and accumulation of primary bile acid by a lack of amidation and secretion.

5.3 TR4 and PPAR α as regulators of fatty acid metabolism and inflammation.

PPAR α is the predominant PPAR isoform expressed in hepatocytes. Its role in lipid metabolism and response to fasting was firstly described using PPAR α $-/-$ mice (Kersten et al., 1999; Leone, Weinheimer, & Kelly, 1999). During fasting, PPAR α mobilizes free fatty acid (FFA) from the white adipose tissue and hepatic uptake of these lipids through FGF21 secretion (Lundåsen et al., 2007). PPAR α will induce the expression of the lipid catabolism program to provide energy to the rest of the body in this low energy context. Loss of PPAR α induces lipid accumulation in the liver, impaired lipid oxidation as well as hypoglycemia, hypothermia and elevated plasma FFA (Kersten et al., 1999). During HFD feeding, loss of PPAR α also promotes lipid accumulation and massive hepatic steatosis. This effect is caused by a combined downregulation of the lipid oxidation enzymes controlled by PPAR α such as *Cyp4a10* and *Cyp4a14* and up-regulation of PPAR γ that promotes lipid synthesis and storage (Patsouris, Reddy, Müller, & Kersten, 2006). Similar effects were observed in liver-specific PPAR α KO mice. Those mice showed lipid accumulation in hepatocytes after fasting or a HFD challenge (Montagner et al., 2016). Also, PPAR α deficiency in the liver aggravates NASH after methionine choline deficient (MCD) diet.

PPAR α activation through ligand treatment can effectively counteract the progression of NASH and fibrosis (Ip, Farrell, Hall, Robertson, & Leclercq, 2004; Shiri-Sverdlov et al., 2006). In ApoE2 deficient mice and in MCD diet fed mice, fibrates and PPAR α ligand Wy14,643 could reverse hepatic fibrosis. In addition to regulation of lipid metabolism, this protective effect was obtained by the strong repressive effect of PPAR α on inflammation (Delerive et al., 1999; Gervois et al., 2001). PPAR α has anti-inflammatory effects through a tethering-based transrepression of AP1, NF- κ B and C/EBP β signaling. Furthermore, it was shown that this transrepressive effect of PPAR α was necessary and sufficient to induce protection against liver fibrosis, independently of lipid metabolism regulation (Pawlak et al., 2014). Liver-specific DNA-binding mutant PPAR α (PPAR α -DIM) rescue in PPAR α null mice showed similar protection against liver fibrosis on MCD diet combined with Wy14,643 treatment than PPAR α wildtype rescue. Importantly, those mice could not regulate lipid oxidation and showed advanced hepatic steatosis but this did not affect the antifibrotic effect of the ligand, showing a predominance of the anti-inflammatory effect of PPAR α in the protection against NASH. Interestingly, L-dKO and L-TR4OE mice show similarities with this model with a susceptibility for hepatic steatosis comparable to wildtype mice but a different propensity to develop liver fibrosis. L-dKO are protected against liver fibrosis on DIAMOND diet, similarly to the PPAR α -DIM mice on MCD diet whereas L-TR4OE show a mirror image of the PPAR α -DIM with a faster progression into NASH. In other words, L-dKO mice resemble PPAR α activation whereas L-

TR4OE mice resemble liver-specific PPAR α knockout mice in their sensitivity to liver fibrosis. This suggests that PPAR α might act as a transcriptional repressor of TR2 and TR4. TR2/4 and PPAR α are opposite regulators of liver fibrosis. An additional cue in that direction is the fact that PPAR α mRNA expression progressively decreases as NASH progresses in humans, impairing the capacity of hepatocytes to counteract lipotoxicity (Francque et al., 2015). In wildtype mice, the measurement of TR2 and TR4 expression on DIAMOND diet showed that these receptors follow an opposite trend than PPAR α with a marked induction of their expression in a pro-fibrotic context.

As seen above with FXR, the regulation of PPAR α signaling could be mediated through DNA binding and chromatin accessibility. In the ChIP-Seq data for TR2 and TR4, motif analysis showed enrichment for PPAR α motif which is very similar to the TR4 motif. Furthermore, bound regions were associated with lipid and cholesterol metabolic genes that are also bound by PPAR α , suggesting a target overlap between these receptors. Similar overlaps have previously been shown between PPAR α , RXRs and LXRs, suggesting that TR2/4 might be a novel partner in this complex regulatory nexus (Boergesen et al., 2012).

Also, ligand availability for PPAR α might be modified by TR2/4 through regulation of PUFA metabolism. In addition to being direct repressors of inflammation, PUFAs have been shown to be natural ligands of PPARs (Calder, 2006; Delerive, Fruchart, & Staels, 2001; Gross et al., 2016). In response to n-3 PUFA supplementation, PPAR α was shown to interact with NF- κ B and prevent inflammation in response to an ischemia-reperfusion injury in the liver (Zúñiga et al., 2011). As seen before, TR2/4 are controlling PUFA composition in hepatocytes. L-dKO mice have increased long chained n-6 PUFA whereas L-TR4OE have reduction in CLA and long chain n-6 and n-3 PUFA. These changes in PUFA composition can affect the activity of PPAR α in the liver. In L-dKO mice, increased PUFA can potentiate the activation of PPAR α and its anti-inflammatory effects. On the other hand, decreased PUFA in L-TR4OE would have the opposite effect with decreased PPAR α signaling and increased inflammation.

Taken together, the crosstalk between TR2/4 and PPAR α probably involves multiple layers of regulation. As DR1 nuclear receptors, they recognize similar DNA sequences and can therefore bind to similar genes and potentially compete with each other. Furthermore, TR2/4 and PPAR α convergence on inflammatory and fibrogenic pathways is possibly mediated through protein-protein interaction where PPAR α would tether and repress the TR2/4 activity. In the L-TR4OE mice, the excess of nuclear TR4 could impair the repressive activity of PPAR α and promote inflammation and fibrosis. Also, TR2/4 activity alters the PUFA composition and could control PPAR α activation through regulation of the available pool of endogenous ligand.

In the L-dKO mice, accessible DR1 motifs and increased PUFA content would allow PPAR α to repress inflammation more effectively. Following that principle, L-TR4OE mice would have reduced PPAR α activity due to the reduction in natural ligand and decreased genomic accessibility.

5.4 TR4 antagonism as a therapeutic strategy against NAFLD.

The identification of a natural ligand for TR4 would be a valuable tool to study in depth the transcriptional program of this receptor. It would also be the initial step for designing potential synthetic ligands and drugs to modulate the action of this receptor in the progression of NAFLD. Indeed, characterizing the type of molecule capable of binding the ligand binding domain of TR4 and activate TR4 activity would give precious information on the desired structure for potential synthetic activators and inhibitors of its ligand binding pocket.

Initial discovery of steroid hormone receptors quickly led to the identification of dozens of related proteins with unknown ligand that were named orphan receptors (R. M. Evans, 1988). Since their discovery, multiple strategies have been successful in de-orphanising some of those receptors. The use of the co-transfection assay combining an expression vector for the nuclear receptor of interest with a reporter sequence containing a hormone response element enabled the identification of specific ligands and target genes (Giguère, Hollenberg, Rosenfeld, & Evans, 1986). By using the co-transfection assay with large libraries of potential ligands, the identification of modulators of orphan nuclear receptors activity flourished, starting with the discovery of 9-cis retinoic acid as the natural ligand of RXR (Levin et al., 1992). This “reverse endocrinology” strategy identified signaling properties for dietary lipids, xenobiotics, vitamins and their derivatives (Kliwer, Lehmann, & Willson, 1999). Those ligands showed lower affinity compared to the previously known hormones. Also, the receptors responding to those ligands were directly regulating the molecular pathways producing them (Ronald M. Evans & Mangelsdorf, 2014). The nature of the ligand was a predictive hallmark of the subsequent metabolic pathway regulated by their bound receptors. For example, the finding that fatty acids are endogenous ligands for PPARs led to the discovery that PPARs govern fatty acid metabolism. Likewise, the binding of cholesterol metabolites by LXR predicted its future role in controlling cholesterol metabolism. Physiologic links were quickly established in the growing list of orphan receptors that were being adopted into the nuclear receptor superfamily. Furthermore, a major role of the receptors for these lipid-derived ligands was to maintain the homeostasis and availability of the ligands themselves. These include fatty acid metabolism for the PPARs, sterol homeostasis for the liver X receptors (LXRs), bile acid homeostasis for the farnesoid X receptor (FXR), and endobiotic/xenobiotic metabolism for pregnane X and

constitutive androstane receptors (PXR and CAR) (Ronald M. Evans & Mangelsdorf, 2014). Over time, the link between the different classes of ligands and their receptors became more complex than it seemed. Most of the RXR partners have been shown to bind more than one specific class of ligands and to share them with other receptors. For example, xenobiotics have been shown to activate both PXR and CAR. LXRs were first identified to respond to cholesterol but have been shown since then to respond to bile acids along with FXR, CAR and VDR (Mazaira et al., 2018). Based on this principle, it seems likely that TR4 could follow the same trend and eventually be added to the list of NR responding to PUFA and BA. The results from this study show that TR2/4 have an impact on BA and PUFA composition in the liver. By controlling lipid, bile acid and xenobiotic metabolism, it is likely that members of these families of metabolite could activate TR2/4.

Published studies on TR4 putative ligands also orientate the search and the type of micromolecule that could act as natural or synthetic ligand for TR4. *In vitro* studies showed that TR4 activity could be modulated by polyunsaturated fatty acid (PUFA) species and intermediary metabolites, as well as thiazolidinedione (TZD) and could act as potential ligands (Xie et al., 2009). The TZD rosiglitazone was identified as a ligand of PPAR γ with the capacity to suppress diabetes (Lebovitz, 2002). The finding that TZD could transactivate TR4 shows the potential for a crosstalk with PPAR γ in the regulation of metabolic pathways. Other studies show that the γ -linoleic acid could induce the TR4 target genes, including *ApoE* and *Pepck*, via induction of TR4 transactivation (N.-C. Liu et al., 2007; Tsai et al., 2009). Retinol and retinoic acid have also been shown to activate TR4 *in vitro* by alleviating the auto-repressed structure of the LBD of TR4 (Zhou et al., 2011). However, the efficiency of those ligands with TR4 has not yet been studied *in vivo*. Furthermore, these classes of ligands have already been described to regulate the activity of other nuclear receptors such as the PPARs, posing the question of ligand specificity (Gross et al., 2016).

To identify specific endogenous ligands, new approaches have been developed since the rise of the co-transfection assay. In *Drosophila*, the UAS-Gal4 system derived from yeast has been used for decades to induce and study the action of specific genes in a tissue dependent manner (Duffy, 2002). Also, fly models were developed to study the impact of nutrients such as lipids on the progression of neurodegenerative diseases (Cho, Bang, & Toh, 2014). A new strategy inspired by the co-transfection assay consists in developing an *in vitro* assay based on a stable cell line expressing a chimeric protein containing the DBD of the Gal4 protein and the LBD of the nuclear receptor of interest. By using a TR4 LBD - Gal4 DBD fusion protein in combination with a UAS-Luciferase reporter, large scale ligand screening can be performed to identify positive hits. In this assay, the affinity of the ligand is proportionate to the luciferase

activity. The stable cell line co-expressing the UAS-Luciferase reporter and the TR4-Gal4 chimeric protein has been generated during this project and further testing for validation is undergoing as well as library designing for ligand screening. The crystal structure of the ligand-free TR4 LBD reveals an auto-repressed conformation with C-terminal half of helix 10 filling the ligand binding pocket similar to RXR α and COUP-TFII (Zhou et al., 2011). The 560 Å³ ligand pocket was predicted to be suitable for an average small molecule such as retinoids or steroids. The final objective is to identify and validate the specificity and efficiency of potential agonists for TR4. From the TR4 targets identified in the liver, co-transfection assays can be performed to validate ligand efficiency. Testing these compounds *in vivo* in the genetic models at our disposal would be an efficient way to validate the potency and specificity of the ligands on TR4. Importantly, using a ligand would allow validation of the direct regulation of the main target genes regulated by TR4 and involved in the progression of NAFLD. Ligand identification will serve as an entry point to decipher in better details the exact transcriptional program of those two receptors. Ultimately, ligand identification for TR2/4 can be applied in the development of novel therapeutic intervention to treat and prevent NAFLD progression.

Taken together, these findings highlight the importance of TR2/4 in liver physiology and their involvement in promoting the metabolic and inflammatory events leading to NASH in response to a dietary challenge. Both receptors, TR4 in particular, bind close to genes involved in inflammation, fibrogenesis, PUFA and bile acid metabolism and regulate their transcription. Their transcriptional programs overlap with known FXR and PPAR α target genes and impact the composition of their ligands in the liver. L-dKO mice show increased BA amidation and secretion. L-TR4OE mice have unconjugated and amidated primary BA accumulation due to decreased BA amidation and secretion. This data suggests that TR2/4 and FXR have opposite effects on the regulation of bile acid metabolism and that TR2/4 promote cholestasis.

Similarly, TR2/4 activity alters the PUFA composition and could mediate PPAR α activation through regulation of the available pool of endogenous ligand. In the L-dKO mice, increased long-chain PUFA could allow PPAR α to repress inflammation more effectively. On the other hand, L-TR4OE mice have reduced PPAR α activity and increased inflammation due to the reduction in specific PUFA species in hepatocytes.

FXR IR1 and PPAR α DR1 motifs were enriched in the vicinity of TR4 binding sites suggesting a crosstalk between these factors and TR2/4 through possible direct interaction and co-regulation of common target genes. This implies a potential binary regulation of RXR partners in metabolic control through genomic and ligand-dependent mechanisms. To study the transcriptional program of these two receptors further, ligand identification will be necessary for the development of novel therapeutic intervention to treat and prevent NAFLD progression.

References

- Abril, N., Ruiz-Laguna, J., & Pueyo, C. (2012). Differential expression of the *Gstp2* gene between the aboriginal species *Mus spretus* and the laboratory mouse *Mus musculus*. *Mutation Research/Genetic Toxicology and Environmental Mutagenesis*, 747(1), 53-61. doi: <https://doi.org/10.1016/j.mrgentox.2012.03.015>
- Adams, D. H. (2003). *Hepatology: a Textbook of Liver Disease*, 4th edition: Edited by Zakim, Boyer. Philadelphia: Saunders, 2003, £230.00, pp 1765. ISBN 0-7216-9051-3. *Gut*, 52(8), 1230-1231.
- Asgharpour, A., Cazanave, S. C., Pacana, T., Seneshaw, M., Vincent, R., Banini, B. A., . . . Sanyal, A. J. (2016). A diet-induced animal model of non-alcoholic fatty liver disease and hepatocellular cancer. *Journal of Hepatology*, 65(3), 579-588. doi: <https://doi.org/10.1016/j.jhep.2016.05.005>
- Beato, M. (1991). Transcriptional control by nuclear receptors. *The FASEB journal*, 5(7), 2044-2051.
- Berg, J. M. (1989). DNA binding specificity of steroid receptors. *Cell*, 57(7), 1065-1068.
- Boergesen, M., Pedersen, T. Å., Gross, B., van Heeringen, S. J., Hagenbeek, D., Bindsbøll, C., . . . Mandrup, S. (2012). Genome-wide profiling of liver X receptor, retinoid X receptor, and peroxisome proliferator-activated receptor α in mouse liver reveals extensive sharing of binding sites. *Molecular and Cellular Biology*, 32(4), 852-867. doi: 10.1128/MCB.06175-11
- Bookout, A. L., Jeong, Y., Downes, M., Yu, R. T., Evans, R. M., & Mangelsdorf, D. J. (2006). Anatomical Profiling of Nuclear Receptor Expression Reveals a Hierarchical Transcriptional Network. *Cell*, 126(4), 789-799. doi: <https://doi.org/10.1016/j.cell.2006.06.049>
- Brown, M. S., & Goldstein, J. L. (2008). Selective versus Total Insulin Resistance: A Pathogenic Paradox. *Cell Metabolism*, 7(2), 95-96. doi: 10.1016/j.cmet.2007.12.009
- Brunt, E. M., Wong, V. W. S., Nobili, V., Day, C. P., Sookoian, S., Maher, J. J., . . . Rinella, M. E. (2015). Nonalcoholic fatty liver disease. *Nature Reviews Disease Primers*, 1, 15080. doi: 10.1038/nrdp.2015.80
- Calder, P. C. (2006). n-3 polyunsaturated fatty acids, inflammation, and inflammatory diseases. *The American journal of clinical nutrition*, 83(6), 1505S-1519S.
- Campbell, A. D., Cui, S., Shi, L., Urbonya, R., Mathias, A., Bradley, K., . . . Engel, J. D. (2011). Forced TR2/TR4 expression in sickle cell disease mice confers enhanced fetal hemoglobin synthesis and alleviated disease phenotypes. *Proceedings of the National Academy of Sciences*, 108(46), 18808. doi: 10.1073/pnas.1104964108
- Chandra, V., Huang, P., Hamuro, Y., Raghuram, S., Wang, Y., Burris, T. P., & Rastinejad, F. (2008). Structure of the intact PPAR- γ -RXR- α nuclear receptor complex on DNA. *Nature*, 456(7220), 350.
- Chang, C., Kokontis, J., Acakpo-Satchivi, L., Liao, S., Takeda, H., & Chang, Y. (1989). Molecular cloning of new human TR2 receptors: A class of steroid receptor with multiple ligand-binding domains. *Biochemical and Biophysical Research Communications*, 165(2), 735-741. doi: [https://doi.org/10.1016/S0006-291X\(89\)80028-2](https://doi.org/10.1016/S0006-291X(89)80028-2)

- Chang, C. S., Kokontis, J., & Liao, S. T. (1988). Molecular cloning of human and rat complementary DNA encoding androgen receptors. *Science*, *240*(4850), 324. doi: 10.1126/science.3353726
- Chang, C. S., L Da Silva, S., Ideta, R., Lee, Y. F., Yeh, S., & Burbach, J. P. H. (1994). Human and rat TR4 orphan receptors specify a subclass of the steroid receptor superfamily. *Proceedings of the National Academy of Sciences of the United States of America*, *91*, 6040-6044. doi: 10.1073/pnas.91.13.6040
- Chen, L.-M., Wang, R.-S., Lee, Y.-F., Liu, N.-C., Chang, Y.-J., Wu, C.-C., . . . Chang, C. (2008). Subfertility with Defective Folliculogenesis in Female Mice Lacking Testicular Orphan Nuclear Receptor 4. *Molecular Endocrinology*, *22*(4), 858-867. doi: 10.1210/me.2007-0181
- Chen, Y.-T., Collins, L. L., Uno, H., & Chang, C. (2005). Deficits in Motor Coordination with Aberrant Cerebellar Development in Mice Lacking Testicular Orphan Nuclear Receptor 4. *Molecular and Cellular Biology*, *25*(7), 2722. doi: 10.1128/MCB.25.7.2722-2732.2005
- Chiang, J. Y. (2009). Bile acids: regulation of synthesis. *Journal of lipid research*, *50*(10), 1955-1966.
- Cho, K. S., Bang, S. M., & Toh, A. (2014). Chapter 26 - Lipids and Lipid Signaling in Drosophila Models of Neurodegenerative Diseases. In R. R. Watson & F. De Meester (Eds.), *Omega-3 Fatty Acids in Brain and Neurological Health* (pp. 327-336). Boston: Academic Press.
- Chong, H. K., Infante, A. M., Seo, Y.-K., Jeon, T.-I., Zhang, Y., Edwards, P. A., . . . Osborne, T. F. (2010). Genome-wide interrogation of hepatic FXR reveals an asymmetric IR-1 motif and synergy with LRH-1. *Nucleic Acids Research*, *38*(18), 6007-6017. doi: 10.1093/nar/gkq397
- Contreras, A. V., Torres, N., & Tovar, A. R. (2013). PPAR- α as a key nutritional and environmental sensor for metabolic adaptation. *Advances in nutrition (Bethesda, Md.)*, *4*(4), 439-452. doi: 10.3945/an.113.003798
- Dawn, X. Z., & Christopher, K. G. (2013). Towards an understanding of cell-specific functions of signal-dependent transcription factors. *Journal of Molecular Endocrinology*, *51*(3), T37-T50. doi: 10.1530/JME-13-0216
- Delerive, P., De Bosscher, K., Besnard, S., Berghe, W. V., Peters, J. M., Gonzalez, F. J., . . . Staels, B. (1999). Peroxisome proliferator-activated receptor α negatively regulates the vascular inflammatory gene response by negative cross-talk with transcription factors NF- κ B and AP-1. *Journal of Biological Chemistry*, *274*(45), 32048-32054.
- Delerive, P., Fruchart, J.-C., & Staels, B. (2001). Peroxisome proliferator-activated receptors in inflammation control. *Journal of Endocrinology*, *169*(3), 453-459.
- Denson, L. A., Sturm, E., Echevarria, W., Zimmerman, T. L., Makishima, M., Mangelsdorf, D. J., & Karpen, S. J. (2001). The Orphan Nuclear Receptor, shp, Mediates Bile Acid-Induced Inhibition of the Rat Bile Acid Transporter, ntcp. *Gastroenterology*, *121*(1), 140-147. doi: 10.1053/gast.2001.25503
- Duffy, J. B. (2002). GAL4 system in drosophila: A fly geneticist's swiss army knife. *genesis*, *34*(1-2), 1-15. doi: 10.1002/gene.10150
- Durinck, S., Spellman, P. T., Birney, E., & Huber, W. (2009). Mapping identifiers for the integration of genomic datasets with the R/Bioconductor package biomaRt. *Nature Protocols*, *4*(8), 1184-1191. doi: 10.1038/nprot.2009.97

- Eden, E., Navon, R., Steinfeld, I., Lipson, D., & Yakhini, Z. (2009). GOrilla: a tool for discovery and visualization of enriched GO terms in ranked gene lists. *BMC Bioinformatics*, *10*(1), 48. doi: 10.1186/1471-2105-10-48
- Erion, D. M., Popov, V., Hsiao, J. J., Vatner, D., Mitchell, K., Yonemitsu, S., . . . Samuel, V. T. (2013). The role of the carbohydrate response element-binding protein in male fructose-fed rats. *Endocrinology*, *154*(1), 36-44. doi: 10.1210/en.2012-1725
- Evans, R. M. (1988). The steroid and thyroid hormone receptor superfamily. *Science (New York, N.Y.)*, *240*(4854), 889-895. doi: 10.1126/science.3283939
- Evans, Ronald M., & Mangelsdorf, David J. (2014). Nuclear Receptors, RXR, and the Big Bang. *Cell*, *157*(1), 255-266. doi: 10.1016/j.cell.2014.03.012
- Fan, Y.-Y., & Chapkin, R. S. (1998). Importance of Dietary γ -Linolenic Acid in Human Health and Nutrition. *The Journal of Nutrition*, *128*(9), 1411-1414. doi: 10.1093/jn/128.9.1411
- Febbraio, M. A., Reibe, S., Shalapur, S., Ooi, G. J., Watt, M. J., & Karin, M. (2019). Preclinical Models for Studying NASH-Driven HCC: How Useful Are They? *Cell Metabolism*, *29*(1), 18-26. doi: <https://doi.org/10.1016/j.cmet.2018.10.012>
- Font-Burgada, J., Sun, B., & Karin, M. (2016). Obesity and Cancer: The Oil that Feeds the Flame. *Cell Metabolism*, *23*(1), 48-62. doi: <https://doi.org/10.1016/j.cmet.2015.12.015>
- Francque, S., Verrijken, A., Caron, S., Prawitt, J., Paumelle, R., Derudas, B., . . . Staels, B. (2015). PPAR α gene expression correlates with severity and histological treatment response in patients with non-alcoholic steatohepatitis. *Journal of Hepatology*, *63*(1), 164-173. doi: 10.1016/j.jhep.2015.02.019
- Gentric, G., Desdouets, C., & Celton-Morizur, S. (2012). Hepatocytes Polyploidization and Cell Cycle Control in Liver Physiopathology. *International journal of hepatology*, *2012*, 8. doi: 10.1155/2012/282430
- Gervois, P., Vu-Dac, N., Kleemann, R., Kockx, M., Dubois, G., Laine, B., . . . Staels, B. (2001). Negative regulation of human fibrinogen gene expression by peroxisome proliferator-activated receptor α agonists via inhibition of CCAAT box/enhancer-binding protein β . *Journal of Biological Chemistry*, *276*(36), 33471-33477.
- Giguère, V., Hollenberg, S. M., Rosenfeld, M. G., & Evans, R. M. (1986). Functional domains of the human glucocorticoid receptor. *Cell*, *46*(5), 645-652. doi: 10.1016/0092-8674(86)90339-9
- Giguère, V., Yang, N., Segui, P., & Evans, R. M. (1988). Identification of a new class of steroid hormone receptors. *Nature*, *331*(6151), 91.
- Glass, C. K. (1994). Differential Recognition of Target Genes by Nuclear Receptor Monomers, Dimers, and Heterodimers*. *Endocrine Reviews*, *15*(3), 391-407. doi: 10.1210/edrv-15-3-391
- Goodwin, B., Jones, S. A., Price, R. R., Watson, M. A., McKee, D. D., Moore, L. B., . . . Kliewer, S. A. (2000). A Regulatory Cascade of the Nuclear Receptors FXR, SHP-1, and LXR-1 Represses Bile Acid Biosynthesis. *Molecular Cell*, *6*(3), 517-526. doi: 10.1016/S1097-2765(00)00051-4
- Greene, G. L., Gilna, P., Waterfield, M. D., Baker, A. M., Hort, Y. J., & Shine, J. D. (1986). Sequence and expression of human estrogen receptor complementary DNA. *Science*, *231* 4742, 1150-1154.

- Greulich, F., Hemmer, M. C., Rollins, D. A., Rogatsky, I., & Uhlenhaut, N. H. (2016). There goes the neighborhood: Assembly of transcriptional complexes during the regulation of metabolism and inflammation by the glucocorticoid receptor. *Steroids*, *114*, 7-15. doi: <https://doi.org/10.1016/j.steroids.2016.05.003>
- Gross, B., Pawlak, M., Lefebvre, P., & Staels, B. (2016). PPARs in obesity-induced T2DM, dyslipidaemia and NAFLD. *Nature Reviews Endocrinology*, *13*, 36. doi: 10.1038/nrendo.2016.135
- Gutierrez-Hartmann, A., Duval, D. L., & Bradford, A. P. (2007). ETS transcription factors in endocrine systems. *Trends in Endocrinology & Metabolism*, *18*(4), 150-158. doi: 10.1016/j.tem.2007.03.002
- Hardy, T., Oakley, F., Anstee, Q. M., & Day, C. P. (2016). Nonalcoholic Fatty Liver Disease: Pathogenesis and Disease Spectrum. *Annual Review of Pathology: Mechanisms of Disease*, *11*(1), 451-496. doi: 10.1146/annurev-pathol-012615-044224
- Heinz, S., Benner, C., Spann, N., Bertolino, E., Lin, Y. C., Laslo, P., . . . Glass, C. K. (2010). Simple Combinations of Lineage-Determining Transcription Factors Prime *cis*-Regulatory Elements Required for Macrophage and B Cell Identities. *Molecular Cell*, *38*(4), 576-589. doi: 10.1016/j.molcel.2010.05.004
- Heyman, R. A., Mangelsdorf, D. J., Dyck, J. A., Stein, R. B., Eichele, G., Evans, R. M., & Thaller, C. (1992). 9-cis retinoic acid is a high affinity ligand for the retinoid X receptor. *Cell*, *68*(2), 397-406. doi: 10.1016/0092-8674(92)90479-V
- Hollenberg, S. M., Weinberger, C., Ong, E. S., Cerelli, G., Oro, A., Lebo, R., . . . Evans, R. M. (1985). Primary structure and expression of a functional human glucocorticoid receptor cDNA. *Nature*, *318*(6047), 635-641. doi: 10.1038/318635a0
- Hsing, M., Wang, Y., Rennie, P. S., Cox, M. E., & Cherkasov, A. (2019). ETS transcription factors as emerging drug targets in cancer. *Medicinal Research Reviews*, *n/a*(*n/a*). doi: 10.1002/med.21575
- Ip, E., Farrell, G., Hall, P., Robertson, G., & Leclercq, I. (2004). Administration of the potent PPAR α agonist, Wy-14,643, reverses nutritional fibrosis and steatohepatitis in mice. *Hepatology*, *39*(5), 1286-1296.
- Jensen, T. L., Kiersgaard, M. K., Sørensen, D. B., & Mikkelsen, L. F. (2013). Fasting of mice: a review. *Laboratory Animals*, *47*(4), 225-240. doi: 10.1177/0023677213501659
- Kang, H. S., Okamoto, K., Kim, Y.-S., Takeda, Y., Bortner, C. D., Dang, H., . . . Jetten, A. M. (2011). Nuclear Orphan Receptor TAK1/TR4-Deficient Mice Are Protected Against Obesity-Linked Inflammation, Hepatic Steatosis, and Insulin Resistance. *Diabetes*, *60*(1), 177. doi: 10.2337/db10-0628
- Kerr, T. A., Saeki, S., Schneider, M., Schaefer, K., Berdy, S., Redder, T., . . . Schwarz, M. (2002). Loss of Nuclear Receptor SHP Impairs but Does Not Eliminate Negative Feedback Regulation of Bile Acid Synthesis. *Developmental Cell*, *2*(6), 713-720. doi: [https://doi.org/10.1016/S1534-5807\(02\)00154-5](https://doi.org/10.1016/S1534-5807(02)00154-5)
- Kersten, S., Seydoux, J., Peters, J. M., Gonzalez, F. J., Desvergne, B., & Wahli, W. (1999). Peroxisome proliferator-activated receptor α mediates the adaptive response to fasting. *The Journal of clinical investigation*, *103*(11), 1489-1498.

- Khan, R. S., Bril, F., Cusi, K., & Newsome, P. N. (2019). Modulation of Insulin Resistance in Nonalcoholic Fatty Liver Disease. *Hepatology*, *70*(2), 711-724. doi: 10.1002/hep.30429
- Kliwer, S. A., Lehmann, J. M., & Willson, T. M. (1999). Orphan Nuclear Receptors: Shifting Endocrinology into Reverse. *Science*, *284*(5415), 757. doi: 10.1126/science.284.5415.757
- Klug, A., & Schwabe, J. (1995). Protein motifs 5. Zinc fingers. *The FASEB journal*, *9*(8), 597-604.
- Law, S. W., Conneely, O. M., & O'Malley, B. W. (1994). Molecular cloning of a novel member of the nuclear receptor superfamily related to the orphan receptor, TR2. *Gene expression*, *4*(1-2), 77-84.
- Leblanc, B. P., & Stunnenberg, H. G. (1995). 9-cis retinoic acid signaling: changing partners causes some excitement. *Genes and Development*, *9*(15), 1811-1816.
- Lebovitz, H. E. (2002). Differentiating members of the thiazolidinedione class: a focus on safety. *Diabetes/Metabolism Research and Reviews*, *18*(S2), S23-S29. doi: 10.1002/dmrr.252
- Lee, J., Seok, S., Yu, P., Kim, K., Smith, Z., Rivas-Astroza, M., . . . Kemper, J. K. (2012). Genomic analysis of hepatic farnesoid X receptor binding sites reveals altered binding in obesity and direct gene repression by farnesoid X receptor in mice. *Hepatology (Baltimore, Md.)*, *56*(1), 108-117. doi: 10.1002/hep.25609
- Lee, Y.-F., Lee, H.-J., & Chang, C. (2002). Recent advances in the TR2 and TR4 orphan receptors of the nuclear receptor superfamily. *The Journal of Steroid Biochemistry and Molecular Biology*, *81*(4), 291-308. doi: [https://doi.org/10.1016/S0960-0760\(02\)00118-8](https://doi.org/10.1016/S0960-0760(02)00118-8)
- Leone, T. C., Weinheimer, C. J., & Kelly, D. P. (1999). A critical role for the peroxisome proliferator-activated receptor α (PPAR α) in the cellular fasting response: the PPAR α -null mouse as a model of fatty acid oxidation disorders. *Proceedings of the National Academy of Sciences*, *96*(13), 7473-7478.
- Levin, A. A., Sturzenbecker, L. J., Kazmer, S., Bosakowski, T., Huselton, C., Allenby, G., . . . Grippo, J. F. (1992). 9-cis retinoic acid stereoisomer binds and activates the nuclear receptor RXR α . *Nature*, *355*(6358), 359.
- Li, H., & Durbin, R. (2010). Fast and accurate long-read alignment with Burrows–Wheeler transform. *Bioinformatics*, *26*(5), 589-595. doi: 10.1093/bioinformatics/btp698
- Li, H., Handsaker, B., Wysoker, A., Fennell, T., Ruan, J., Homer, N., . . . Genome Project Data Processing, S. (2009). The Sequence Alignment/Map format and SAMtools. *Bioinformatics*, *25*(16), 2078-2079. doi: 10.1093/bioinformatics/btp352
- Li, T., & Chiang, J. Y. L. (2014). Bile Acid Signaling in Metabolic Disease and Drug Therapy. *Pharmacological Reviews*, *66*(4), 948. doi: 10.1124/pr.113.008201
- Lin, D.-L., Wu, S.-Q., & Chang, C. (1998). The genomic structure and chromosomal location of the human TR2 orphan receptor, a member of the steroid receptor superfamily. *Endocrine*, *8*(2), 123-134. doi: 10.1385/ENDO:8:2:123
- Lin, S.-J., Ho, H.-C., Lee, Y.-F., Liu, N.-C., Liu, S., Li, G., . . . Chang, C. (2012). Reduced osteoblast activity in the mice lacking TR4 nuclear receptor leads to osteoporosis. *Reproductive Biology and Endocrinology*, *10*(1), 43. doi: 10.1186/1477-7827-10-43

- Lin, S.-J., Yang, D.-R., Yang, G., Lin, C.-Y., Chang, H.-C., Li, G., & Chang, C. (2017). Chapter Thirteen - TR2 and TR4 Orphan Nuclear Receptors: An Overview. In D. Forrest & S. Tsai (Eds.), *Current Topics in Developmental Biology* (Vol. 125, pp. 357-373): Academic Press.
- Liu, H., Zhang, S., Xu, S., Koroleva, M., Small, E. M., & Jin, Z. G. (2019). Myofibroblast-specific YY1 promotes liver fibrosis. *Biochemical and Biophysical Research Communications*, *514*(3), 913-918. doi: <https://doi.org/10.1016/j.bbrc.2019.05.004>
- Liu, N.-C., Lin, W.-J., Kim, E., Collins, L. L., Lin, H.-Y., Yu, I. C., . . . Chang, C. (2007). Loss of TR4 Orphan Nuclear Receptor Reduces Phosphoenolpyruvate Carboxykinase-Mediated Gluconeogenesis. *Diabetes*, *56*(12), 2901. doi: [10.2337/db07-0359](https://doi.org/10.2337/db07-0359)
- Lou, X., Toresson, G., Benod, C., Suh, J. H., Philips, K. J., Webb, P., & Gustafsson, J.-A. (2014). Structure of the retinoid X receptor α -liver X receptor β (RXR α -LXR β) heterodimer on DNA. *Nature structural & molecular biology*, *21*(3), 277.
- Love, M. I., Huber, W., & Anders, S. (2014). Moderated estimation of fold change and dispersion for RNA-seq data with DESeq2. *Genome Biology*, *15*(12), 550. doi: [10.1186/s13059-014-0550-8](https://doi.org/10.1186/s13059-014-0550-8)
- Lu, Y., Ma, Z., Zhang, Z., Xiong, X., Wang, X., Zhang, H., . . . Li, X. (2014). Yin Yang 1 promotes hepatic steatosis through repression of farnesoid X receptor in obese mice. *Gut*, *63*(1), 170. doi: [10.1136/gutjnl-2012-303150](https://doi.org/10.1136/gutjnl-2012-303150)
- Lundåsen, T., Hunt, M. C., Nilsson, L.-M., Sanyal, S., Angelin, B., Alexson, S. E. H., & Rudling, M. (2007). PPAR α is a key regulator of hepatic FGF21. *Biochemical and Biophysical Research Communications*, *360*(2), 437-440. doi: <https://doi.org/10.1016/j.bbrc.2007.06.068>
- Maeda, T., Miyata, M., Yotsumoto, T., Kobayashi, D., Nozawa, T., Toyama, K., . . . Tamai, I. (2004). Regulation of Drug Transporters by the Farnesoid X Receptor in Mice. *Molecular Pharmaceutics*, *1*(4), 281-289. doi: [10.1021/mp0499656](https://doi.org/10.1021/mp0499656)
- Mangelsdorf, D. J., Borgmeyer, U., Heyman, R. A., Zhou, J. Y., Ong, E. S., Oro, A. E., . . . Evans, R. M. (1992). Characterization of three RXR genes that mediate the action of 9-cis retinoic acid. *Genes & development*, *6*(3), 329-344.
- Mangelsdorf, D. J., & Evans, R. M. (1995). The RXR heterodimers and orphan receptors. *Cell*, *83*(6), 841-850. doi: [https://doi.org/10.1016/0092-8674\(95\)90200-7](https://doi.org/10.1016/0092-8674(95)90200-7)
- Mangelsdorf, D. J., Ong, E. S., Dyck, J. A., & Evans, R. M. (1990). Nuclear receptor that identifies a novel retinoic acid response pathway. *Nature*, *345*(6272), 224.
- Mangelsdorf, D. J., Thummel, C., Beato, M., Herrlich, P., Schütz, G., Umesono, K., . . . Evans, R. M. (1995). The nuclear receptor superfamily: the second decade. *Cell*, *83*(6), 835-839. doi: [10.1016/0092-8674\(95\)90199-x](https://doi.org/10.1016/0092-8674(95)90199-x)
- Marschall, H. U., & Beuers, U. (2013). When Bile Acids Don't Get Amidated. *Gastroenterology*, *144*(5), 870-873. doi: [10.1053/j.gastro.2013.03.018](https://doi.org/10.1053/j.gastro.2013.03.018)
- Martin, S., Juliane, R., Katrin, W., Walter, J., & Theresia, T. (2011). Organic Anion Transporting Polypeptides (OATPs): Regulation of Expression and Function. *Current Drug Metabolism*, *12*(2), 139-153. doi: <http://dx.doi.org/10.2174/138920011795016863>

- Matsubara, T., Li, F., & Gonzalez, F. J. (2013). FXR signaling in the enterohepatic system. *Molecular and cellular endocrinology*, *368*(1-2), 17-29. doi: 10.1016/j.mce.2012.05.004
- Mazaira, G. I., Zgajnar, N. R., Lotufo, C. M., Daneri-Becerra, C., Sivils, J. C., Soto, O. B., . . . Galigniana, M. D. (2018). The Nuclear Receptor Field: A Historical Overview and Future Challenges. *Nuclear receptor research*, *5*, 101320. doi: 10.11131/2018/101320
- McLean, C. Y., Bristor, D., Hiller, M., Clarke, S. L., Schaar, B. T., Lowe, C. B., . . . Bejerano, G. (2010). GREAT improves functional interpretation of cis-regulatory regions. *Nature Biotechnology*, *28*(5), 495-501. doi: 10.1038/nbt.1630
- McNelis, Joanne C., & Olefsky, Jerrold M. (2014). Macrophages, Immunity, and Metabolic Disease. *Immunity*, *41*(1), 36-48. doi: 10.1016/j.immuni.2014.05.010
- Mi, L.-Z., Devarakonda, S., Harp, J. M., Han, Q., Pellicciari, R., Willson, T. M., . . . Rastinejad, F. (2003). Structural Basis for Bile Acid Binding and Activation of the Nuclear Receptor FXR. *Molecular Cell*, *11*(4), 1093-1100. doi: 10.1016/S1097-2765(03)00112-6
- Milbrandt, J. (1988). Nerve growth factor induces a gene homologous to the glucocorticoid receptor gene. *Neuron*, *1*(3), 183-188.
- Mir, A. A., Dyar, K. A., Greulich, F., Quagliarini, F., Jouffe, C., Hubert, M. J., . . . Uhlenhaut, N. H. (2019). In Vivo ChIP-Seq of Nuclear Receptors: A Rough Guide to Transform Frozen Tissues into High-Confidence Genome-Wide Binding Profiles. In M. Z. Badr (Ed.), *Nuclear Receptors: Methods and Experimental Protocols* (pp. 39-70). New York, NY: Springer New York.
- Montagner, A., Polizzi, A., Fouché, E., Ducheix, S., Lippi, Y., Lasserre, F., . . . Guillou, H. (2016). Liver PPAR α is crucial for whole-body fatty acid homeostasis and is protective against NAFLD. *Gut*, *65*(7), 1202-1214. doi: 10.1136/gutjnl-2015-310798
- Moschetta, A., Bookout, A. L., & Mangelsdorf, D. J. (2004). Prevention of cholesterol gallstone disease by FXR agonists in a mouse model. *Nature medicine*, *10*(12), 1352.
- Mu, X., Lee, Y.-F., Liu, N.-C., Chen, Y.-T., Kim, E., Shyr, C.-R., & Chang, C. (2004). Targeted Inactivation of Testicular Nuclear Orphan Receptor 4 Delays and Disrupts Late Meiotic Prophase and Subsequent Meiotic Divisions of Spermatogenesis. *Molecular and Cellular Biology*, *24*(13), 5887. doi: 10.1128/MCB.24.13.5887-5899.2004
- Müller, A., Ringseis, R., Düsterloh, K., Gahler, S., Eder, K., & Steinhart, H. (2005). Detection of conjugated dienoic fatty acids in human vascular smooth muscle cells treated with conjugated linoleic acid. *Biochimica et Biophysica Acta (BBA) - Molecular and Cell Biology of Lipids*, *1737*(2), 145-151. doi: <https://doi.org/10.1016/j.bbalip.2005.09.011>
- O'Geen, H., Lin, Y.-H., Xu, X., Echipare, L., Komashko, V. M., He, D., . . . Farnham, P. J. (2010). Genome-wide binding of the orphan nuclear receptor TR4 suggests its general role in fundamental biological processes. *BMC Genomics*, *11*(1), 689. doi: 10.1186/1471-2164-11-689
- O'Malley, B. (1990). MINIREVIEW: The Steroid Receptor Superfamily: More Excitement Predicted for the Future. *Molecular Endocrinology*, *4*(3), 363-369.
- Oldfield, Andrew J., Yang, P., Conway, Amanda E., Cinghu, S., Freudenberg, Johannes M., Yellaboina, S., & Jothi, R. (2014). Histone-Fold Domain Protein NF-Y Promotes Chromatin Accessibility for

- Cell Type-Specific Master Transcription Factors. *Molecular Cell*, 55(5), 708-722. doi: 10.1016/j.molcel.2014.07.005
- Olivares, A. M., Han, Y., Soto, D., Flattery, K., Marini, J., Mollema, N., . . . Haider, N. B. (2017). The nuclear hormone receptor gene Nr2c1 (Tr2) is a critical regulator of early retina cell patterning. *Developmental Biology*, 429(1), 343-355. doi: <https://doi.org/10.1016/j.ydbio.2017.05.021>
- Patsouris, D., Reddy, J. K., Müller, M., & Kersten, S. (2006). Peroxisome Proliferator-Activated Receptor α Mediates the Effects of High-Fat Diet on Hepatic Gene Expression. *Endocrinology*, 147(3), 1508-1516. doi: 10.1210/en.2005-1132
- Pawlak, M., Baugé, E., Bourguet, W., De Bosscher, K., Lalloyer, F., Tailleux, A., . . . Staels, B. (2014). The transrepressive activity of peroxisome proliferator-activated receptor alpha is necessary and sufficient to prevent liver fibrosis in mice. *Hepatology*, 60(5), 1593-1606.
- Perlmann, T., Rangarajan, P. N., Umesono, K., & Evans, R. M. (1993). Determinants for selective RAR and TR recognition of direct repeat HREs. *Genes & development*, 7(7b), 1411-1422.
- Petkovich, M., Brand, N. J., Krust, A., & Chambon, P. (1987). A human retinoic acid receptor which belongs to the family of nuclear receptors. *Nature*, 330(6147), 444-450. doi: 10.1038/330444a0
- Pircher, P. C., Kitto, J. L., Petrowski, M. L., Tangirala, R. K., Bischoff, E. D., Schulman, I. G., & Westin, S. K. (2003). Farnesoid X Receptor Regulates Bile Acid-Amino Acid Conjugation. *Journal of Biological Chemistry*, 278(30), 27703-27711.
- Plass, J. R., Mol, O., Heegsma, J., Geuken, M., Faber, K. N., Jansen, P. L., & Müller, M. (2002). Farnesoid X receptor and bile salts are involved in transcriptional regulation of the gene encoding the human bile salt export pump. *Hepatology*, 35(3), 589-596.
- Potthoff, M. J., Kliewer, S. A., & Mangelsdorf, D. J. (2012). Endocrine fibroblast growth factors 15/19 and 21: from feast to famine. *Genes & development*, 26(4), 312-324. doi: 10.1101/gad.184788.111
- Rui, L. (2014). Energy metabolism in the liver. *Comprehensive Physiology*, 4(1), 177-197. doi: 10.1002/cphy.c130024
- Russell, D. W., & Setchell, K. D. R. (1992). Bile acid biosynthesis. *Biochemistry*, 31(20), 4737-4749. doi: 10.1021/bi00135a001
- Sakuma, T., Kitajima, K., Nishiyama, M., Mashino, M., Hashita, T., & Nemoto, N. (2004). Suppression of female-specific murine Cyp2b9 gene expression by growth or glucocorticoid hormones. *Biochemical and Biophysical Research Communications*, 323(3), 776-781. doi: <https://doi.org/10.1016/j.bbrc.2004.08.158>
- Samuel, V. T., & Shulman, G. I. (2018). Nonalcoholic Fatty Liver Disease as a Nexus of Metabolic and Hepatic Diseases. *Cell Metabolism*, 27(1), 22-41. doi: <https://doi.org/10.1016/j.cmet.2017.08.002>
- Sanders, F. W. B., & Griffin, J. L. (2016). De novo lipogenesis in the liver in health and disease: more than just a shunting yard for glucose. *Biological reviews of the Cambridge Philosophical Society*, 91(2), 452-468. doi: 10.1111/brv.12178

- Schmitt, J., Kong, B., Stieger, B., Tschopp, O., Schultze, S. M., Rau, M., . . . Geier, A. (2015). Protective effects of farnesoid X receptor (FXR) on hepatic lipid accumulation are mediated by hepatic FXR and independent of intestinal FGF15 signal. *Liver International*, *35*(4), 1133-1144. doi: 10.1111/liv.12456
- Schuppan, D., Surabattula, R., & Wang, X. Y. (2018). Determinants of fibrosis progression and regression in NASH. *Journal of Hepatology*, *68*(2), 238-250. doi: 10.1016/j.jhep.2017.11.012
- Schuster, S., Cabrera, D., Arrese, M., & Feldstein, A. E. (2018). Triggering and resolution of inflammation in NASH. *Nature Reviews Gastroenterology & Hepatology*, *15*(6), 349-364. doi: 10.1038/s41575-018-0009-6
- Shi, L., Sierant, M. C., Gurdziel, K., Zhu, F., Cui, S., Kolodziej, K. E., . . . Engel, J. D. (2014). Biased, Non-equivalent Gene-Proximal and -Distal Binding Motifs of Orphan Nuclear Receptor TR4 in Primary Human Erythroid Cells. *PLOS Genetics*, *10*(5), e1004339. doi: 10.1371/journal.pgen.1004339
- Shin, D.-J., & Wang, L. (2019). Bile Acid-Activated Receptors: A Review on FXR and Other Nuclear Receptors. In S. Fiorucci & E. Distrutti (Eds.), *Bile Acids and Their Receptors* (pp. 51-72). Cham: Springer International Publishing.
- Shin, S.-Y., Fauman, E. B., Petersen, A.-K., Krumsiek, J., Santos, R., Huang, J., . . . Soranzo, N. (2014). An atlas of genetic influences on human blood metabolites. *Nature Genetics*, *46*, 543. doi: 10.1038/ng.2982
- <https://www.nature.com/articles/ng.2982#supplementary-information>
- Shiri-Sverdlov, R., Wouters, K., van Gorp, P. J., Gijbels, M. J., Noel, B., Buffat, L., . . . Hofker, M. H. (2006). Early diet-induced non-alcoholic steatohepatitis in APOE2 knock-in mice and its prevention by fibrates. *Journal of Hepatology*, *44*(4), 732-741.
- Shulman, A. I., & Mangelsdorf, D. J. (2005). Retinoid x receptor heterodimers in the metabolic syndrome. *New England Journal of Medicine*, *353*(6), 604-615.
- Shyr, C.-R., Kang, H.-Y., Tsai, M.-Y., Liu, N.-C., Ku, P.-Y., Huang, K. E., & Chang, C. (2009). Roles of Testicular Orphan Nuclear Receptors 2 and 4 in Early Embryonic Development and Embryonic Stem Cells. *Endocrinology*, *150*(5), 2454-2462. doi: 10.1210/en.2008-1165
- Sinal, C. J., Tohkin, M., Miyata, M., Ward, J. M., Lambert, G., & Gonzalez, F. J. (2000). Targeted Disruption of the Nuclear Receptor FXR/BAR Impairs Bile Acid and Lipid Homeostasis. *Cell*, *102*(6), 731-744. doi: [https://doi.org/10.1016/S0092-8674\(00\)00062-3](https://doi.org/10.1016/S0092-8674(00)00062-3)
- Sizemore, G. M., Pitarresi, J. R., Balakrishnan, S., & Ostrowski, M. C. (2017). The ETS family of oncogenic transcription factors in solid tumours. *Nature Reviews Cancer*, *17*(6), 337-351. doi: 10.1038/nrc.2017.20
- Stieger, B., Meier, Y., & Meier, P. J. (2007). The bile salt export pump. *Pflügers Archiv-European Journal of Physiology*, *453*(5), 611-620.
- Tanabe, O., Katsuoka, F., Campbell, A. D., Song, W., Yamamoto, M., Tanimoto, K., & Engel, J. D. (2002). An embryonic/fetal beta-type globin gene repressor contains a nuclear receptor TR2/TR4 heterodimer. *The EMBO journal*, *21*(13), 3434-3442. doi: 10.1093/emboj/cdf340

- Torer, N., Ozenirler, S., Yucel, A., Bukan, N., & Erdem, O. (2007). Importance of cytokines, oxidative stress and expression of BCL-2 in the pathogenesis of non-alcoholic steatohepatitis. *Scandinavian Journal of Gastroenterology*, *42*(9), 1095-1101. doi: 10.1080/00365520701286680
- Trauner, M., & Boyer, J. L. (2003). Bile Salt Transporters: Molecular Characterization, Function, and Regulation. *Physiological Reviews*, *83*(2), 633-671. doi: 10.1152/physrev.00027.2002
- Tsai, N.-P., Huq, M., Gupta, P., Yamamoto, K., Kagechika, H., & Wei, L.-N. (2009). Activation of testicular orphan receptor 4 by fatty acids. *Biochim Biophys Acta*, *1789*(11-12), 734-740. doi: 10.1016/j.bbagr.2009.09.010
- Wallace, M. C., Friedman, S. L., & Mann, D. A. (2015). Emerging and Disease-Specific Mechanisms of Hepatic Stellate Cell Activation. *Semin Liver Dis*, *35*(02), 107-118. doi: 10.1055/s-0035-1550060
- Wang, H., Chen, J., Hollister, K., Sowers, L. C., & Forman, B. M. (1999). Endogenous Bile Acids Are Ligands for the Nuclear Receptor FXR/BAR. *Molecular Cell*, *3*(5), 543-553. doi: 10.1016/S1097-2765(00)80348-2
- Wang, L., Lee, Y.-K., Bundman, D., Han, Y., Thevananther, S., Kim, C.-S., . . . Karin, M. (2002). Redundant pathways for negative feedback regulation of bile acid production. *Developmental Cell*, *2*(6), 721-731.
- Weintraub, A. S., Li, C. H., Zamudio, A. V., Sigova, A. A., Hannett, N. M., Day, D. S., . . . Young, R. A. (2017). YY1 Is a Structural Regulator of Enhancer-Promoter Loops. *Cell*, *171*(7), 1573-1588.e1528. doi: <https://doi.org/10.1016/j.cell.2017.11.008>
- Weir, J. B. d. V. (1949). New methods for calculating metabolic rate with special reference to protein metabolism. *The Journal of Physiology*, *109*(1-2), 1-9. doi: 10.1113/jphysiol.1949.sp004363
- Weisberg, S. P., McCann, D., Desai, M., Rosenbaum, M., Leibel, R. L., & Ferrante, A. W., Jr. (2003). Obesity is associated with macrophage accumulation in adipose tissue. *The Journal of clinical investigation*, *112*(12), 1796-1808. doi: 10.1172/JCI19246
- WHO. (2018). Obesity and overweight. <https://www.who.int/news-room/fact-sheets/detail/obesity-and-overweight>.
- Xie, S., Lee, Y.-F., Kim, E., Chen, L.-M., Ni, J., Fang, L.-Y., . . . Chang, C. (2009). TR4 nuclear receptor functions as a fatty acid sensor to modulate CD36 expression and foam cell formation. *Proceedings of the National Academy of Sciences*, *106*(32), 13353. doi: 10.1073/pnas.0905724106
- Yang, X., Downes, M., Yu, R. T., Bookout, A. L., He, W., Straume, M., . . . Evans, R. M. (2006). Nuclear Receptor Expression Links the Circadian Clock to Metabolism. *Cell*, *126*(4), 801-810. doi: <https://doi.org/10.1016/j.cell.2006.06.050>
- Yoshikawa, T., DuPont, B. R., Leach, R. J., & Detera-Wadleigh, S. D. (1996). New Variants of the Human and Rat Nuclear Hormone Receptor, TR4: Expression and Chromosomal Localization of the Human Gene. *Genomics*, *35*(2), 361-366. doi: <https://doi.org/10.1006/geno.1996.0368>

- Younossi, Z., Anstee, Q. M., Marietti, M., Hardy, T., Henry, L., Eslam, M., . . . Bugianesi, E. (2017). Global burden of NAFLD and NASH: trends, predictions, risk factors and prevention. *Nature Reviews Gastroenterology & Hepatology*, *15*, 11. doi: 10.1038/nrgastro.2017.109
<https://www.nature.com/articles/nrgastro.2017.109#supplementary-information>
- Zhang, M., Zhang, Y., Yang, S., Zhou, J., Gao, W., Yang, X., . . . Ni, B. (2017). Multifunctional YY1 in Liver Diseases. *Semin Liver Dis*, *37*(04), 363-376. doi: 10.1055/s-0037-1607451
- Zhang, Y., Jiang, R., Zheng, X., Lei, S., Huang, F., Xie, G., . . . Jia, W. (2019). Ursodeoxycholic acid accelerates bile acid enterohepatic circulation. *British Journal of Pharmacology*, *176*(16), 2848-2863. doi: 10.1111/bph.14705
- Zhang, Y., Liu, T., Meyer, C. A., Eeckhoute, J., Johnson, D. S., Bernstein, B. E., . . . Liu, X. S. (2008). Model-based Analysis of CHIP-Seq (MACS). *Genome Biology*, *9*(9), R137. doi: 10.1186/gb-2008-9-9-r137
- Zhou, X. E., Suino-Powell, K. M., Xu, Y., Chan, C.-W., Tanabe, O., Kruse, S. W., . . . Xu, H. E. (2011). The orphan nuclear receptor TR4 is a vitamin A-activated nuclear receptor. *The Journal of biological chemistry*, *286*(4), 2877-2885. doi: 10.1074/jbc.M110.168740
- Zúñiga, J., Cancino, M., Medina, F., Varela, P., Vargas, R., Tapia, G., . . . Fernández, V. (2011). N-3 PUFA supplementation triggers PPAR- α activation and PPAR- α /NF- κ B interaction: anti-inflammatory implications in liver ischemia-reperfusion injury. *PLoS one*, *6*(12), e28502.

Supplemental data

Supplemental Table 1: TR2 ChIP-Sequencing peaks in wildtype liver.

TR2 ChIP-Seq data from liver of chow-fed wildtype mice. Selected peaks discussed in results are listed. Data represents the overlapping peaks from 2 biological replicates.

Gene symbol	Chromosome	Start	End	Width	annotation	Distance to TSS	Gene name
Rps6kc1	chr1	190911600	190912052	453	Promoter	0	ribosomal protein S6 kinase polypeptide 1
Cwc15	chr9	14500410	14500894	485	Promoter	0	CWC15 spliceosome-associated protein
Fam114a2	chr11	57518379	57518861	483	Promoter	0	family with sequence similarity 114 member A2
Romo1	chr2	156143978	156144704	727	Promoter	0	reactive oxygen species modulator 1

Supplemental Table 2: TR4 ChIP-Sequencing peaks in wildtype liver.

TR4 ChIP-Seq data from liver of chow-fed wildtype mice. Selected peaks discussed in results are listed. Data represents the overlapping peaks from 2 biological replicates.

Gene symbol	Chromosome	Start	End	Width	annotation	Distance to TSS	Gene name
Rps6kc1	chr1	190911244	190912327	1084	Promoter	0	ribosomal protein S6 kinase polypeptide 1
Rps6kc1	chr1	190880585	190881182	598	Intron	30588	ribosomal protein S6 kinase polypeptide 1
Cwc15	chr9	14500122	14501376	1255	Promoter	0	CWC15 spliceosome-associated protein
Fam114a2	chr11	57517632	57519255	1624	Promoter	0	family with sequence similarity 114 member A2
Romo1	chr2	156143644	156144662	1019	Promoter	0	reactive oxygen species modulator 1
Slc27a5	chr7	12995893	12996291	399	Exon	1901	solute carrier family 27 , member 5
Slc27a5	chr7	12998970	12999311	342	Promoter	-778	solute carrier family 27 , member 5
Elovl5	chr9	77910504	77911196	693	Distal Intergenic	-6169	elongation of long chain fatty acids family member 5
Elovl5	chr9	77917075	77917691	617	Promoter	0	elongation of long chain fatty acids family member 5
Elovl5	chr9	77943398	77943756	359	Intron	26033	elongation of long chain fatty acids family member 5
Elovl5	chr9	77950864	77951218	355	Intron	33499	elongation of long chain fatty acids family member 5
Fads2	chr19	10101559	10102268	710	Promoter	-56	fatty acid desaturase 2
Fads2	chr19	10122109	10123246	1138	Distal Intergenic	-20606	fatty acid desaturase 2

Supplemental Table 3: TR4 ChIP-Sequencing peaks in L-TR4OE liver.

TR4 ChIP-Seq data from liver of chow-fed L-TR4OE mice. Selected peaks discussed in results are listed. Data represents the overlapping peaks from 2 biological replicates.

Gene symbol	Chromosome	Start	End	Width	annotation	Distance to TSS	Gene name
Baat	chr4	49485246	49486708	1463	Exon	19850	bile acid-Coenzyme A: amino acid N-acyltransferase
Baat	chr4	49510194	49510663	470	Distal Intergenic	-3636	bile acid-Coenzyme A: amino acid N-acyltransferase
Slc27a5	chr7	12995730	12996375	646	Exon	1817	solute carrier family 27 , member 5
Slc27a5	chr7	12997981	12999493	1513	Promoter	0	solute carrier family 27 , member 5
Elovl5	chr9	77910065	77911397	1333	Distal Intergenic	-5968	elongation of long chain fatty acids family member 5
Elovl5	chr9	77917056	77917648	593	Promoter	0	elongation of long chain fatty acids family member 5
Elovl5	chr9	77921604	77922011	408	Intron	4239	elongation of long chain fatty acids family member 5
Elovl5	chr9	77926161	77927429	1269	Intron	8796	elongation of long chain fatty acids family member 5
Elovl5	chr9	77943254	77943802	549	Intron	25889	elongation of long chain fatty acids family member 5
Elovl5	chr9	77950860	77951380	521	Intron	33495	elongation of long chain fatty acids family member 5
Elovl5	chr9	77951982	77952441	460	Intron	34617	elongation of long chain fatty acids family member 5
Fads2	chr19	10101224	10102239	1016	Promoter	0	fatty acid desaturase 2
Fads2	chr19	10121513	10123297	1785	Distal Intergenic	-20010	fatty acid desaturase 2
Fads2	chr19	10126600	10127621	1022	Distal Intergenic	-25097	fatty acid desaturase 2

Supplemental Table 4: Genes differentially expressed in livers of L-dKO livers on chow diet.

Results from RNA-Seq in liver indicating the fold change (FC) in gene expression as log₂ (log₂FC). The 11 up and 28 downregulated genes (log₂ FC >0,58 or <-0,58 ; adjusted p-value<0.05) are listed. Data represents n=3 per genotype.

Ensembl gene ID	Log2 FC	adjusted p-value	MGI (Mouse Genome Interactive) symbol
ENSMUSG00000069307	6.774	0.000	Hist1h2bq
ENSMUSG00000040660	3.431	0.017	Cyp2b9
ENSMUSG00000038155	2.164	0.000	Gstp2
ENSMUSG00000029822	1.989	0.000	Osbpl3
ENSMUSG00000029207	1.769	0.018	Apbb2
ENSMUSG00000020319	1.738	0.000	Wdpcp
ENSMUSG00000021376	1.391	0.000	Tpmt
ENSMUSG00000074183	1.320	0.006	Gsta1
ENSMUSG00000057068	1.103	0.002	Fam47e
ENSMUSG00000074794	1.004	0.001	Arrdc3
ENSMUSG00000064368	0.883	0.002	mt-Nd6
ENSMUSG00000053333	-0.712	0.041	Dis3l2
ENSMUSG00000014791	-0.798	0.018	Elmo3
ENSMUSG00000018102	-0.880	0.037	Hist1h2bc
ENSMUSG00000020311	-0.907	0.026	Erlec1
ENSMUSG00000040471	-0.919	0.024	Ggt6
ENSMUSG00000097148	-1.040	0.041	Gm3839
ENSMUSG00000033918	-1.116	0.006	Parl
ENSMUSG00000027618	-1.124	0.001	Nfs1
ENSMUSG00000063929	-1.151	0.033	Cyp4a32
ENSMUSG00000030364	-1.284	0.020	Clec2h
ENSMUSG00000056501	-1.340	0.006	Cebpb
ENSMUSG00000038005	-1.452	0.026	Hpf1
ENSMUSG00000063019	-1.474	0.012	Manbal
ENSMUSG00000060373	-1.575	0.002	Hnrnpc
ENSMUSG00000096768	-1.675	0.009	Gm47283
ENSMUSG00000040669	-1.703	0.012	Phc1
ENSMUSG00000025218	-1.755	0.000	Poll
ENSMUSG00000024423	-1.922	0.001	Impact
ENSMUSG00000040327	-1.950	0.001	Cul9
ENSMUSG00000067847	-2.047	0.000	Romo1
ENSMUSG00000030882	-2.370	0.001	Dnhd1
ENSMUSG00000089872	-2.479	0.000	Rps6kc1
ENSMUSG00000002781	-2.500	0.011	Tmem143
ENSMUSG00000020523	-2.689	0.000	Fam114a2
ENSMUSG00000035351	-2.805	0.000	Nup37
ENSMUSG00000004096	-3.022	0.000	Cwc15
ENSMUSG00000022223	-3.241	0.000	Sdr39u1
ENSMUSG00000042589	-7.189	0.001	Cux2

Supplemental Table 5: Genes differentially expressed in livers of L-TR4OE livers on chow diet.

Results from RNA-Seq in liver indicating the fold change (FC) in gene expression as log₂ (log₂FC). The 52 up and 11 downregulated genes (log₂ FC >0,58 or <-0,58 ; adjusted p-value<0.05) are listed. Data represents n=3 per genotype.

Ensembl gene ID	Log2 FC	adjusted p-value	MGI (Mouse Genome Interactive) symbol
ENSMUSG00000005893	4.334	0.000	Nr2c2
ENSMUSG000000091705	3.345	0.000	H2-Q2
ENSMUSG000000020000	3.259	0.003	Moxd1
ENSMUSG000000091867	3.188	0.001	Cyp2a22
ENSMUSG000000021208	3.058	0.000	Ifi2712b
ENSMUSG000000034634	2.696	0.001	Ly6d
ENSMUSG000000021508	2.562	0.018	Cxcl14
ENSMUSG000000028970	2.539	0.000	Abcb1b
ENSMUSG000000020911	2.523	0.030	Krt19
ENSMUSG000000027635	2.505	0.002	Dsn1
ENSMUSG000000032098	2.443	0.000	Treh
ENSMUSG000000074240	2.207	0.000	Cib3
ENSMUSG000000006398	2.100	0.002	Cdc20
ENSMUSG000000079507	2.078	0.000	H2-Q1
ENSMUSG000000027699	2.061	0.028	Ect2
ENSMUSG000000032718	2.033	0.001	Mansc1
ENSMUSG000000054932	1.803	0.041	Afp
ENSMUSG000000061132	1.793	0.000	Blnk
ENSMUSG000000045934	1.760	0.000	Mtmr11
ENSMUSG000000046402	1.698	0.004	Rbp1
ENSMUSG000000025014	1.680	0.002	Dntt
ENSMUSG000000064215	1.656	0.000	Ifi27
ENSMUSG000000029482	1.594	0.000	Aacs
ENSMUSG000000074183	1.530	0.043	Gsta1
ENSMUSG000000021670	1.430	0.000	Hmgcr
ENSMUSG000000041827	1.412	0.002	Oasl1
ENSMUSG000000047228	1.349	0.032	A2ml1
ENSMUSG000000032068	1.335	0.000	Plet1
ENSMUSG000000043013	1.311	0.004	Onecut1
ENSMUSG000000070348	1.283	0.007	Ccnd1
ENSMUSG000000068220	1.280	0.031	Lgals1
ENSMUSG000000021665	1.268	0.000	Hexb
ENSMUSG000000006517	1.246	0.001	Mvd
ENSMUSG000000042834	1.174	0.001	Nrep
ENSMUSG0000000037379	1.153	0.047	Spon2
ENSMUSG000000001642	1.134	0.002	Akr1b3
ENSMUSG000000022351	1.124	0.000	Sqle
ENSMUSG000000028551	1.084	0.046	Cdkn2c
ENSMUSG000000005968	1.052	0.006	Tuft1
ENSMUSG000000031604	1.039	0.001	Msmo1
ENSMUSG000000027907	1.016	0.033	S100a11

ENSMUSG00000051579	0.997	0.002	Tceal8
ENSMUSG00000030605	0.941	0.003	Mfge8
ENSMUSG00000022587	0.898	0.002	Ly6e
ENSMUSG00000036446	0.896	0.022	Lum
ENSMUSG00000058216	0.807	0.039	Gstp3
ENSMUSG00000001467	0.771	0.001	Cyp51
ENSMUSG00000055447	0.763	0.039	Cd47
ENSMUSG00000032231	0.762	0.050	Anxa2
ENSMUSG00000027712	0.714	0.002	Anxa5
ENSMUSG00000023832	0.609	0.002	Acat2
ENSMUSG00000020258	-0.610	0.004	Glyctk
ENSMUSG00000047417	-0.646	0.042	Rexo1
ENSMUSG00000029162	-0.700	0.017	Khk
ENSMUSG00000028999	-0.835	0.002	Rint1
ENSMUSG00000031161	-0.835	0.019	Hdac6
ENSMUSG00000006800	-1.099	0.002	Sulf2
ENSMUSG00000035245	-1.457	0.002	Eogt
ENSMUSG00000022025	-1.533	0.002	Cnmd
ENSMUSG00000062061	-1.739	0.039	Obp2a
ENSMUSG00000026475	-2.779	0.000	Rgs16
ENSMUSG00000040441	-9.322	0.000	Slc26a10

Supplemental Table 6: Genes differentially expressed in livers of L-dKO livers after 12 weeks of HFD.

Results from RNA-Seq in liver indicating the fold change (FC) in gene expression as log₂ (log₂FC). The top 50 up and downregulated genes (log₂ FC >0,58 or <-0,58 ; adjusted p-value<0.05) are listed. Data represents n=3 per genotype.

Ensembl gene ID	Log ₂ FC	adjusted p-value	MGI (Mouse Genome Interactive) symbol
ENSMUSG00000069307	7.10	0.00	Hist1h2bq
ENSMUSG00000037071	3.81	0.03	Scd1
ENSMUSG00000040583	3.68	0.00	Cyp2b13
ENSMUSG00000038155	3.47	0.00	Gstp2
ENSMUSG00000027577	3.43	0.04	Chrna4
ENSMUSG00000074240	2.30	0.01	Cib3
ENSMUSG00000060803	2.28	0.00	Gstp1
ENSMUSG00000061780	2.27	0.01	Cfd
ENSMUSG00000028072	2.02	0.05	Ntrk1
ENSMUSG00000057933	1.99	0.04	Gsta2
ENSMUSG00000056035	1.97	0.00	Cyp3a11
ENSMUSG00000020319	1.93	0.00	Wdpcp
ENSMUSG00000029822	1.76	0.02	Osbpl3
ENSMUSG00000020623	1.69	0.04	Map2k6
ENSMUSG00000027559	1.68	0.00	Car3
ENSMUSG00000003477	1.65	0.00	Inmt
ENSMUSG00000025986	1.49	0.04	Slc39a10
ENSMUSG00000021704	1.35	0.00	Mtx3
ENSMUSG00000036769	1.32	0.01	Wdr44
ENSMUSG00000001998	1.31	0.00	Ap4e1
ENSMUSG00000038370	1.27	0.01	Pcp411

ENSMUSG00000056973	1.18	0.00	Ces1d
ENSMUSG00000079110	1.18	0.01	Capn3
ENSMUSG00000021376	1.16	0.00	Tpmt
ENSMUSG00000053846	1.16	0.02	Lipg
ENSMUSG00000058135	1.14	0.04	Gstm1
ENSMUSG00000049493	1.12	0.00	Pls1
ENSMUSG00000038188	1.08	0.02	Scarf1
ENSMUSG00000002032	1.08	0.05	Tmem25
ENSMUSG00000019232	1.06	0.00	Etnppl
ENSMUSG00000074182	1.00	0.00	Znhit6
ENSMUSG00000027820	0.99	0.00	Mme
ENSMUSG00000027810	0.98	0.00	Eif2a
ENSMUSG00000033114	0.96	0.00	Slc35d2
ENSMUSG00000037709	0.95	0.00	Fam13a
ENSMUSG00000096215	0.94	0.01	Smim22
ENSMUSG00000060227	0.93	0.01	Casc4
ENSMUSG00000061959	0.91	0.00	Ces1e
ENSMUSG00000025870	0.90	0.01	Arl10
ENSMUSG00000010025	0.89	0.00	Aldh3a2
ENSMUSG00000030649	0.88	0.00	Anapc15
ENSMUSG00000050856	0.86	0.00	Atp5k
ENSMUSG00000030256	0.85	0.02	Bhlhe41
ENSMUSG00000008976	0.84	0.00	Gabpa
ENSMUSG00000051615	0.82	0.01	Rap2a
ENSMUSG00000017309	0.81	0.04	Cd300lg
ENSMUSG00000034729	0.80	0.00	Mrps10
ENSMUSG00000033715	0.79	0.02	Akr1c14
ENSMUSG00000025934	0.79	0.00	Gsta3
ENSMUSG00000031725	0.79	0.00	Ces1f
ENSMUSG00000061947	-1.26	0.00	Serpina10
ENSMUSG00000074093	-1.26	0.00	Svip
ENSMUSG00000006014	-1.28	0.00	Prg4
ENSMUSG00000031722	-1.30	0.02	Hp
ENSMUSG00000018459	-1.30	0.00	Slc13a3
ENSMUSG00000019737	-1.31	0.01	Syne4
ENSMUSG00000012428	-1.32	0.00	Steap4
ENSMUSG00000031451	-1.34	0.04	Gas6
ENSMUSG00000021091	-1.34	0.00	Serpina3n
ENSMUSG00000051225	-1.34	0.01	Fam83a
ENSMUSG00000021922	-1.35	0.01	Itih4
ENSMUSG00000006522	-1.36	0.03	Itih3
ENSMUSG00000022146	-1.36	0.02	Osmr
ENSMUSG00000024036	-1.38	0.02	Slc37a1
ENSMUSG00000039738	-1.41	0.02	Slx4
ENSMUSG00000034795	-1.47	0.00	Ccdc122
ENSMUSG00000067847	-1.48	0.00	Romo1
ENSMUSG00000022223	-1.50	0.00	Sdr39u1
ENSMUSG00000020926	-1.50	0.00	Adam11
ENSMUSG00000029380	-1.51	0.00	Cxcl1
ENSMUSG00000040026	-1.51	0.00	Saa3
ENSMUSG00000035299	-1.55	0.04	Mid1
ENSMUSG00000025218	-1.56	0.00	Poll
ENSMUSG00000073755	-1.56	0.00	5730409E04Rik
ENSMUSG00000037095	-1.62	0.00	Lrg1

ENSMUSG00000039196	-1.64	0.00	Orm1
ENSMUSG00000060981	-1.65	0.00	Hist1h4h
ENSMUSG00000015702	-1.68	0.04	Anxa9
ENSMUSG00000026558	-1.68	0.00	Uck2
ENSMUSG00000061048	-1.76	0.02	Cdh3
ENSMUSG00000031150	-1.92	0.00	Ccdc120
ENSMUSG00000029304	-1.97	0.00	Spp1
ENSMUSG00000026542	-2.21	0.02	Apcs
ENSMUSG00000038524	-2.34	0.00	Fchsd1
ENSMUSG00000042638	-2.36	0.00	Gucy2c
ENSMUSG00000089872	-2.51	0.00	Rps6kc1
ENSMUSG00000020523	-2.53	0.00	Fam114a2
ENSMUSG00000020522	-2.54	0.00	Mfap3
ENSMUSG00000029352	-2.60	0.01	Crybb3
ENSMUSG00000004096	-2.66	0.00	Cwc15
ENSMUSG00000026822	-2.77	0.02	Lcn2
ENSMUSG00000035351	-2.80	0.00	Nup37
ENSMUSG00000040809	-3.12	0.01	Chil3
ENSMUSG00000021614	-3.21	0.00	Vcan
ENSMUSG00000034634	-3.30	0.05	Ly6d
ENSMUSG00000031765	-3.36	0.00	Mt1
ENSMUSG00000095648	-3.61	0.00	Gm2004
ENSMUSG00000031762	-4.13	0.00	Mt2
ENSMUSG00000078867	-5.63	0.00	Gm14418
ENSMUSG00000032816	-5.76	0.00	Igdcc4

Supplemental Table 7: Genes differentially expressed in livers of L-TR4OE livers after 12 weeks of HFD.

Results from RNA-Seq in liver indicating the fold change (FC) in gene expression as log₂ (log₂FC). The top 50 up and downregulated genes (log₂ FC >0,58 or <-0,58 ; adjusted p-value<0.05) are listed. Data represents n=3 per genotype.

Ensembl gene ID	Log ₂ FC	adjusted p-value	MGI (Mouse Genome Interactive) symbol
ENSMUSG00000020159	5.841	0.000	Gabrp
ENSMUSG00000043501	4.618	0.000	Lgals2
ENSMUSG00000021214	4.417	0.000	Akr1c18
ENSMUSG00000020911	4.092	0.000	Krt19
ENSMUSG00000005893	4.056	0.000	Nr2c2
ENSMUSG00000025630	3.573	0.008	Hprt
ENSMUSG00000047517	3.462	0.000	Dmbt1
ENSMUSG00000024029	3.425	0.000	Tff3
ENSMUSG00000021795	3.222	0.000	Sftpd
ENSMUSG00000075189	2.808	0.002	Olf1055
ENSMUSG00000023039	2.600	0.000	Krt7
ENSMUSG00000047139	2.580	0.000	Cd24a
ENSMUSG00000012350	2.486	0.000	Ehf
ENSMUSG00000032357	2.320	0.000	Tinag
ENSMUSG00000039187	2.265	0.001	Fanci
ENSMUSG00000037995	2.249	0.000	Igsf9
ENSMUSG00000042784	2.217	0.000	Muc1
ENSMUSG00000091345	2.216	0.000	Col6a5
ENSMUSG00000057092	2.137	0.000	Fxyd3
ENSMUSG00000074240	2.036	0.000	Cib3
ENSMUSG00000000303	2.021	0.000	Cdh1

ENSMUSG00000042961	2.013	0.002	Egflam
ENSMUSG00000034127	1.995	0.000	Tspan8
ENSMUSG00000045394	1.971	0.000	Epcam
ENSMUSG00000032091	1.910	0.011	Tmprss4
ENSMUSG00000037736	1.899	0.004	Limch1
ENSMUSG00000026479	1.872	0.000	Lamc2
ENSMUSG00000031995	1.851	0.000	St14
ENSMUSG00000027315	1.846	0.000	Spint1
ENSMUSG00000043719	1.840	0.000	Col6a6
ENSMUSG00000068037	1.829	0.019	Mas1
ENSMUSG00000029086	1.787	0.000	Prom1
ENSMUSG00000016763	1.777	0.000	Scube1
ENSMUSG00000034634	1.734	0.031	Ly6d
ENSMUSG00000031274	1.727	0.000	Col4a5
ENSMUSG00000003534	1.719	0.001	Ddr1
ENSMUSG00000031075	1.713	0.000	Ano1
ENSMUSG00000020758	1.681	0.000	Itgb4
ENSMUSG00000038943	1.592	0.000	Prc1
ENSMUSG00000054932	1.577	0.000	Afp
ENSMUSG00000074254	1.565	0.000	Cyp2a4
ENSMUSG00000002265	1.557	0.000	Peg3
ENSMUSG00000066877	1.557	0.029	Nck2
ENSMUSG00000029675	1.549	0.000	Eln
ENSMUSG00000028716	1.517	0.008	Pdzk1ip1
ENSMUSG00000002980	1.512	0.000	Bcam
ENSMUSG00000039131	1.504	0.042	Gipc2
ENSMUSG00000028357	1.487	0.000	Kif12
ENSMUSG00000001025	1.470	0.000	S100a6
ENSMUSG00000024270	1.458	0.001	Slc39a6
ENSMUSG00000041684	-0.747	0.000	Bivm
ENSMUSG00000021091	-0.750	0.049	Serpina3n
ENSMUSG00000022871	-0.772	0.017	Fetub
ENSMUSG00000017718	-0.777	0.015	Afmid
ENSMUSG00000029656	-0.783	0.049	C8b
ENSMUSG00000037286	-0.788	0.000	Stag1
ENSMUSG00000016194	-0.794	0.000	Hsd11b1
ENSMUSG00000032561	-0.795	0.023	Acpp
ENSMUSG00000038836	-0.797	0.000	Agbl3
ENSMUSG00000046532	-0.810	0.023	Ar
ENSMUSG00000022139	-0.810	0.026	Mbnl2
ENSMUSG00000022877	-0.816	0.002	Hrg
ENSMUSG00000026839	-0.817	0.005	Upp2
ENSMUSG00000030378	-0.817	0.003	Sult2a8
ENSMUSG00000040213	-0.836	0.004	Kyat3
ENSMUSG00000038641	-0.838	0.004	Akr1d1
ENSMUSG00000028838	-0.856	0.001	Extl1
ENSMUSG00000020017	-0.864	0.000	Hal
ENSMUSG00000027556	-0.866	0.000	Car1
ENSMUSG00000093485	-0.884	0.000	Gm20708
ENSMUSG00000040017	-0.901	0.018	Saa4
ENSMUSG00000021259	-0.919	0.014	Cyp46a1
ENSMUSG00000042851	-0.928	0.018	Zc3h6
ENSMUSG00000024411	-0.935	0.000	Aqp4
ENSMUSG00000005268	-0.956	0.000	Prlr
ENSMUSG00000040035	-1.055	0.011	Disp2

ENSMUSG00000039533	-1.074	0.000	Mmd2
ENSMUSG00000028238	-1.075	0.038	Atp6v0d2
ENSMUSG00000061928	-1.080	0.006	Dsg1b
ENSMUSG00000034774	-1.147	0.000	Dsg1c
ENSMUSG00000036027	-1.156	0.004	1810046K07Rik
ENSMUSG00000028556	-1.165	0.025	Dock7
ENSMUSG00000000739	-1.166	0.010	Sult5a1
ENSMUSG00000042248	-1.180	0.001	Cyp2c37
ENSMUSG00000061601	-1.229	0.002	Pclo
ENSMUSG00000079492	-1.301	0.000	Gm11127
ENSMUSG00000022129	-1.360	0.000	Dct
ENSMUSG00000025004	-1.384	0.018	Cyp2c40
ENSMUSG00000027870	-1.439	0.019	Hao2
ENSMUSG00000030237	-1.476	0.000	Slco1a4
ENSMUSG00000027677	-1.664	0.002	Ttc14
ENSMUSG00000040660	-1.801	0.002	Cyp2b9
ENSMUSG00000028008	-2.256	0.012	Asic5
ENSMUSG00000092008	-2.399	0.006	Cyp2c69
ENSMUSG00000029752	-2.682	0.002	Asns
ENSMUSG00000024211	-2.743	0.000	Grm8
ENSMUSG00000025757	-2.969	0.000	Hspa4l
ENSMUSG00000023036	-4.368	0.014	Pcdhgc4
ENSMUSG00000025326	-4.822	0.009	Ube3a
ENSMUSG00000041750	-6.101	0.001	Cd1d2

Supplemental Table 8: PUFA and bile acid profiling in WT and L-dKO livers.

Metabolite profiling results from metabolomics for all detected PUFA, primary and secondary bile acids identified in wildtype and L-dKO livers after 12 weeks of HFD. Data represents the average of 7 biological replicates per genotype.

Biochemical	Class of lipid	Component ID	Chemical ID	Average WT	Average KO	KO/WT ratio
stearidonate (18:4n3)	PUFA (n3 and n6)	33969	100001229	23035392.14	15254681.86	0.662
linolenate [alpha or gamma; (18:3n3 or 6)]	PUFA (n3 and n6)	34035	100001337	376120907.4	313822667.4	0.834
eicosapentaenoate (EPA; 20:5n3)	PUFA (n3 and n6)	18467	2050	204654483.4	171480666.3	0.838
hexadecatrienoate (16:3n3)	PUFA (n3 and n6)	57651	100009393	8002688.571	6712528.429	0.839
nisinate (24:6n3)	PUFA (n3 and n6)	57810	100015785	32576537.14	28812417.43	0.884
hexadecadienoate (16:2n6)	PUFA (n3 and n6)	57652	100009394	47993268.29	42692634.57	0.890
docosapentaenoate (n3 DPA; 22:5n3)	PUFA (n3 and n6)	32504	100001181	183101634.3	165772438.9	0.905
arachidonate (20:4n6)	PUFA (n3 and n6)	1110	229	1902574720	1762608695	0.926
docosahexaenoate (DHA; 22:6n3)	PUFA (n3 and n6)	44675	100000665	895505746.3	848197814.9	0.947
linoleate (18:2n6)	PUFA (n3 and n6)	1105	180	4181557175	3979945765	0.952
mead acid (20:3n9)	PUFA (n3 and n6)	35174	100001472	194798688	210371780.6	1.080
dihomo-linolenate (20:3n3 or n6)	PUFA (n3 and n6)	35718	100001739	199995492.6	222100217.1	1.111
docosadienoate (22:2n6)	PUFA (n3 and n6)	32415	100001182	11764823.14	13924009.29	1.184
dihomo-linoleate (20:2n6)	PUFA (n3 and n6)	17805	1231	226425718.9	279506589.7	1.234
docosapentaenoate (n6 DPA; 22:5n6)	PUFA (n3 and n6)	37478	100001580	97057637.71	120936172.6	1.246
heneicosapentaenoate (21:5n3)	PUFA (n3 and n6)	57658	100015797	1462453.429	1891897.429	1.294
adrenate (22:4n6)	PUFA (n3 and n6)	32980	100001193	126425432	169087010.3	1.337
docosatrienoate (22:3n6)	PUFA (n3 and n6)	57467	100015762	54828652.29	80468362.29	1.468
chenodeoxycholate	Primary Bile Acid	1563	1123	5235211.571	8706044.714	1.663
cholate	Primary Bile Acid	22842	136	11947002.86	18032263.29	1.509
tauro-beta-muricholate	Primary Bile Acid	33983	100001250	22896289.71	45685034.86	1.995
taurochenodeoxycholate	Primary Bile Acid	18494	1629	5764080.714	11494787.43	1.994
taurocholate	Primary Bile Acid	18497	1648	160840602.9	258854153.1	1.609
glycocholate	Primary Bile Acid	18476	342	444021.8	224409.5714	0.505
beta-muricholate	Primary Bile Acid	31885	100001066	56979671.43	69689565.71	1.223
6-beta-hydroxylithocholate	Secondary Bile Acid	36807	100001625	2981018.286	4835218.714	1.622

6-oxolithocholate	Secondary Bile Acid	46336	100001068	130823.7143	320395.2857	2.449
hyocholate	Secondary Bile Acid	34093	100001279	311993.1667	455499	1.460
hyodeoxycholate	Secondary Bile Acid	27531	100000777	4677428.286	8263357.714	1.767
taurodeoxycholate	Secondary Bile Acid	12261	1668	46319573.71	88931995.71	1.920
taurohyocholate	Secondary Bile Acid	42603	100004084	209417.1667	412384	1.969
tauroolithocholate	Secondary Bile Acid	31889	100001065	543247.3333	1577797.286	2.904
tauroursodeoxycholate	Secondary Bile Acid	39378	100002912	2737951	6379313.143	2.330
ursodeoxycholate	Secondary Bile Acid	1605	1135	4463123.571	6916759	1.550
3-dehydrocholate	Secondary Bile Acid	43835	100001062	94896.5	64870	0.684
taurochenodeoxycholic acid 7-sulfate	Secondary Bile Acid	52976	100006643	198958.8571	267552.1429	1.345
7-ketodeoxycholate	Secondary Bile Acid	31904	100001063	2788049.143	3809741.571	1.366

Supplemental Table 9: PUFA and bile acid profiling in WT and L-TR4OE livers.

Metabolite profiling results from metabolomics for all detected PUFA, primary and secondary bile acids identified in wildtype and L-TR4OE livers after 12 weeks of HFD. Data represents the average of 5 biological replicates per genotype.

Biochemical	Class of lipid	Component ID	Chemical ID	Average WT	Average OE	OE/WT ratio
hexadecatrienoate (16:3n3)	PUFA (n3 and n6)	57651	100009393	8346290.2	4090718.4	0.490
adrenate (22:4n6)	PUFA (n3 and n6)	32980	100001193	161752733.6	130918881.6	0.809
arachidonate (20:4n6)	PUFA (n3 and n6)	1110	229	2942259952	2577283456	0.876
dihomo-linoleate (20:2n6)	PUFA (n3 and n6)	17805	1231	261214113.6	291034457.6	1.114
dihomo-linolenate (20:3n3 or n6)	PUFA (n3 and n6)	35718	100001739	265451717.2	238410358.4	0.898
docosadienoate (22:2n6)	PUFA (n3 and n6)	32415	100001182	16287315	19071738.6	1.171
docosahexaenoate (DHA; 22:6n3)	PUFA (n3 and n6)	44675	100000665	797950491.2	707155993.6	0.886
docosapentaenoate (n3 DPA; 22:5n3)	PUFA (n3 and n6)	32504	100001181	131181589.6	110583265.6	0.843
docosapentaenoate (n6 DPA; 22:5n6)	PUFA (n3 and n6)	37478	100001580	122870942.2	130061755.2	1.059
docosatrienoate (22:3n6)	PUFA (n3 and n6)	57467	100015762	79267943.8	85853635.2	1.083
eicosapentaenoate (EPA; 20:5n3)	PUFA (n3 and n6)	18467	2050	160335125.6	172305875.2	1.075
heneicosapentaenoate (21:5n3)	PUFA (n3 and n6)	57658	100015797	1298536.25	909129	0.700
hexadecadienoate (16:2n6)	PUFA (n3 and n6)	57652	100009394	46753520	39424838.4	0.843
linoleate (18:2n6)	PUFA (n3 and n6)	1105	180	3639812198	3634452787	0.999

linolenate [alpha or gamma; (18:3n3 or 6)]	PUFA (n3 and n6)	34035	100001337	268183267.2	267185929.6	0.996
mead acid (20:3n9)	PUFA (n3 and n6)	35174	100001472	273625753.2	302842768	1.107
nisinate (24:6n3)	PUFA (n3 and n6)	57810	100015785	29729757.2	32657886	1.098
stearidonate (18:4n3)	PUFA (n3 and n6)	33969	100001229	13164609	12248087.2	0.930
taurocholate	Primary Bile Acid	18497	1648	219781067.2	336087235.2	1.529
chenodeoxycholate	Primary Bile Acid	1563	1123	7410802.2	13770793	1.858
glyco-beta-muricholate	Primary Bile Acid	62066	100020214	119171.75	191481.8	1.607
beta-muricholate	Primary Bile Acid	31885	100001066	113185372.8	244068076.8	2.156
tauro-beta-muricholate	Primary Bile Acid	33983	100001250	43574052.4	112253290	2.576
taurochenodeoxycholate	Primary Bile Acid	18494	1629	6700501.6	22146103.6	3.305
cholate	Primary Bile Acid	22842	136	20952695.4	24801484.4	1.184
cholate sulfate	Primary Bile Acid	52973	100006637	70240.75	67182.5	0.956
glycocholate	Primary Bile Acid	18476	342	276547.2	208962.8	0.756
6-oxolithocholate	Secondary Bile Acid	46336	100001068	469900	127132.8	0.271
hyodeoxycholate	Secondary Bile Acid	27531	100000777	8463615.75	4870147	0.575
taurochenodeoxycholic acid 7-sulfate	Secondary Bile Acid	52976	100006643	223831.2	347082.4	1.551
hyocholate	Secondary Bile Acid	34093	100001279	230975.4	397424.6	1.721
ursodeoxycholate	Secondary Bile Acid	1605	1135	10377398.4	18427048.2	1.776
7-ketodeoxycholate	Secondary Bile Acid	31904	100001063	4506217.8	8391027	1.862
taurohyocholate	Secondary Bile Acid	42603	100004084	211054.4	416403.8	1.973
tauroursodeoxycholate	Secondary Bile Acid	39378	100002912	5152094.8	14830903.4	2.879
3-dehydrocholate	Secondary Bile Acid	43835	100001062	96373.33333	85175	0.884
6-beta-hydroxylithocholate	Secondary Bile Acid	36807	100001625	3984685.2	2890677.6	0.725
taurodeoxycholate	Secondary Bile Acid	12261	1668	46463206.8	51733164.8	1.113
tauroolithocholate	Secondary Bile Acid	31889	100001065	390358.6	582841.4	1.493

List of publications

- [1] Mir, A. A.*, Dyar, K. A.*, Greulich, F., Quagliarini, F., Jouffe, C., **Hubert, M. J.**, Hemmer M.C., Uhlenschaut, N. H. (2019). **In Vivo ChIP-Seq of Nuclear Receptors: A Rough Guide to Transform Frozen Tissues into High-Confidence Genome-Wide Binding Profiles.** In M. Z. Badr (Ed.), *Nuclear Receptors: Methods and Experimental Protocols* (pp. 39-70). New York, NY: Springer New York. *: these authors contributed equally to the work

- [2] Dyar, K. A., **Hubert, M. J.**, Mir, A. A., Ciciliot, S., Lutter, D., Greulich, F., . . . Uhlenschaut, N. H. (2018). **Transcriptional programming of lipid and amino acid metabolism by the skeletal muscle circadian clock.** *PLOS Biology*, 16(8), e2005886. doi: 10.1371/journal.pbio.2005886

Conference attendance and poster presentations

- [1] Progression of non-alcoholic fatty liver disease by increased activity of testicular nuclear receptors, *Cold Spring Harbor: Mechanisms of Metabolic Signaling* (New York, USA, 2019)

- [2] Role of the Testicular Nuclear Receptors in hepatic lipid and glucose metabolism, *DZD Second german french conference on diabetes research* (Berlin, Germany, 2018)

- [3] Role of the transcriptional regulation of Insulin and the Glut-transporter family by Nuclear Receptors in glucose homeostasis., *FEBS advanced lecture course: Nuclear Receptors Signaling in Physiology and Disease* (Spetses, Greece, 2015)